Distribution Agreement

In presenting this thesis or dissertation as a partial fulfillment of the requirements for an advanced degree from Emory University, I hereby grant to Emory University and its agents the non-exclusive license to archive, make accessible, and display my thesis or dissertation in whole or in part in all forms of media, now or hereafter known, including display on the world wide web. I understand that I may select some access restrictions as part of the online submission of this thesis or dissertation. I retain all ownership rights to the copyright of the thesis or dissertation. I also retain the right to use in future works (such as articles or books) all or part of this thesis or dissertation.

Signature:

_____ _____

Scott Christopher Wilkinson Date

The role of LKB1 in regulating actin and cellular polarization during motility

By

Scott Christopher Wilkinson
Doctor of Philosophy

Graduate Division of Biological and Biomedical Sciences
Cancer Biology

Adam I Marcus
Advisor

George Beck
Committee Member

Andrew Kowalczyk
Committee Member

Shoichiro Ono
Committee Member

Wei Zhou
Committee Member

Accepted:

Lisa A. Tedesco, Ph.D.
Dean of the James T. Laney School of Graduate Studies

Date

The role of LKB1 in regulating actin and cellular polarization during motility

By

Scott Christopher Wilkinson
B.S., Berry College, 2009

Advisor: Adam I Marcus, Ph.D.

An abstract of
A dissertation submitted to the Faculty of the
James T. Laney School of Graduate Studies of Emory University
in partial fulfillment of the requirements for the degree of
Doctor of Philosophy
in Graduate Division of Biological and Biomedical Sciences
Cancer Biology
2016

Abstract

The role of LKB1 in regulating actin and cellular polarization during motility

By Scott Christopher Wilkinson

Lung cancer is the leading cause of cancer related deaths in the United States, with an estimated 158,080 deaths in 2016. Importantly, 90% of all cancer related deaths are due to metastasis, highlighting the importance of understanding the biological basis of cancer cell invasion and metastasis.

LKB1 is the 3rd most-commonly mutated gene in lung adenocarcinoma, with the majority of mutations being truncations disrupting kinase activity and removing its C-terminal domain (CTD). Since LKB1 inactivation drives cancer metastasis in mice, we examined how LKB1 inactivation impacts cytoskeletal structure, single cell motility, and cell polarization during invasion. Cells re-expressing wildtype LKB1 colocalize strongly with actin in a farnesylation-dependent but kinase-independent manner. These cells also exhibit actin stress fiber assembly, which we show is through RhoA-ROCK signaling. Further, LKB1 kinase activity regulates cell membrane ruffling, through the regulation of FAK activity. A combination of the LKB1 farnesylation and kinase activity coordinate to spatially regulate focal adhesion deposition and size during cell motility.

While examining 3D invasion, we show that cells re-expressing wildtype LKB1 or CTD alone exhibited mesenchymal polarity with strong directional persistence, which is completely abrogated upon farnesylation loss. Since the CTD is kinase-dead, these data highlight a farnesylation-dependent but kinase-independent regulation of polarity and directionality during invasion. We then examined how farnesylation regulates cellular polarity, and show rescuing RhoA activity in farnesylation-compromised cells restores this polarized phenotype. Importantly, activating RhoA in the absence of LKB1 fails to restore mesenchymal polarity, indicating a region of LKB1 is necessary for the regulation of polarity. Inverse of polarity, LKB1 signals to MARK1 in a farnesylation-independent but kinase-dependent manner to repress FAK, which represses collagen remodeling during 3D invasion. Since LKB1 frequently undergoes truncations affecting farnesylation and kinase activity, cancer cells with LKB1-loss would lose regulation of the actin cytoskeleton, exhibit unique amoeboid morphologies with hyperactive FAK, and acquire the ability to remodel collagen. Together, these data suggest that a combination of kinase-dependent and -independent defects create a uniquely invasive cell upon LKB1 inactivation.

The role of LKB1 in regulating actin and cellular polarization during motility

By

Scott Christopher Wilkinson
B.S., Berry College, 2009

Advisor: Adam I Marcus, Ph.D.

A dissertation submitted to the Faculty of the
James T. Laney School of Graduate Studies of Emory University
in partial fulfillment of the requirements for the degree of
Doctor of Philosophy
in Graduate Division of Biological and Biomedical Sciences
Cancer Biology
2016

Acknowledgements

I am deeply indebted to many individuals who have provided me with support throughout my time at Emory. First, thank you to the entire Marcus lab for all of your support over the years. Ranging from experimental advice to lending a friendly ear at times of stress, I cannot stress enough my gratitude for your friendship and help over the past five years. Jessica, Ale, Emily, Rachel, Junghui, Yue, Lauren, Brian, Melissa, Erik, Carrie… Thank you all for all your help and friendship over the past 5 years. And to Adam… thank you for all your individual support. Ranging from encouraging me to keep fighting in the very beginning, to supporting me as I conducted my search for my next position, you've been there for me every step of the way and have been someone I can comfortably call both an advisor and a friend.

To other members of the Emory community, to my classmates and colleagues, to the people who I see almost every day of the week as we continue our journey: Thank you for being there with me and encouraging me forward. To the one who helped me every step of the way and was always there for me: thank you for keeping me alive and kicking. To the Integrated Cellular Imaging core and Debby, Neil, Songli, and Alexa, thank you for your assistance with the microscopes and learning how to actually take an image without breaking anything. To my collaborators: Wei, LaTonia, Haian, Minion, Fadlo, Lee, Byoungkoo, Ji, Fakeng, Rui, Xiuju, Kaisheng, Rachel, Tanisha, Tiffany, Tongrui, Ruth, and the countless others: Thank you for the opportunity, the assistance, and the consideration you provided as I've completed this journey.

To members of the Cancer Biology program and GDBBS, thank you for being there with me and working with us as we learn the ins and outs of becoming a new program. To Cytoskeleton, Inc.: Nope. Not at all. To my thesis committee, thank you for your helpful advice and encouragement over the past several years.

Finally, to my family and especially my parents Jean and Hal Wilkinson: Thank you for your constant encouragement. I know it's been a long and tough 5 years, and I value your support more than I could ever begin to express. Thank you for helping me push through this and understanding as things got difficult. Your support and encouragement are second to none, and I could not have asked for anything better.

Table of Contents

List of Figures

List of Abbreviations

In Order of Appearance

EMT: Epithelial-to-Mesenchymal Transition

VEGF: Vascular Endothelial Growth Factor

MMP: Matrix Metalloproteinase

TP53: Tumor Protein 53

KRAS: V-Ki-ras2 Kirsten rat sarcoma viral oncogene homolog

KEAP1: Kelch-like ECH-associated protein 1

STK11: Serine/Threonine Kinase 11

Rho-GTPases: Ras superfamily of small guanosine triphosphatases

kDa: Kilodalton

GTP: Guanosine Triphosphate

GDP: Guanosine Diphosphate

PI3K: phosphoinositide 3-kinase

PDGF: Platelet-Derived Growth Factor

EGF: Endothelial Growth Factor

N-WASp: neuronal Wiskott–Aldrich Syndrome protein

Arp2/3: Actin-related proteins 2/3

ECM: Extracellular Matrix

NA: Nascent Adhesion

FAK: Focal Adhesion Kinase

MLCK: Myosin Light Chain Kinase

MLC: Myosin Light Chain

ROCK: Rho-associated protein kinase

LKB1: Liver Kinase B1

NTD: N-terminal domain

CTD: C-terminal domain

NLS: Nuclear Localization Signal

NES: Nuclear Export Signal

STRADα: STE20-Related Kinase Adaptor alpha

CRM1: Chromosomal Maintenance 1

ATM: Ataxia telangiectasia mutated

PKA: Protein Kinase A

PJS Peutz-Jeghers Syndrome

NSCLC: Non-Small Cell Lung Cancer

AMPK: 5' AMP-activated protein kinase

MARK: Microtubule Affinity Regulating Kinase

SIK: Salt-Inducible Kinase

BRSK: Brain-Specific Kinase

SNRK: Sucrose Non-Fermenting Related Kinase

GEMM: Genetically Engineered Mouse Model

AP: Anterior-Posterior

MYPT: Myosin Phosphatase Targeting Protein

ATCC: American Type Culture Collection

DMEM: Dulbecco’s Minimum Essential Medium

GFP: Green Fluorescent Protein

ROI: Region of Interest

WT: Wildtype

C:N: Cytoplasmic:Nuclear

CADE: Cellular Analysis of Dynamic Events

siRNA: Small Interfering RNA

RPMI: Roswell Park Memorial Institute

GAPDH: Glyceraldehyde 3-phosphate dehydrogenase

BCA: Bicinchoninic Acid Assay

HRP: Horseradish Peroxidae

RBD: Rho Binding Domain

PAK: p21 Activated Kinase

PBD: PAK Binding Domain

SDS: Sodium Dodecyl Sulfate

PAGE: Polyacrylamide Gel Electrophoresis

PVDF: Polyvinylidene Fluoride

PBS: Phosphate-Buffered Saline

CCD: Charge-Coupled Device

NIH: National Institutes of Health

CT-FIRE: Curvelet Transform Fiber Extraction

DMSO: Dimethyl Sulfoxide

LOX: Lysyl Oxidase

mTOR: Mammalian Target of Rapamycin

HIF1α: Hypoxia-Inducible Factor 1α

Chapter 1: Introduction

1.1 Lung Cancer

Cancer deaths are the second leading cause of death in the United States, with an estimated 595,690 deaths due to cancer in 2016[1]. An estimated 224,390 new cases of lung cancer will be diagnosed in 2016, placing lung cancer as the second-most commonly diagnosed new cancer in both men and women, behind prostate and breast cancers, respectively[1]. Importantly, when examining deaths due to cancer, lung cancer remains the leading cause of cancer-related deaths, with an estimated 158,080 deaths in 2016[1]. The 5-year survival rate for lung cancer remains at a mere 17%, which is directly correlated with only 16% of lung cancers being diagnosed at a localized stage. Importantly, when examining survival rates for lung cancers diagnosed in early non-metastatic stages, the 5-year survival soars to 55%, highlighting the critical role of early detection in maintaining non-disseminated cancer and increasing survival. The reason for this strong disparity in survival based on lung cancer stage directly lies with deaths due to metastasis. An estimated 90% of cancer-related deaths are due to metastasis to distal organs rather than the primary lesion[2]. Taken together, the low 5-year survival rate due to metastatic lung cancer highlights the need to further examine lung cancer development, invasion, and metastasis to uncover novel treatment mechanisms to curtail this devastating disease.

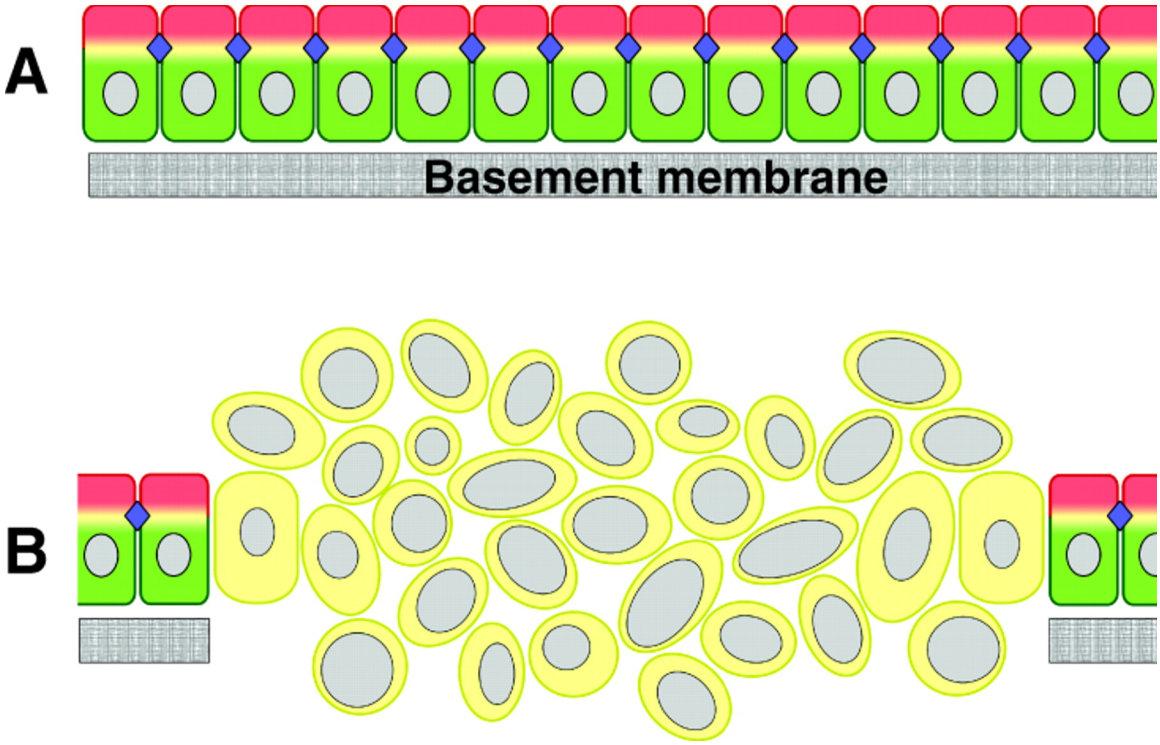

Figure 1.1: Cellular polarization switches between apical-basal and unidirectional polarity. (A) Normal epithelial cells exhibit an apical-basal polarity with distinct apical surfaces and basal regions at the basement membrane. (B) Unidirectional polarity occurs to promote cell motility, and results in a loss of normal apical and basal regions and acquisition of a unidirectional polarization towards a stimulus.

Image adapted from [3]

1.1.1 Lung Cancer Invasion and Metastasis

Lung cancer development begins with localized invasion at the primary tumor site. When normal epithelial cells transform and disseminate into localized cancer, the cells undergo a series of genetic and epigenetic events to change their phenotype. Coined the Epithelial-to-Mesenchymal Transition (EMT), this process oversees a down-regulation of stationary epithelial programming with an up-regulation of mesenchymal programming to induce cellular changes[4-8]. Specifically, cells undergoing EMT will lose normal cell-cell contacts, reorient themselves, and begin to invade into surrounding tissue[8]. This localized dissemination of a primary tumor is the initial step that ultimately results in the metastatic cascade.

After localized invasion, cancer cells will begin the process of metastasis. For this to occur, a localized primary tumor must first induce angiogenesis to induce blood vessel development, typically through the secretion of VEGF. Cancer cells will then utilize matrix metalloproteinases (MMPs) to intravasate into the blood vessels[9-12]. Upon intravasation, the cancer cells will travel to secondary sites, with lung cancer cells typically metastasizing to the adrenal glands, bone, brain, and liver[1]. Cells will then use MMPs to extravasate from the blood vessel, where the cells will then set up a micrometastasis in the secondary location. Eventually, the micrometastasis will develop into a metastatic lesion, completing the process of localized cancer invasion and metastasis to secondary locations.

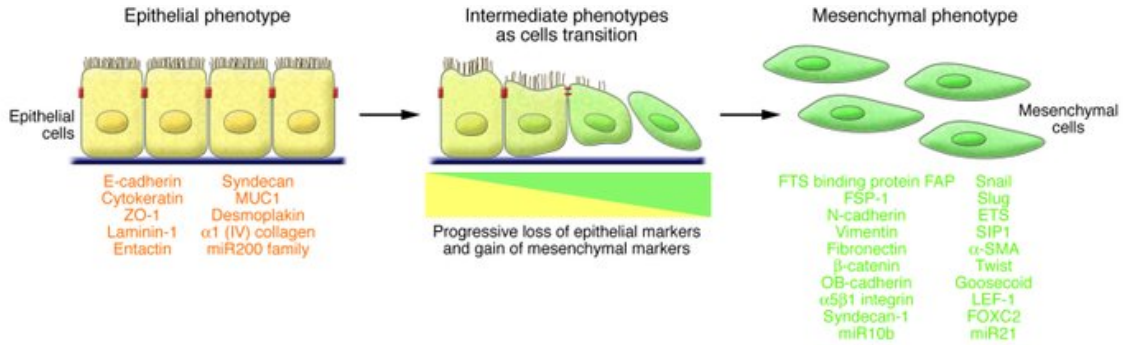

Figure 1.2: The Epithelial-to-Mesenchymal Transition (EMT) promotes mesenchymal cell motility. EMT occurs with a downregulation of epithelial proteins, including E-cadherin, Cytokeratin, and ZO-1. Conversely, mesenchymal proteins, including N-cadherin, vimentin, and the transcription factors Snail and Slug are upregulated to promote a mesenchymal motile cell.

Image adapted from [13].

1.1.2 Common Lung Cancer Mutations

The most common gene mutations in lung adenocarcinoma are TP53, KRAS, KEAP1, and STK11, mutated in 46%, 33%, 17%, and 17% of all lung adenocarcinomas, respectively[14, 15]. Importantly, the TP53 and STK11 tumor suppressors are frequently mutated in lung adenocarcinoma, although as of yet these inactivations cannot be targeted in the clinic. Rather than restoring the function of these tumor suppressors, research is currently focused on understanding and restoring downstream targets of these genes, as well as the interaction between different sets of mutated genes within the same cancer.

Lung adenocarcinomas with oncogenic KRAS mutations are frequently co-mutated with both TP53 and STK11. Of 154 tumors with KRAS mutations examined, 35 (22.73%) of the tumors exhibited co-mutation with STK11, while 31 (20.13%) of the tumors exhibited co-mutation with TP53. Importantly, only 4 (2.59%) tumors exhibited mutations for all KRAS, STK11, and TP53[16]. Together, these data appear to indicate that KRAS oncogenic mutations in lung adenocarcinomas are typically paired with either STK11 or TP53 tumor suppressor mutations, indicating that, while oncogenic mutations are frequently paired with tumor suppressive mutations, typically only one of these tumor suppressive mutations is required within lung adenocarcinoma.

1.2 Cellular Polarization in Lung Cancer

Cell polarization is essential to generate distinctive shapes that guide cellular function. This is perhaps best observed in stationary epithelial cells, which form an epithelial sheet to maintain normal tissue function. Within the epithelial sheet, normal cells maintain an apical-basal polarity with specific apical proteins aggregating at the apical surface, while

basolateral proteins are found in the basal region of the cell (Figure 1.1). This distinct apical-basal polarity is important for cell-cell contacts, cell signaling, and normal tissue physiology[17]. Upon induction of EMT, normal apical and basal regions are disrupted and cell-cell contacts are broken upon disruption of adherins junction proteins. Rather, these cells instead acquire a unidirectional polarity conducive for cell motility, acquiring a distinct leading edge that undergoes actin polymerization to form the lamellipodia during 2D motility and invadopodia during 3D invasion[18]. In all cases, cell polarity and motility are overseen by dynamic signaling networks that ultimately influence the phenotype of the cell[18-25].

1.2.1 Rho-GTPases and Polarity

The Rho family of GTPases are master regulators of cell polarity and motility[12]. In humans, the Rho family of GTPases is composed of 20 different members, 21-25 kDa in size, that share 40-95% homology with each other[26]. Most Rho-GTPases contain a C-terminal prenylation motif, allowing for post-translational addition of a hydrophobic geranylgeranyl or farnesyl group and subsequent insertion into the plasma membrane[12, 26, 27]. Rho-GTPases cycle between an active GTP-bound and inactive GDP-bound state through the addition of a phosphate group by a guanine nucleotide exchange factor (GEF)[22]. The most well-studied Rho-GTPases are cdc42, RhoA, and Rac1. Importantly, the coordination of both apical-basal and unidirectional cell motility relies on coordinated signaling amongst these three polarity proteins.

During unidirectional motility, cdc42 is activated by a GEF in response to a variety of different stimuli, including the phosphoinositide 3-kinase (PI3K) pathway and the binding of PDGF and EGF to their respective ligands at the leading edge[28-30]. Importantly, Vav2, a GEF for cdc42, also serves as a GEF for the Rho-GTPase Rac1 at the leading edge, leading to the hypothesis that a coordination of cdc42 and Rac1 activation at the leading edge promotes unidirectional polarization[30]. Upon activation, cdc42 induces centrosome and Golgi realignment in the direction of polarization, allowing for secretion of polarity proteins towards the cellular leading edge[17]. Additionally, active-cdc42 rapidly translocates to the cellular leading edge, where it signals to neuronal Wiskott-Aldrich Syndrome protein (N-WASp) to complex with Arp2/3 and promote actin polymerization and lamellipodia development[31, 32].

In motile cells, RhoA is typically thought to be active at the rear of the cell, where it signals to downstream proteins to induce actomyosin contractility to induce stress fiber formation and contractility, generating a force to propel the cell forward in the direction of polarization[20, 33]. Further, RhoA and its associated kinase ROCK (Rho-associated protein kinase) complex at the rear of the cell to phosphorylate Par3 and prevent formation of the Par polarity complex to spatially disrupt Rac1 activation at the rear of the cell[34], thus coordinating with leading edge Rac1 activation to define the cellular leading edge. Although the spatial localization of the canonical Rho-GTPases cdc42, Rac1, and RhoA is well understood, the upstream coordination of all three GTPases to drive cell polarization during normal motility remains an area of intense interest.

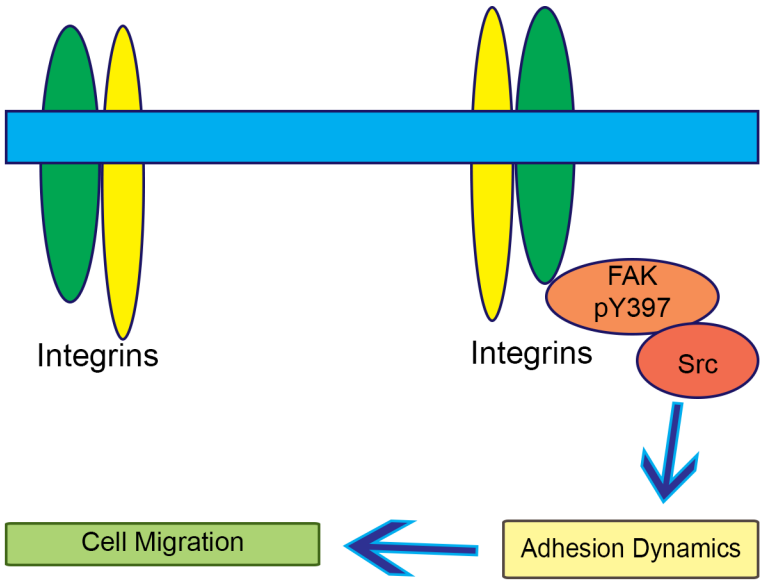

Figure 1.3: Focal Adhesion Kinase (FAK) drives cellular adhesion dynamics. Extracellular signals are transmitted to transmembrane integrin proteins. FAK forms a focal adhesion complex at these integrin sites to regulate adhesion dynamics and cell migration.

1.2.2 Epithelial-to-Mesenchymal Transition and Cancer

Stationary epithelial cells can lose their apical-basal polarity and become motile through the pro-invasive epithelial to mesenchymal transition (EMT)[10, 35]. EMT is triggered by genetic and epigenetic changes resulting in downregulation of normal epithelial proteins (Figure 1.2)[10, 35, 36]. Normal cell-cell contacts are disrupted upon downregulation of claudin, occludin, and E-cadherin at adherins junctions[4], while loss of the Crumbs complex disrupts a defined apical-basal polarity[37]. At the same time, mesenchymal proteins, including vimentin, N-cadherin, fibronectin, and transcription factors Snail and Slug, are upregulated to induce cellular changes[4]. These cells now acquire a mesenchymal phenotype with a unidirectional polarity through coordination of RhoA, cdc42, and Rac1 to drive cell motility. The upregulation of mesenchymal proteins, such as vimentin, Snail, and Slug, induces cell motility to promote directed migration[8]. EMT is critical for normal embryogenesis, being implicated in both gastrulation and formation of mesoderm and endoderm[4, 34]. EMT is also involved in other normal physiological processes, such as tissue regeneration and fibrosis in response to wound healing[5, 6, 38].

Cancer cells also undergo EMT to become more invasive and metastatic[7, 8, 39]. EMT has been implicated in many epithelial tumors, where the invasive front shows a mesenchymal expression pattern[40, 41]. EMT is well-correlated with invasive and more metastatic tumors, significantly decreasing clinical outcome and patient survival[42]. After undergoing EMT, cancer cells acquire aberrant polarity[19, 43-45]. This polarity is regulated by the small Rho-GTPases, and it is likely that the defects observed in cell polarity are due to defective Rho-GTPase signaling[44]. While aberrant cell polarity serves

as a prerequisite for cancer development, the Rho family of GTPases are infrequently mutated[46]. This raises the interesting possibility that there are other defects in the cell polarity pathway that can trigger aberrant cell motility and invasion.

1.3 Cell Motility During Invasion

Upon acquiring a unidirectional polarization to orient in a direction of motility, cells will next begin the complex process of motility to migrate in 2D and invade in 3D. Cell motility is a complex interplay of multiple cellular processes, coordinating cellular adhesion to the extracellular matrix (ECM) with a reorientation of cellular cytoskeletal proteins to drive motility. Upon induction of motility, broad lamellipodia in 2D cells and invadopodia in 3D cells form at the cellular leading edge[47]. These cellular protrusions occur at the leading edge of migrating cells to facilitate cellular adhesion and migration[47].

1.3.1 Focal Adhesions

The process of cell migration is dependent on the cell being able to interact with and adhere to its ECM. Within lamellipodia in 2D and invadopodia in 3D, nascent adhesion (NA) sites represent the early interaction of the cell with its ECM. Within these lamelli- and invadopodia, transmembrane integrin proteins interact with and bind to the ECM at the cellular leading edge, which activates the Rho-GTPase Rac1 to stimulate formation of a NA[48, 49]. These adhesion sites then rapidly recruit other proteins within the focal adhesion complex, including talin, paxillin, vinculin, and focal adhesion kinase (FAK) to further engage the ECM and form a mature focal adhesion site, which is seen throughout

the entire cell-ECM interaction (Figure 1.3)[50, 51]. These NA and focal adhesion sites together coordinate to drive directed cell migration.

Within these focal adhesion sites, FAK serves as a major regulate of focal adhesion assembly, persistence, and disassembly. Phosphorylation of FAK at Tyr-397 creates a docking site to allow Src to bind to FAK, resulting in Src activation[52]. Further, this FAK-Src complex can then contribute to the focal adhesion complex by inducing further FAK phosphorylation and recruiting other adhesion proteins to the site to promote intracellular signaling and migration[53]. At the rear of the cell, FAK^{Y397} is dephosphorylated to promote focal adhesion disassembly, promoting integrin disengagement and allowing the rear of the cell to travel forward[53]. Together, this dynamic process of FAK phosphorylation and dephosphorylation are critical for the formation, maturation, and disassembly of focal adhesion sites during cell motility.

1.3.2 Actin Dynamics During Motility

Within leading edge lamellipodia and invadopodia, actin polymerization occurs at the leading edge to facilitate migration or invasion[54]. At the leading edge, formin induces actin nucleation through binding of three actin monomers[55]. Actin monomers then continue to join the nascent filament to ultimately create actin filaments through retrograde actin polymerization. The actin-related protein 2/3 (Arp2/3) complex is also capable of attaching to pre-existing actin filaments and inducing further actin polymerization through actin branching, again occurring in a retrograde polymerization[55]. This retrograde flow

of actin polymerization at the leading edge combines with nascent and mature focal adhesion sites to extend lamelli/invadopodia and drive cell migration.

While actin polymerization is driving cell migration at the leading edge, actin stress fibers also facilitate migration through contracting the cell to promote directed migration. These stress fibers are composed of actin and myosin filaments and span the length of the cell, terminating in focal adhesions at the cell membrane[56, 57]. During cell motility, multiple pathways are capable of inducing stress fiber contraction. In one, the myosin light chain kinase (MLCK) phosphorylates myosin light chain (MLC) to induce actomyosin contractility along the stress fiber[58]. Alternatively, RhoA can activate Rho-kinase (ROCK), which then phosphorylates MLC to induce this stress fiber contractility[58]. Upon undergoing actomyosin contractility, stress fiber contraction contributes to cell migration by bringing the trailing edge of the cell forward while also working to stabilize leading edge focal adhesions[59]. Together, this combination of leading edge actin polymerization and actin stress fiber contractility coordinate to drive cell migration. Importantly, although actin dynamics drives cell migration and invasion, actin and actin-related proteins are infrequently mutated in cancer[14], again raising the intriguing question as to what is driving this cancer cell invasion.

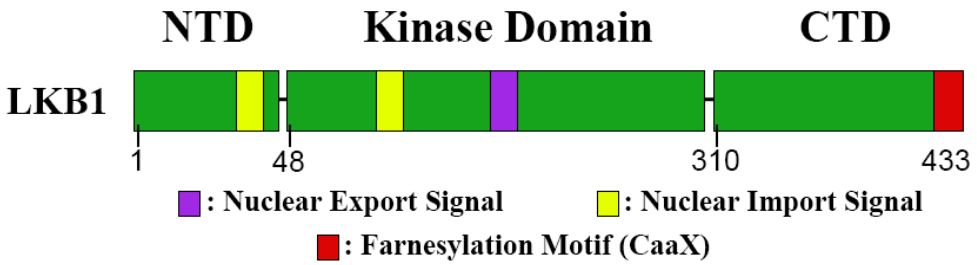

Figure 1.4 LKB1 functional domains. LKB1 consists of a short N-terminal domain (NTD), a central kinase domain, and an extensive C-terminal domain (CTD). Nuclear import signals are found in the NTD and kinase domain, while a Nuclear Export Signal is located within the kinase domain. The CTD contains a C-terminal farnesylation motif for membrane targeting.

1.4 LKB1 is a membrane-targeted tumor suppressor kinase

LKB1 (liver kinase B1, also known as STK11) is a tumor suppressor kinase that is evolutionarily conserved across multiple species[60]. In humans, LKB1 consists of a short N-terminal domain (NTD), a central kinase domain, and an extensive C-terminal domain (CTD) with C-terminal membrane-targeting farnesylation motif (Figure 1.4)[60]. LKB1 is found primarily in its farnesylated form *in vivo*[61]. LKB1 contains two nuclear localization signals (NLS): one in the NTD and one in the kinase domain. In addition, LKB1 contains one nuclear export signal (NES) in the kinase domain[62]. In its inactive state, the two LKB1 NLS motifs promote its interaction with importin α/β to import it into the nucleus[63, 64]. However, upon LKB1 activation, the LKB1 binding partner STRADα induces a conformational shift to expose the LKB1 NES, which is recognized by the exportins CRM1 and exportin7 drive nuclear export[63, 65, 66]. LKB1 and STRADα complex with the scaffolding protein MO25, with the catalytic activity of LKB1 ten times greater in the LKB1-STRADα-MO25 complex than alone[67-69].

Phosphorylation residues have been found throughout the LKB1 gene, although the significance of these residues is less well understood. LKB1 can be autophosphorylated at T189, T189, T336, and S404, although this phosphorylation is not required for LKB1 kinase activity[70]. Further, LKB1 contains multiple phosphorylation residues within the C-terminal domain, including S428, which is phosphorylated by ATM, PKA, and p90RSK[71-74]. Importantly, although the S428 residue is only two amino acids away from the LKB1 farnesylation motif (430-433), S428 phosphorylation does not impact LKB1 farnesylation, nor does farnesylation impact the phosphorylation[75]. Although

LKB1 contains multiple phosphorylation residues and a farnesylation motif for membrane targeting, the functional significance of these motifs on the role of LKB1 in normal cellular functions remains a focus of intense study.

1.4.1 Identification of LKB1 Through Peutz-Jeghers Syndrome

The tumor suppressor Liver Kinase B1 (LKB1, also known as STK11) was first identified as the causative agent of the autosomal dominant Peutz-Jeghers syndrome (PJS)[76-81]. PJS patients exhibit hamartomatous gastrointestinal polyps, mucocutaneous pigmentation, and present an elevated risk of developing breast, cervical, testicular, gastric, and pancreatic cancers upon loss of heterozygosity[77-80, 82]. When examining mutations within PJS patients, scientists identified mutations throughout the LKB1 gene, with a majority of these mutations disrupting LKB1 kinase activity[83]. LKB1 deletion *in vivo* is embryonic lethal, highlighting the role of LKB1 in development and necessitating other methods for examining LKB1 status[84]. Given that LKB1 loss is embryonic lethal, *in vivo* studies initially used heterozygous lkb1 alleles, and showed that these mice also exhibit hamartomatous gastric polyps with approximately half the LKB1 expression of normal tissue in these cells, thus phenocopying PJS, and demonstrating that LKB1 loss promotes tumor development and highlighting a role of LKB1 as a tumor suppressor gene[84-86].

In addition to serving as the causative agent for PJS, LKB1 is the third-most commonly mutated gene in non-small cell lung carcinoma (NSCLC) tumors, behind p53 and Ras[14]. Inactivating mutations are seen in approximately ⅓ of all NSCLC patients[72, 87]. Importantly, LKB1 mutations are found throughout the entire gene, with a majority of

mutations (75%) occurring as truncating mutations that would predictably disrupt LKB1 farnesylation and potentially interfere with LKB1 kinase activity[15]. When examining kinase activity, LKB1 was first identified as the upstream kinase for AMPK in the energy sensing pathway[88, 89], and has since been identified as the upstream kinase for the 14 members of the AMPK family (AMPK 1/2, MARK1-4, NUAK1/2, SIK1-3, BRSK1/2, and SNRK) (Figure 1.5)[90-97]. Using a $Kras^{G12D}$-driven genetically engineered mouse model (GEMM), LKB1 loss results in increased tumor burden shortened survival time, and increased metastasis compared to $Kras^{G12D}$ control mice[87].

1.4.2 LKB1 Regulates Cell Polarity

LKB1 orthologs have previously been shown as critical for driving cell polarity across multiple species. In *C. elegans*, the LKB1 ortholog, PAR-4, was shown to drive embryonic asymmetry[98, 99]. *C. elegans* embryos with PAR-4 mutations show a smaller and more-rounded oocyte compared to wildtype, which is believed to be due to PAR-4 regulating the distribution of PAR36 and PAR6 throughout the zygote[99]. In *D. melanogaster*, *lkb1* drives epithelial polarization and the formation of the anterior-posterior (A-P) axis during embryogenesis[100, 101]. *Lkb1*-mutant oocytes exhibit mislocalized *Staufen* and *oskar* mRNA, while over-expressing GFP-*lkb1* in the same oocytes restores this A-P axis[100]. Together, these data indicate LKB1 is an evolutionarily-conserved master regulator of cell polarity.

In humans, LKB1 tumor suppressive function also regulates both epithelial and unidirectional cell polarity. A seminal report examining LKB1 function showed LKB1 was able to guide epithelial polarization when re-expressed in LKB1-null single epithelial cells

with no cell-cell junctions[60, 67, 68, 102, 103]. Upon re-expression, these cells show establishment of apical and basolateral surfaces, as well as formation of acinar actin caps[103]. When examining this further, it was identified that LKB1 drives this polarity through activation of p114RhoGEF to activate RhoA (Figure 1.6), resulting in maintenance of apical junctions in normal epithelial cells[104]. Further, this LKB1-RhoA interaction also results in activation of the RhoA-ROCK pathway to phosphorylate myosin light chain and promote stress fiber assembly [58, 105-109]. This LKB1-RhoA interaction thus coordinates to activate RhoA and drive actin rearrangement during cell polarity.

LKB1 loss in epithelial cells has been shown to disrupt both apical-basal polarity and basement membrane integrity, resulting in mixing of apical and basolateral junctions throughout the membrane, as well as promoting EMT to drive mesenchymal cell migration[101, 110, 111]. When examining planar polarity, upon activation LKB1 rapidly translocates to the cellular leading edge. At the leading edge, LKB1 then recruits active cdc42 and associates with both leading edge actin and cdc42[112]. After this association, the LKB1-actin-cdc42 complex induces Golgi reorientation to drive polarization, which is lost upon LKB1 knockdown[112]. When inactive, LKB1 is unable to regulate cell polarity and motility, resulting in aberrant polarity and ultimately invasion into surrounding tissue[87, 113]. Together, these data highlight a role of LKB1 in promoting and maintaining a normal apical-basal polarization in epithelial cell structures, while driving Golgi reorientation and polarization during mesenchymal motility.

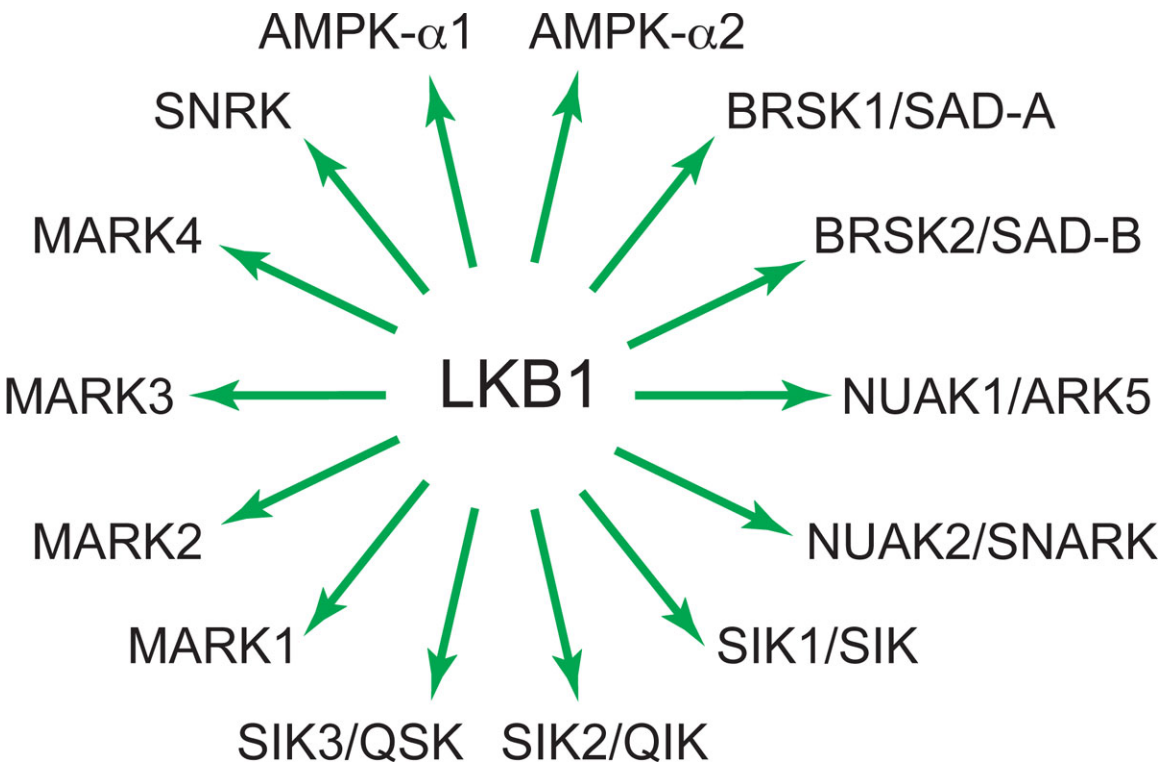

Figure 1.5 LKB1 phosphorylates 14 members of the AMPK family. LKB1 was first identified as the upstream kinase of AMPK. It has since been shown to phosphorylate the 14 members of the AMPK family: AMPK1/2, BRSK1/2, NUAK1/2, SIK1-3, MARK1-4, and SNRK.

Image adapted from [114].

1.4.3 LKB1 Drives Adhesion Dynamics

LKB1 loss causes aberrant adhesion signaling. Depletion of LKB1 leads to FAK hyperactivation, highlighting a role of LKB1 as a FAK repressor[115]. Subcellular localization studies highlighted LKB1 as a selective FAK repressor, whereby LKB1 and FAK^{Y397} are spatially exclusive of each other at the cellular leading edge[115]. LKB1 also phosphorylates the downstream targets MARK1/4, which then phosphorylate the scaffolding protein DIXDC1 to repress FAK activity and stabilize focal adhesions (Figure 1.6)[116]. Although LKB1 serves as a selective FAK repressor, it also drives elongated focal adhesion formation with adhesion sites terminating at newly-formed stress fibers[105]. Further, upon LKB1 depletion focal adhesions exhibit rapid turnover resulting in increased migration with limited directional persistence[115]. *In vivo* models examining FAK status also highlight the role of LKB1 as a FAK repressor, with LKB1-deficient tumors exhibiting hyperactive FAK and activated Src compared to control, with the tumors exhibiting abnormal focal adhesions[117]. This hyperactivation of FAK and Src directly correlates with more invasive and migratory tumors[117]. These data highlight a role of LKB1 in both spatially regulating FAK activity and promoting elongated focal adhesion formation throughout the cell-ECM interaction.

NUAK1/2, a target of LKB1 kinase activity, also drives adhesion by phosphorylating myosin phosphatase targeting-1 (MYPT1) at Ser^{445}, Ser^{472}, and Ser^{910}[96, 97, 118]. This MYPT phosphorylation promotes its association with 14-3-3 and enhancing MLC phosphorylation. Importantly, cellular adhesion is directly impacted through this LKB1-NUAK1/2 pathway, whereby LKB1 or NUAK1/2 loss impairs cell detachment[97].

Together, these data indicate LKB1 regulates cellular adhesion through its phosphorylation of members of the AMPK family and downstream MLC activity to regulate adhesion, while also serving as a selective FAK repressor in motile cells. Given the importance of adhesion in tumor cells, LKB1 loss could thus have enormous implications in increasing adhesion and migration during invasion.

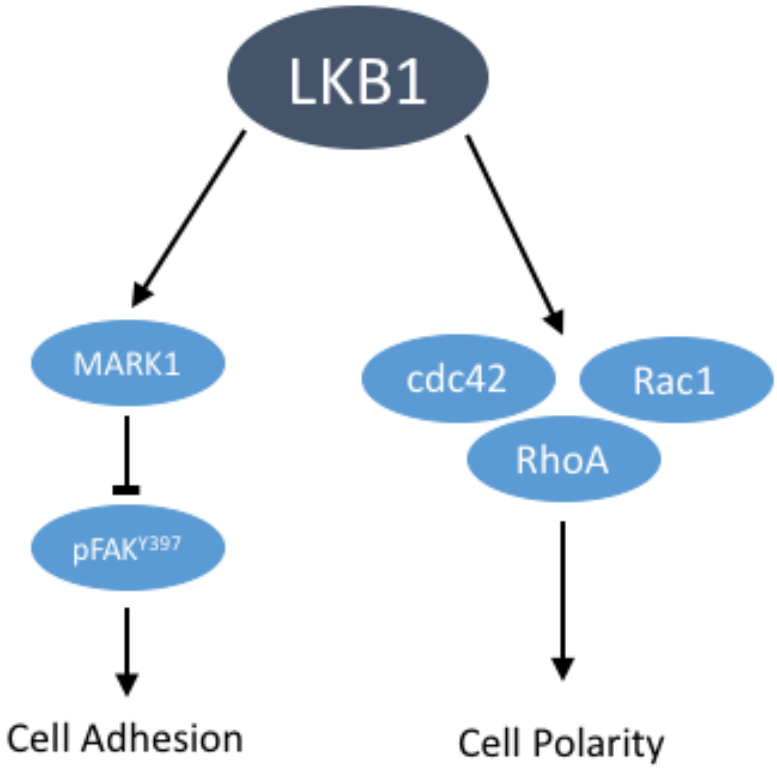

Figure 1.6 LKB1 regulates cell adhesion and cell polarity. LKB1 phosphorylates the AMPK family member MARK1, which results in pFAK repression and regulates cell adhesion. Conversely, LKB1 activates the Rho-GTPases cdc42, Rac1, and RhoA to regulate cell polarity during motility.

1.5 Identifying LKB1-mediated Cancer Cell Polarization and Invasion

LKB1 has been identified as a critical tumor suppressor kinase that is frequently lost in lung adenocarcinoma patients. While LKB1 phosphorylation has remained a focus over the past decade, very little is understood about kinase-independent roles of LKB1 in regulating cellular function[71, 75, 119]. Given that LKB1 is implicated in cell polarity through signaling to RhoA and cdc42, cell-ECM interaction through its regulation of FAK activity, and actin dynamics during motility through its signaling to RhoA (Figure 1.6), the impacts of LKB1 loss in lung adenocarcinoma patients presents dire circumstances with the potential for multiple avenues of loss of normal cell function. Thus, an important goal of current research focuses on further understanding how a combination of LKB1 kinase activity and its localization due to farnesylation drive its tumor suppressive activities. The Marcus lab focuses on these aspects to further address this gap in the knowledge of lung cancer.

The Marcus lab has previously shown that LKB1 associates with leading edge actin during cell migration[112], although the functional significance of this association remained largely unknown. Chapter 2 presents data in which we further evaluate the significance of this association. We show that LKB1 associates with leading edge actin and signals through the RhoA-ROCK pathway to drive stress fiber assembly in a farnesylation-dependent manner, while LKB1 kinase activity regulates membrane dynamics during motility. Further, we show that a combination of LKB1 farnesylation and its kinase activity drive cellular adhesion dynamics and ultimately regulate cell migration.

In addition, the Marcus lab has invested significant resources into examining the role of LKB1 in regulating cellular polarization and 3D invasion. In Chapter 3, we present data highlighting a role of LKB1 farnesylation in activating RhoA to drive mesenchymal cell polarization and directional persistence during invasion. Further, we report that LKB1 kinase activity is critical for signaling to MARK1 to repress FAK activity, and that this kinase activity also drives collagen remodeling during 3D invasion. Together, cancer cells exhibiting LKB1 loss would result in a uniquely invasive cell with aberrant amoeboid polarity, as well as aberrant adhesion signaling to drive invasion into the microenvironment.

Chapter 2: Coordinated cell motility is regulated by a combination of LKB1 farnesylation and kinase activity

2.1 Author's Contribution and Acknowledgement of Reproduction

This chapter is reproduced with minor edits from S Wilkinson, Y Hou, JT Zoine, J Saltz, LAD Cooper, and AI Marcus. *Coordinated cell motility is regulated by a combination of LKB1 farnesylation and kinase activity*. In Revision to Scientific Reports, 2016.

SW, YH, and JTZ performed the experiments. SW and AIM conceived the initial idea for this study. YH performed CADE analysis. LADC, JS, and AIM contributed to experimental design and analysis. SW and AIM wrote the manuscript with feedback from all authors.

2.2 Abstract

Cell motility requires the precise coordination of cell polarization, lamellipodia formation, adhesion, and force generation. LKB1 is a multi-functional serine/threonine kinase that associates with actin at the cellular leading edge of motile cells and suppresses FAK. We sought to understand how LKB1 coordinates these multiple events by systematically dissecting LKB1 protein domain function in combination with live cell imaging and computational approaches. We show that LKB1-actin colocalization is dependent upon LKB1 farnesylation leading to RhoA-ROCK-mediated stress fiber formation, but membrane dynamics is reliant on LKB1 kinase activity. We propose that LKB1 kinase activity controls membrane dynamics through FAK since loss of LKB1 kinase activity results in morphologically defective nascent adhesion sites. In contrast, defective farnesylation mislocalizes nascent adhesion sites, suggesting that LKB1 farnesylation serves as a targeting mechanism for properly localizing adhesion sites during cell motility. Together, we propose a model where coordination of LKB1 farnesylation and kinase activity serve as a multi-step mechanism to coordinate cell motility during migration.

2.3 Introduction

LKB1 (liver kinase B1; also known as STK11) is a multifunctional, serine/threonine kinase that serves as the upstream activator of 14 members of the AMPK (5' AMP-activated protein kinase) family to regulate energy sensing[88, 89], cell motility[17, 120], polarity[121-123], adhesion[115, 116, 121, 124], and axon differentiation[90, 93]. In lung adenocarcinoma, LKB1 is the 2nd most-commonly mutated tumor suppressor where the majority of mutations (~72%) are inactivating truncation mutations found within its kinase domain[14, 15, 72, 125, 126]. Although LKB1 loss is correlated with increased tumor burden and metastasis in a murine model[87], how LKB1 inactivation impacts its function remains poorly understood.

LKB1 has three major protein domains: the kinase, N-terminal (NTD), and C-terminal (CTD) domains. The LKB1 kinase domain is responsible for phosphorylating and activating the AMPK family, while the LKB1 CTD contains multiple phosphorylation residues and a C-terminal farnesylation motif for post-translational membrane targeting[60, 61]. LKB1 phosphorylation at residue S431 in murine models (90% homology to human, 436 amino acids vs 433 amino acids in human[71]) does not affect its farnesylation, suggesting that farnesylation is functionally distinct from phosphorylation[75]. Although LKB1 kinase activity is not impacted by farnesylation[75], *in vivo* studies suggest farnesylation promotes membrane localization to activate myristoylated AMPK, highlighting the role of post-translational farnesylation in localizing LKB1 kinase activity[61].

Several studies have implicated LKB1 as a major regulator of cell polarity and downstream motility. Restoring LKB1 activity in single epithelial cells induces cellular polarization with an acinar actin cap even in the absence of cell:cell contacts[103]. Cell biological studies show that upon activation in lung cancer cells, LKB1 rapidly translocates to the cellular leading edge, where it associates with actin in lamellipodia[112]. LKB1 promotes stress fiber assembly in contractile cells to help drive actin dynamics during cell motility[105]. These events are likely through small Rho-GTPases[104, 112], where LKB1 signals to RhoA to drive mesenchymal polarization during 3D invasion in a farnesylation-dependent but kinase-independent manner[121]. Although LKB1 colocalizes with actin at the leading edge and regulates Rho-GTPase activity to drive polarity, the functional significance of these events in the context of cell motility remains largely unstudied.

Recent *in vivo* and *in vitro* experiments show LKB1 loss also leads to adhesion defects, specifically FAK hyperphosphorylation[87, 115-117, 121, 124]. LKB1 depletion results in individual FAK sites that fail to mature properly[115, 116] and is overseen through an LKB1-MARK1/4-FAK pathway[116]. Further, recent studies highlight the role of FAK in promoting lamellipodia protrusion through nascent adhesion (NA) assembly[127]. Together, these highlight the major question of how LKB1 coordinates its actin-based function described above with its role in cell adhesion during motility; therefore, the goal of these studies was to examine how the different LKB1 protein domains impact the interplay between its role on actin and focal adhesion function during cell motility. Our data support a model whereby LKB1 farnesylation, independent of its kinase activity, promotes its cytoplasmic actin co-localization and retrograde actin flow through a RhoA-

Rho-associated protein kinase (ROCK) pathway to induce actin stress fiber assembly. In contrast, LKB1 kinase activity regulates membrane dynamics and represses membrane ruffling. When we examine LKB1 within nascent lamellipodia, we show that LKB1 farnesylation localizes LKB1 to the membrane, where LKB1 kinase activity then regulates NA formation and deposition. Together, we propose a model where coordination of LKB1 farnesylation and kinase activity serve as a multi-step mechanism to coordinate cell motility during migration.

2.4 Methods

Cell culture and generating stable cells:

HeLa cells (ATCC, Manassas, VA) were cultured in Dulbecco's Modified Eagle Medium (DMEM) media supplemented with 10% fetal bovine serum and 100 units/mL of penicillin/streptomycin, and maintained at 37°C and 5% CO_2.

To generate HeLa cells stably expressing GFP-tagged LKB1 and constitutively active RhoA or cdc42, wildtype LKB1 and the various LKB1 domains and mutations were cloned into a pEGFP-C1 vector. Empty GFP or the GFP-LKB1 constructs were then subcloned from the pEGFP-C1 vector into a pBabe-puro vector. Constitutively active RhoA (Q63L) and cdc42 (Q61L) were subcloned from a pCDNA3 vector into pBabe-Hygro. The pBabe constructs were then transfected into Phoenix-ampho cells with Lipofectamine 2000 and PLUS reagent (Invitrogen, Grand Island, NY). Cells expressing only empty GFP or GFP-LKB1 were selected with 1 μg/ml puromycin, while cells co-expressing the constitutively active RhoA or cdc42 mutants were selected with 1 μg/ml puromycin and 300 μg/ml hygromycin (EMD Millipore, Billerica, MA). Proper expression of GFP-LKB1 was verified using IF and Western blot to confirm phenotype and molecular weight. Expression of constitutively active RhoA and cdc42 was confirmed using a Rho-GTPase activity assay comparing the constitutively active mutants to their isogenic partner lines.

Transfection and Microscopy:

Live-Cell Imaging:

For colocalization and membrane analysis experiments, HeLa cells (LKB1-null) were co-transfected with either pEGFP-C1 control or wildtype LKB1 and its various constructs (Figure 2.1A), Flag-STRADα, and LifeAct-mRuby (Ibidi, Madison, WI) to visualize f-actin filaments using Lipofectamine 2000 (Invitrogen), per manufacturer's protocol. For paxillin experiments, cells were co-transfected with either pEGFP-C1 control or pEGFP-C1 LKB1 and various constructs, Flag-STRADα, and pmRuby-Paxillin-22. mRuby-Paxillin-22 was a gift from Michael Davidson (Addgene plasmid # 55877). 24 hours later, cells were imaged using a Perkin Elmer Ultraview spinning disk confocal microscope at 63x (1.40 NA) mounted onto a Zeiss Axiovert encased at 37^{o}C with 5% CO_2. For colocalization and membrane analysis experiments, fluorescent images were acquired using a 488 and 568 nm laser line every 5 seconds for up to 5 minutes using a Hamamatsu Orca Flash 4.0 v2 CMOS camera with exposure times ranging from 250-1000 ms. For paxillin experiments, fluorescent images were acquired using a 488 and 568 nm laser line every 30 seconds for up to 30 minutes using a Hamamatsu Orca Flash 4.0 v2 CMOS camera with exposure times ranging from 250-1000 ms. For scratch wound assays, HeLa cells stably expressing our panel of GFP-LKB1 constructs were plated on a fibronectin-coated plate (40 ug/ml). 24 hours later, a confluent monolayer was scratched using a p10 tip and washed 3 times with PBS. Complete media was replaced, and cells were imaged using a Perkin Elmer Ultraview spinning disk confocal microscope at 10x (0.3 NA) mounted onto a Zeiss Axiovert encased at 37^{o}C with 5% CO_2, with images acquired every 8 minutes for 21 hours.

Fixed Tissue Microscopy:

HeLa cells (LKB1-null) were co-transfected with either pEGFP-C1 control or our panel of LKB1 constructs and Flag-STRADα using Lipofectamine 2000 (Invitrogen), per manufacturer's protocol. 24 hours later, cells were fixed using Phemo buffer with a final concentration of: 3.7% paraformaldehyde (Electron Microscopy Sciences, Hatfield, PA), 0.05% glutaraldehyde (MP Biomedicals, Santa Ana, CA), and 0.5% Triton-X (Promega, Madison, WI) for 10 minutes at room temperature. Fixed cells were rinsed with PBS and stained with Alexa Fluor® 555 Phalloidin (1:200 in PBS) for 1 hour, rinsed three times with PBS, and stained with 350 nM DAPI for 10 minutes followed by three more PBS washes. Coverslips were then mounted with ProLong® Diamond Antifade Mountant. Fixed cells were imaged using a Leica SP8 inverted confocal microscope at 63x (HP PL APO 1.40 NA oil) using a 488 and 514 nm argon laser.

Drug Treatments:

ROCK Inhibitor

Cells were plated and transfected as previously described. 1 hour prior to fixation, the ROCK inhibitor Y-27632 (Millipore) was added at 10 μM to fresh complete DMEM. After 1 hour, cells were fixed as described.

FAK Inhibitor

Cells were plated and transfected as previously described. 8 hours after transfection, media was replaced with complete DMEM containing 1 μM FAK inhibitor PF-562271 (Pfizer)

and incubated overnight. The next day, media was replaced with fresh DMEM with 1 μM PF-562271, and 1 hour later cells were imaged as described.

Image Analysis:

Stress Fiber Quantification

Images were analyzed using ImageJ/Fiji (NIH, Bethesda, MD) image analysis software. Stress fiber formation was quantified through manual counting of cells containing lateral stress fibers. Each HeLa GFP-LKB1 cell line was compared with the respective empty GFP control lines and also to its farnesylation mutant partner (WT vs. C430S, K78I vs. K78I-C430S, CTD vs. CTD-C430S) using Fisher's exact test with a p value of 0.05. ****$p \leq 0.0001$.

Colocalization and Membrane Dynamics

In order to study dynamic protein colocalization and the relationships between membrane dynamics and colocalization we developed several enhancements to Machacek and Danuser's CellEdgeTracker algorithm[128, 129]. CellEdgeTracker software provides boundary tracking and discretization. We used CellEdgeTracker as a platform to develop Cellular Analysis of Dynamic Events (CADE) which uses tracked discretized boundaries to measure protein colocalization dynamics and associations between colocalization membrane motion dynamics. Time-lapse fluorescent images were first segmented using 3D graph cuts algorithm developed by [130] and analyzed with CellEdgeTracker to obtain membrane positions $(x(t), y(t), t)$. The boundary was then divided into a sequence of sectors approximately 10 μm in length. The velocity V of each sector is calculated by equation (1),

where is the displacement vector and is the normal vector for sector *i*. Normalized *V* is plotted in a heat map as a function of time (x-axis) and the position around the cell edge (left y-axis). Heatmap color is used to encode boundary velocity with red, blue and green denoting protrusion (*V*=1), retraction (*V*=−1) and quiescence (*V*=0) of the cell edge velocity respectively.

$$V = \frac{\sum_{i=1}^{N} \vec{d_i} * \vec{n_i}}{N\Delta t} \quad (1)$$

Based on the cell membrane algorithm, we develop our colocalization algorithm to quantify the spatiotemporal colocalization of two proteins. We first erode the binary cell mask to obtain a 2 μm * 10 μm band at the cell edge, and then partition this band into *N* contiguous regions where protein expression *G, R* and colocalization signals between green and red channels c*oloc(G,R)* can be quantified as in equations (2)-(4), where and denote the average background signals from green and red channels, respectively. μ_G and μ_R are the mean value of green and red signals. *Cov* and *Var* are the covariance and the variance of the mean subtracted green and red signals, respectively. The normalized colocalization is finally plotted as a heat map both in time and spatial domain. Red indicates high colocalization (*coloc*=1) and blue indicates low colocalization (*coloc*=0).

$$G = G(x, y, t) - \overline{\underline{BG}}_{G,t} \quad (2)$$

$$R = R(x, y, t) - \overline{\underline{BG}}_{R,t} \quad (3)$$

$$coloc(G, R) = \frac{Cov(G-\mu_G, R-\mu_R)}{\sqrt{Var(G-\mu_G)}\sqrt{Var(R-\mu_R)}} \quad (4)$$

To investigate the spatiotemporal relationship *C* between membrane dynamics and protein colocalization, we calculated the dot product between *V* and *coloc* using equation (5), where *N* and *t* are the number of rows and columns in velocity heat maps. *C* is also normalized according to the maximum and minimum *C* values among all cells. Similarly as velocity and colocalization heat maps, normalized *C* is plotted into heat maps. Red indicates highly coupled protrusion and high colocalization (*C*=1); Orange indicates highly coupled protrusion and low colocalization (*C*=0.5); Green indicates coupling between quiescence and low colocalization (*C*=0); Cyan indicates coupling between retraction and low colocalization (*C*=−0.5) and blue indicates highly coupled retraction and high colocalization (*C*=−1).

$$C_{N,t} = V_{N,t} \times coloc_{N,t} \quad (5)$$

Quantification of Membrane Dynamic Patterns

We developed a semi-automated graphical user interface to facilitate measuring protrusion/retraction regions on the membrane velocity heatmap. Several regions of interest (ROIs) were manually selected on the heatmap to represent the protrusion/retraction regions using CROIEditor algorithm written by Jonas Reber (http://www.mathworks.com/matlabcentral/fileexchange/31388-multi-roi-mask-editor-class/content/CROIEditor/CROIEditor.m). Then these ROIs were segmented into binary masks. Several morphology features for each ROI was calculated using regionprops function in Matlab. The features for each ROI are the number of ROIs, the area of the ROI, angle of the ROI from major axis to the x-axis, and the duration time, which is the length

in x-axis converted to time unit. Since there is no standard definition of a protrusion/retraction region, we asked multiple users to select the ROIs for the same heatmap, similar to [128, 129, 131, 132]. We then performed a one-way ANOVA test amongst all users to check reproducibility and found the p-value larger than 0.05, which indicated the selection among different users was similar. The ROIs of the multiple users was then averaged for statistical analysis. Colocalization duration and events/cell/minute was compared between empty GFP control and either LKB1 K78I or LKB1 CTD using the student's t-test with a p-value of 0.05. Membrane event duration, angle, and number of events/cell/minute was compared between empty GFP control and the panel of LKB1 constructs (Figure 2.1A), as well as each parental construct and their respective farnesylation mutant, using the student's t-test with a p-value of 0.05. **$p \leq 0.01$, ***$p \leq 0.001$, ****$p \leq 0.0001$.

Paxillin Adhesion

Volocity (PerkinElmer) image analysis software was used to quantify fluorescent paxillin sites. A ROI was drawn around a single lamellipodia and the image was cropped around the ROI. The images were then thresholded and the smoothing filter was used. Automatic detection of objects was employed and objects less than a volume of 0.1 μm^3 were excluded from the analysis. We manually identified the cell boundary for each image and used this for the analysis. Fluorescent site area, elongation, and distance from the membrane were then analyzed and recorded. The site area, elongation, and distance to membrane of each HeLa GFP-LKB1 cell line was compared with empty GFP control lines, and each LKB1

mutant was compared to LKB1 wildtype, using an unpaired t-test with a p value of 0.05. **p ≤ 0.01, ***p ≤ 0.001, ****p ≤ 0.0001.

Scratch wound analysis

Volocity (Perkin Elmer, Waltham, MA) image analysis software and manual tracking was used to quantify meandering index and percent area invaded. An ROI was manually drawn around the scratch wound at 0, 3, 6, 9, 12, 15, 18, and 21 hours, and the percent area closed was quantified over time. Meandering index (displacement/distance) and area closed was compared between empty GFP and the LKB1 constructs, as well as wildtype LKB1 and the various LKB1 constructs, using the 2-tailed Student's t-test with a p-value of 0.05. * ≤0.05; ** ≤0.01; *** ≤0.001; **** ≤0.0001.

Subcellular localization

Non-confluent cells were imaged and image analysis using Imaris Cell (Bitplane, South Windsor, CT) was performed using the cell tracking function. Cytoplasmic LKB1 was identified using phalloidin as a cytoplasmic marker, while nuclear LKB1 was identified using DAPI. Mean intensity of LKB1 was quantified in both the cytoplasmic and nuclear regions, and the cytoplasmic:nuclear ratio was determined for each cell. C:N ratio was compared between wildtype LKB1 and the various constructs, as well as the isogenic parental and farnesyl-mutant condition (WT vs C430S, K78I vs K78I-C430S, CTD vs CTD-C430S), using the 2-tailed Student's t-test with a p-value of 0.05. * ≤0.05; **** ≤0.0001.

2.5 Results

LKB1 farnesylation is required to promote actin stress fiber formation through RhoA signaling

To probe how different LKB1 domains impact actin stress fiber formation, we created a series of LKB1 mutants that modify LKB1 farnesylation and kinase activity. GFP-tagged: wildtype LKB1, a C430S mutation to disrupt farnesylation, a K78I kinase-dead mutation[81], the CTD alone (kinase dead as well), and the CTD with a C430S mutation (Figure 2.1A, [121]) were transiently re-expressed in HeLa (LKB1-null) cells. Empty GFP control cells exhibit a predominantly amoeboid phenotype with only 18.5% of cells exhibiting lateral stress fibers spanning the cell length (Figure 2.1B, C); however, upon re-expression of wildtype LKB1, cells revert to a mesenchymal morphology with 70.2% of cells exhibiting lateral stress fibers (Figure 2.1B, C). Preventing LKB1 farnesylation with a C430S mutation resulted in reduced stress fiber assembly compared to LKB1 wildtype cells, with only 22.7% of cells exhibiting lateral stress fibers (Figure 2.1B, C). Disrupting kinase activity with the LKB1 K78I mutant induced less stress fiber assembly (47.7%) than LKB1 wildtype, though the lack of stress fiber assembly was more apparent when disrupting farnesylation alone (LKB1 C430S, 22.7%) or disrupting both farnesylation and kinase activity in the double mutant (LKB1 K78I-C430S, 17.28%). Expression of the LKB1 CTD alone promoted the greatest amount of stress fiber assembly (82%), but this effect was abolished (26.67%) with a single point mutation in the CTD farnesylation site (CTD-C430S; Figure 2.1B, C). Together, these data indicate that the LKB1 CTD alone can induce stress fiber assembly and LKB1 farnesylation is critical for this to occur.

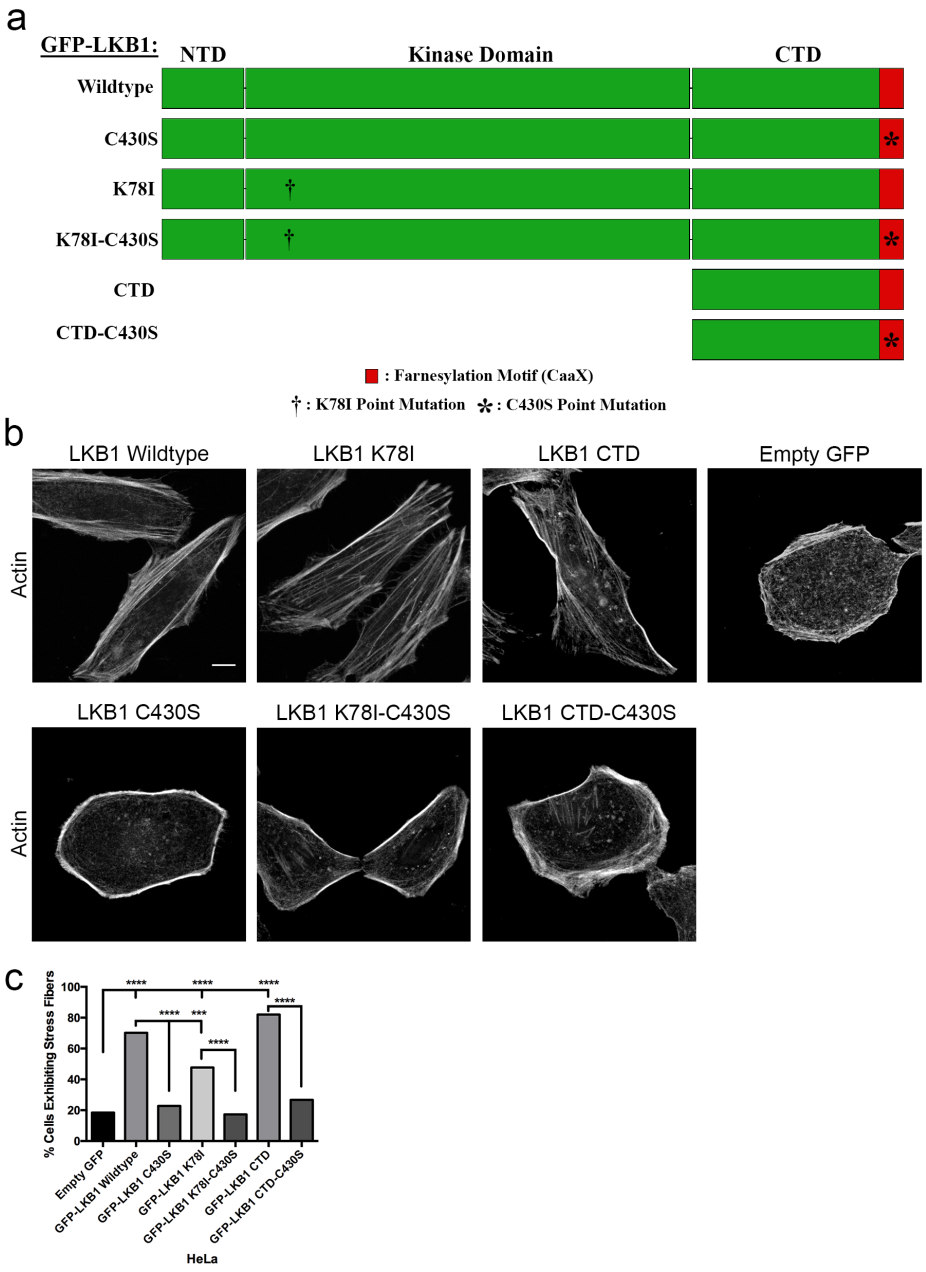

Figure 2.1: LKB1 promotes actin stress fibers in a farnesylation-dependent manner. (A) Schematic showing HeLa cells that were transfected to express GFP-tagged: wildtype LKB1, a C430S mutation to disrupt farnesylation, a K78I kinase dead mutation, a double mutation with both K78I and C430S, the C-terminal domain (CTD) alone, or the CTD alone with a C430S mutation. (B) Immunofluorescent images of HeLa cells transfected with GFP-LKB1 and stained with phalloidin-555. (C) The percentage of cells containing lateral stress fibers was quantified 24 hours after transfection. Significance was measured between comparisons using a 2-tailed Fisher's exact Chi-squared analysis, where ****=$p \leq 0.0001$. $n \geq 50$ cells/condition. Scale bar: 10 µm.

LKB1 signals to RhoA, and RhoA is required for stress fiber assembly through ROCK and subsequent myosin light chain phosphorylation[104-106, 133]; therefore, we sought to determine whether LKB1 farnesylation promotes stress fiber assembly through RhoA. Using HeLa cells stably expressing constitutively active RhoA or cdc42 and co-expressing members of the panel of LKB1 plasmids (Figure 2.1A), we observe activating either RhoA or cdc42 in cells re-expressing wildtype LKB1 or the LKB1 CTD did not impact mesenchymal morphology and lateral stress fiber formation with cells maintaining this LKB1-induced phenotype (Figure 2.2A, B). However, restoring RhoA activity in either empty GFP control or farnesyl-mutant cells induced a rescue of lateral stress fiber assembly, suggesting LKB1 farnesylation lies upstream of RhoA activity in the stress fiber assembly pathway (Figure 2.2A, B). Furthermore, restoring cdc42 activity in empty GFP or farnesyl-compromised cells failed to rescue the stress fiber phenotype, highlighting the role of LKB1 farnesylation in signaling to RhoA and not cdc42 to drive stress fiber assembly.

To determine how LKB1 drives stress fiber assembly through RhoA, a similar experiment was performed in the presence of the ROCK inhibitor Y-27632. As expected, ROCK inhibition had limited impact on empty GFP control cells with 16.22% (vs 18.75% untreated control) of cells exhibiting lateral stress fibers upon ROCK inhibition. However, in cells re-expressing both wildtype LKB1 and the LKB1 CTD alone, ROCK inhibition abrogated the stress fiber assembly rescue by reducing the percent of cells containing stress fibers from 77.89% to 15.31% in LKB1 WT and 80.45% to 15.15% in

LKB1 CTD (Figure 2.3A, B). Together, these data suggest LKB1 farnesylation promotes lateral stress fiber assembly through a RhoA-ROCK signaling pathway.

LKB1 colocalizes with actin at the cell periphery through C-terminal domain farnesylation

LKB1 associates with actin at the cell periphery of motile cells[112]; however, how this is regulated and the functional consequences of the LKB1-actin association have not been investigated. Using the LKB1 panel described in Figure 2.1A, we noted no significant difference in cell footprint based on LKB1 status (Figure 2.4). However, while examining cell area, we noticed striking differences in LKB1 subcellular localization; therefore, using quantitative imaging we generated a cytoplasmic:nuclear ratio (C:N ratio) of LKB1 localization, where a C:N ratio of 1 indicates equal GFP:LKB1 signal in the nucleus and cytoplasm, while a C:N higher than 1 indicates greater cytoplasmic GFP:LKB1 localization. When re-expressing wildtype LKB1, a C:N ratio of 0.51 was observed, indicating that the basal LKB1 signal was two times higher in the nucleus than the cytoplasm. However, when disrupting LKB1 farnesylation with a C430S mutation (or K78I-C430S or CTD-C430S), the signal shifted more into the nucleus with a C:N ratio of 0.25 (Figure 2.4), suggesting that LKB1 farnesylation promotes its cytoplasmic localization. The K78I LKB1 mutant or the LKB1 CTD-only truncate had no impact on GFP:LKB1 localization, suggesting that kinase domain functionality does not impact LKB1 nuclear or cytoplasmic localization.

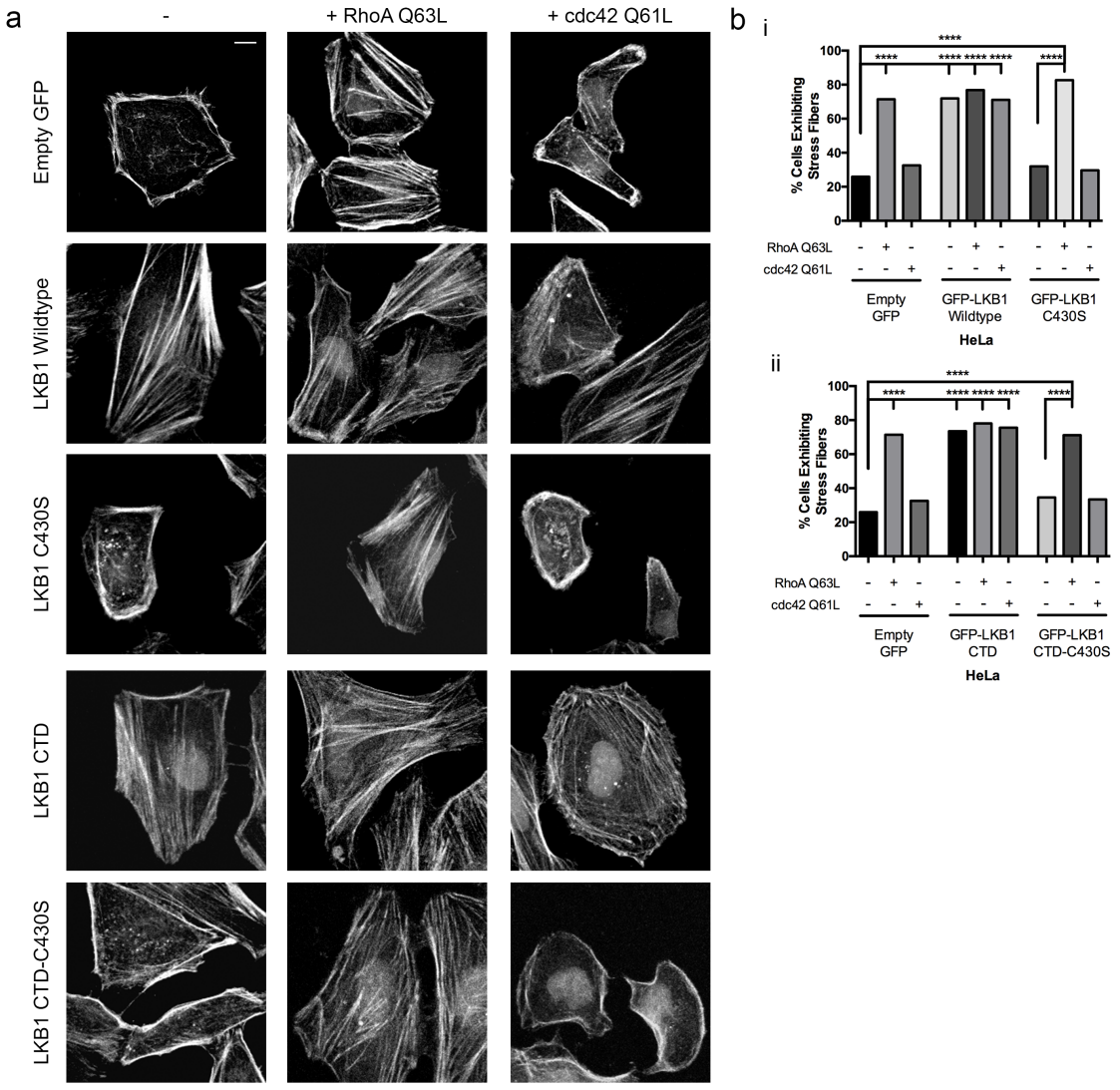

Figure 2.2: LKB1 signals to activate RhoA to promote stress fiber assembly. (A) Immunofluorescent images of HeLa cells expressing GFP-LKB1, constitutively active RhoA (Q63L), and constitutively active cdc42 (Q61L) and stained with phalloidin-555. (B) Percent of cells containing lateral stress fibers was quantified 24 hours after transfection. i) Percentage of cells containing stress fibers for empty GFP control, GFP-LKB1 Wildtype, and GFP-LKB1 C430S with their respective Rho-GTPase mutants. ii) Percentage of cells containing stress fibers for empty GFP control, GFP-LKB1 CTD, and GFP-LKB1 CTD-C430S with their respective Rho-GTPase mutants.

Using live-cell imaging, we confirmed that cytoplasmic LKB1 colocalizes with actin in living HeLa cells primarily in the cell periphery with smaller actin filaments (Figure 2.5A, B). This colocalization originates at the membrane and travels towards the cell interior, presumably through actin retrograde flow. Since LKB1-actin colocalization occurs proximal to the cell membrane with primarily cortical actin filaments, we wanted to determine if LKB1 farnesylation mediates its actin colocalization. When LKB1 farnesylation is disrupted with the C430S mutant, we observed that the LKB1-actin colocalization is almost completely abrogated, returning to empty GFP control levels (Figure 2.5A, B). The impact of LKB1 kinase activity on LKB1-actin colocalization was then tested by re-expressing a K78I kinase-dead mutant. In this case, similar LKB1-actin colocalization as wildtype LKB1 was observed, suggesting that kinase activity is not required for its actin association (Figure 2.5A, B).

We next wanted to determine if the LKB1 CTD alone, which contains the farnesylation motif but lacks kinase activity, is responsible for its actin colocalization. Re-expression of the LKB1 CTD alone led to extensive LKB1-actin colocalization, again primarily with short actin filaments traveling towards the cell interior (Figure 2.5A, B). Importantly, the LKB1 CTD-C430S farnesylation mutant completely abolished the LKB1-actin colocalization (Figure 2.5A, B), further supporting a critical role for farnesylation in promoting LKB1-actin colocalization.

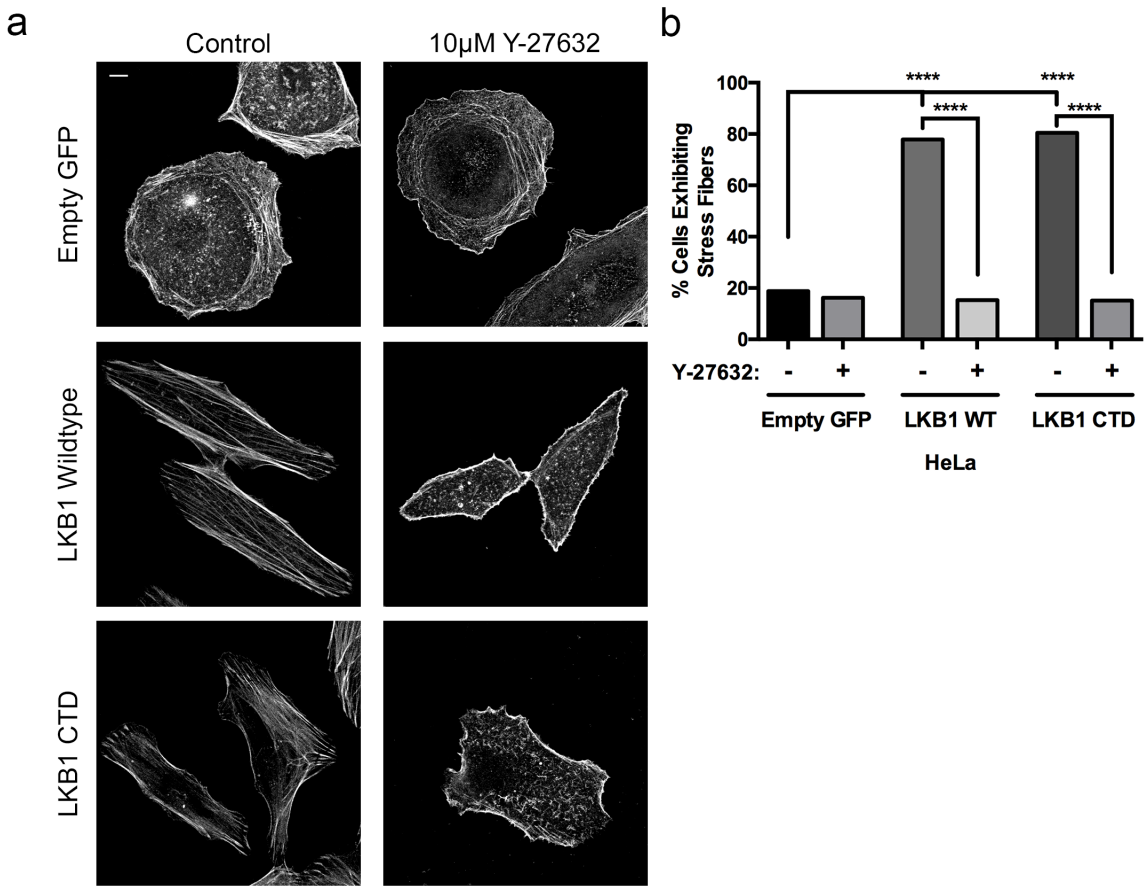

Figure 2.3: LKB1 signals via the RhoA-ROCK pathway to promote stress fiber assembly. (A) Immunofluorescent images of HeLa cells expressing GFP-LKB1 with or without 10 μM Y-27632 ROCK inhibitor treatment and stained with phalloidin-555. (B) Percentage of cells containing stress fibers in response to ROCK inhibitor treatment. Significance was measured between comparisons using a two-tailed Fisher's exact Chi-squared analysis, where ****=$p \leq 0.0001$. $N \geq 50$ cells/condition. Scale bar: 10 μm.

Given that the LKB1-actin association appears to originate at the membrane and maintains this colocalization while traveling towards the cell interior, we assessed this association over time using live cell confocal imaging of the GFP-tagged LKB1 constructs (Figure 2.1A) and LifeAct-mRuby, using Cellular Analysis of Dynamic Events (Figure 2.6A, CADE, see methods). When examining LKB1 colocalization over time, re-expression of wildtype LKB1 induced a persistent actin colocalization, with the LKB1-actin colocalization event averaging 63s (Figure 2.6Bi, C, Figure 2.7). A similar analysis was done with the LKB1 K78I kinase dead mutant and the LKB1 CTD (lacking the kinase domain). As shown previously, inhibition of LKB1 kinase activity did not impact its actin colocalization; however, it does impact actin colocalization persistence. Specifically, when re-expressing the LKB1 K78I kinase dead mutant or the CTD alone (also kinase dead), the LKB1-actin colocalization pattern shifts from persistent dynamics averaging over 60s to transient associations lasting 24.3s and 20.0s, respectively (Figure 2.6Bii, iii, C, Figure 2.7). In addition, the persistent colocalization with wildtype LKB1 results in only 0.6 colocalization events/cell/minute, while disrupting kinase activity increases colocalization events to 1.8 (LKB1 K78I) and 2.8 (LKB1 CTD) events/cell/minute (Figure 2.6D). These results suggest that abolishing farnesylation results in loss of actin colocalization while loss of kinase activity reduces actin colocalization persistence.

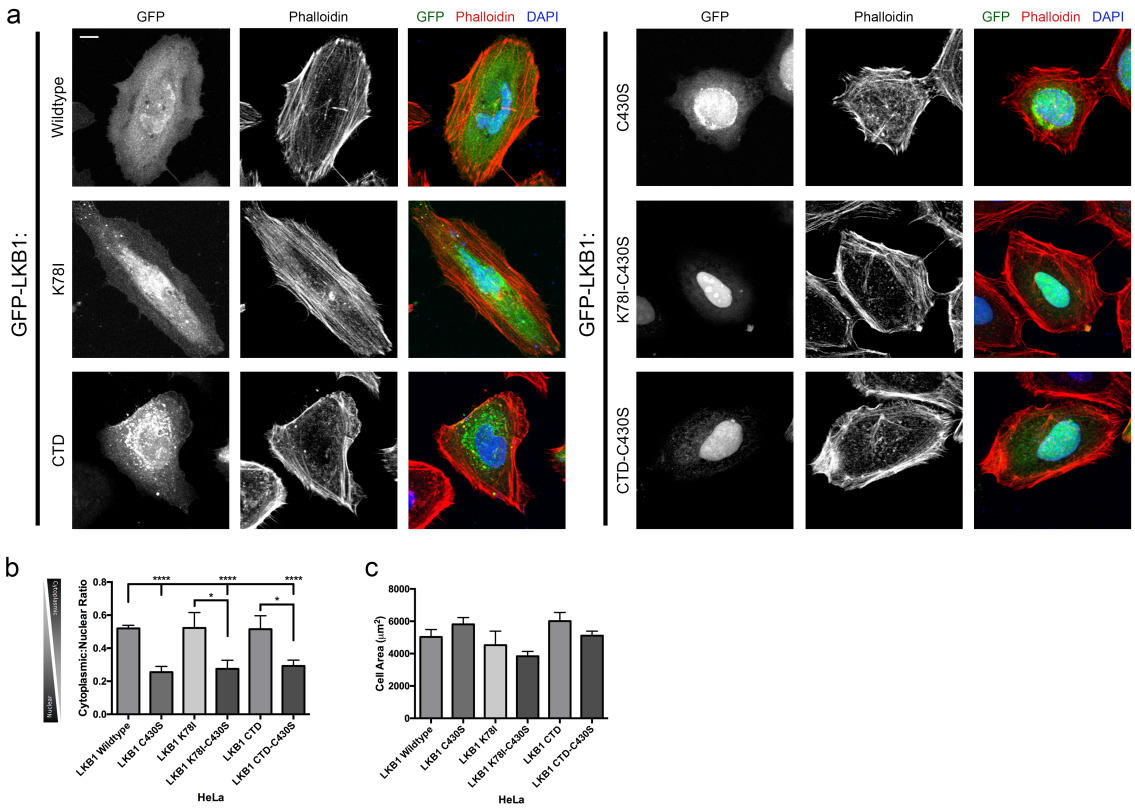

Figure 2.4: LKB1 farnesylation promotes its cytoplasmic localization. (A) Our panel of GFP-LKB1 constructs was transfected into HeLa (LKB1-null) cells. 24 hours later, cells were fixed and stained with phalloidin and DAPI. (B) Mean cytoplasmic and nuclear intensities GFP-LKB1 were calculated in each cell to calculate a Cytoplasmic:Nuclear (C:N) ratio. A C:N ratio of 1:1 indicates an even amount of LKB1 in the cytoplasm and nucleus, while a C:N of 0.5 indicates twice as much nuclear LKB1 as cytoplasmic. (C) Average cell footprint was measured in non-confluent cells. Significance was measured between comparisons using 2-tailed unpaired t-test, where *=p≤0.05; ****=p≤0.0001. N=≥15 cells/condition. Scale bar: 10 μm. Error bars = SEM.

LKB1 kinase activity represses membrane dynamics and traveling membrane waves through FAK

Since actin assembly is critical for lamellipodia elongation[54], we determined how the LKB1-actin colocalization impacts membrane protrusion and retraction events by observing membrane dynamics with the LKB1 truncates and mutants. Using CADE analysis, empty GFP control cells exhibit an average membrane event (defined as either a membrane protrusion or retraction) for a duration of 22±1.1 seconds (Figure 2.8A, Bi, C, Figure 2.9); however, upon re-expression of wildtype LKB1 or a C430S farnesyl mutant, cells had significantly reduced mean membrane event duration to 14±0.8s and 16±0.9s, respectively, (Figure 2.8Bii-iii, C, Figure 2.9). Re-expressing wildtype LKB1 or the C430S mutant also resulted in a decreased number of membrane events per cell, from 6.0±0.8 events/cell/minute for empty GFP to 3.4±0.6 events/cell/min and 2.5±0.4 events/cell/min, respectively (Figure 2.8D). Although farnesylation does not impact membrane dynamics, disrupting LKB1 kinase activity with either a K78I mutation or the LKB1 CTD alone (also lacking kinase activity), induced a reversion back to membrane event durations and number of events/cell/minute similar to empty GFP control (Figure 2.8C, D, Figure 2.9). Together, these data indicate the LKB1 kinase activity, independent of its farnesylation, is responsible for repressing both duration of membrane activity and number of membrane events/cell.

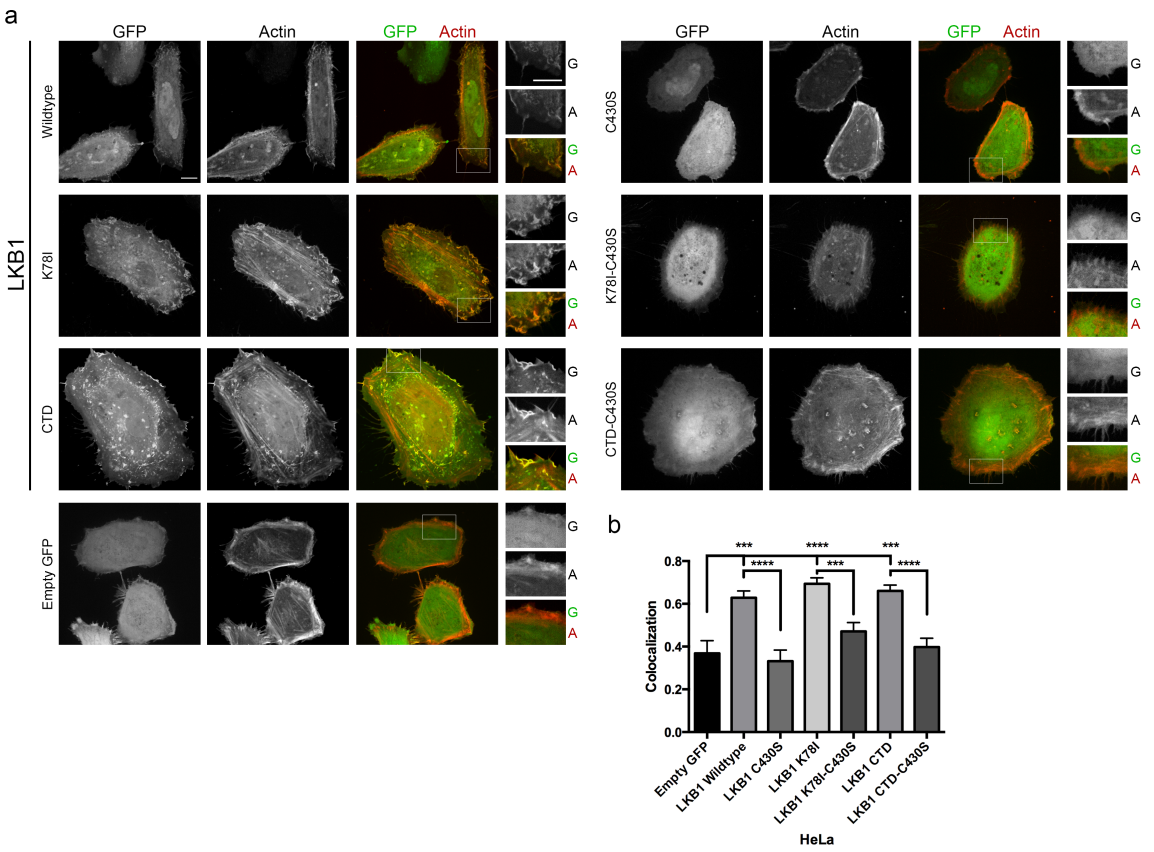

Figure 2.5: LKB1 farnesylation promotes its actin colocalization. (A) Live-cell images of HeLa cells transfected with GFP-LKB1 and LifeAct-mRuby. Inserts are cropped from the white box in the merged image. G: GFP; A: Actin. (B) LKB1-actin colocalization values for the respective constructs from (A). Significance was measured between comparisons using a 2-tailed unpaired t-test, where ***=p≤0.001; ****=p≤0.0001. N≥13 cells/condition. Scale bar: 10 μm. Error bars = SEM.

Traveling membrane waves are defined as a cell membrane protrusion traveling laterally along the membrane, and are typically associated with leading edge actin polymerization[128, 134-136]. We examined traveling wave formation during protrusion/retraction with our panel of LKB1 constructs (Figure 2.1A). To do this, we quantified the angle of membrane events by defining a traveling wave as any membrane event with an angle greater than 10^{o}. In empty GFP control cells, protrusion/retraction events generally occur within the same region of the cell, with only 35.0% of all membrane events exhibiting traveling waves (mean event angle of 12.9 ± 0.7^{o}) (Figure 2.8E, F). Similarly, cells re-expressing wildtype LKB1 and the LKB1 C430S mutant exhibited 32.6% and 28.7% of membrane events as traveling waves, with an average membrane event angle of 12.1 ± 0.8^{o} and 10.7 ± 0.9^{o}, respectively (Figure 2.8E, F). In contrast, re-expressing either the LKB1 K78I (kinase dead) or the LKB1 CTD alone (lacking the kinase domain) resulted in greater traveling waves with 47.8% and 57.0% of membrane events exhibiting traveling waves, with an average angle of 19.5 ± 0.9^{o} and 22.9 ± 1.2^{o}, respectively (Figure 2.8E, F). The CTD-C430S construct also resulted in abrogation of traveling waves, potentially due to the lack of farnesylation to target LKB1 to the membrane. Together, these data suggest that LKB1 functions in a farnesylation-independent, but kinase-dependent manner to repress traveling membrane waves during protrusion and retraction events.

Since LKB1 kinase activity represses membrane dynamics (Figure 2.8) and pFAK[115, 116, 121], we determined whether LKB1 represses membrane dynamics through FAK activity. To do this, cells were treated with the pharmacological FAK inhibitor PF-

562271[137]. Empty GFP control cells treated with 1 μM FAK inhibitor show a reduced duration of membrane events from 22.4±1.1s to 17.3±1.6s and a reduced number of events/cell from 30.6±0.8 to 17.3±1.0 events/cell (Figure 2.10Ai-ii, B, C, Figure 2.11).

In cells re-expressing the LKB1 K78I kinase dead mutant or the LKB1 CTD alone (also lacking kinase activity), FAK inhibition also reduced the duration of membrane events, from 21.8±1.0s to 15.7±1.5s (LKB1 K78I) and from 23.4±1.1s to 13.1±0.7s (LKB1 CTD), as well as reducing the number of membrane events/cell from 6.8±0.6 to 2.8±0.6 events/cell/minute (LKB1 K78I) and 5.9±0.8 to 3.2±0.9 events/cell/minute (LKB1 CTD) (Figure 2.10Aiii-vi, B, C, Figure 2.11). Together, these data show that FAK inhibition significantly decreased membrane activity in kinase activity-compromised cells, suggesting that the FAK pathway is at least in part responsible for driving membrane activity in these cells.

To probe the mechanism underlying traveling waves, we examined the angle of the traveling membrane waves in response to FAK inhibition. Although 35.0% membrane events in empty GFP control cells exhibited traveling waves, FAK inhibition reduced the percentage to 29.2%, with reduction in the average angle of these waves from 12.9±0.7^{o} to 8.7±0.8^{o} (Figure 2.10D, E). In addition, when inhibiting LKB1 kinase activity, the percent of traveling waves decreased from 47.8% to 27.5% (K78I) and from 57.0% to 24.03% (CTD), with the average angle of the waves also reduced from 19.5±1.0^{o} to 10.7±1.5^{o} (LKB1 K78I), and 22.9±1.1^{o} to 10.0±0.7^{o} (LKB1 CTD) (Figure 2.10D, E). Together, these

data indicate membrane activity is impacted by FAK activity, as disrupting FAK inhibits membrane events and traveling waves associated with these events.

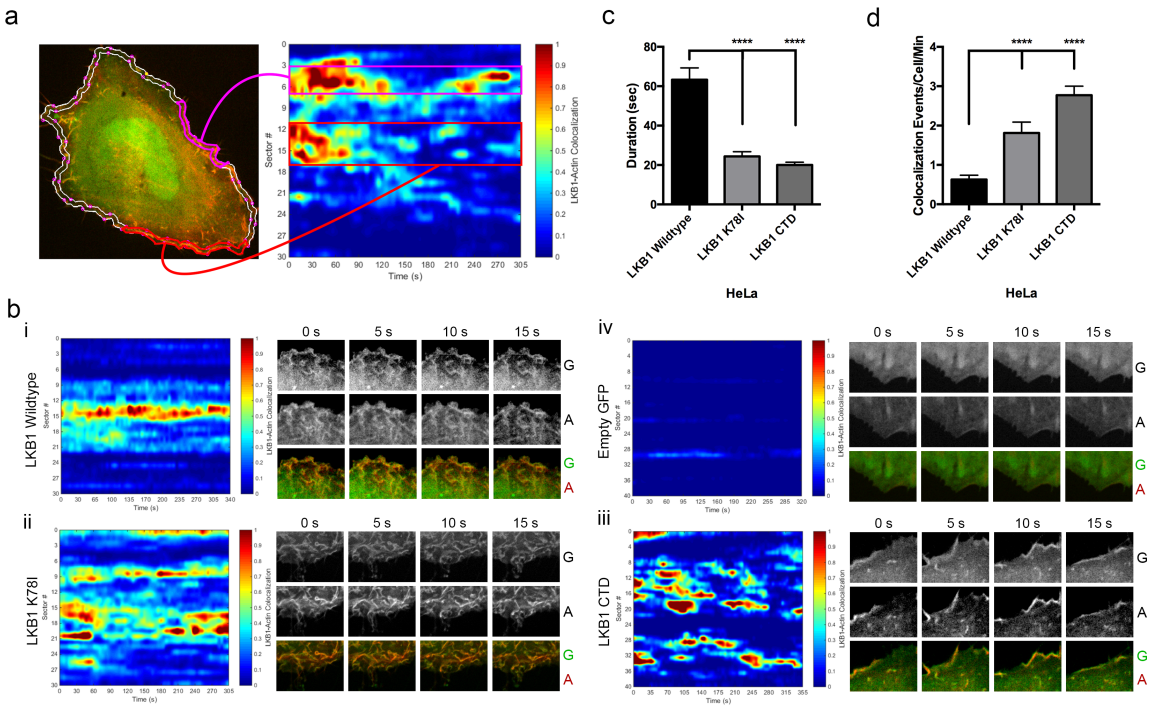

Figure 2.6: LKB1 farnesylation and kinase activity combine to drive actin colocalization over time. (A) Cellular Analysis of Dynamic Events (CADE) was used (see methods). Briefly, live-cell movies were segmented to identify the cell border and a region 2 µm interior of that border. Spatiotemporal colocalization was then measured for the duration of the image acquisition and plotted. Different sectors of the cell boundary are on the y-axis, and time is on the x-axis. Red indicates strong colocalization, blue indicates no colocalization. (B) i-iii) CADE analysis of various LKB1 constructs. ii-iv) CADE analysis of empty GFP control. (C) Graph of the average duration of colocalization events/condition. (D) Graph of the average number of colocalization events/cell/minute for each condition. Significance was measured between comparisons using a 2-tailed unpaired t-test, where ***=p≤0.001; ****=p≤0.0001. N≥13 cells/condition. Scale bar: 10 µm. Error bars = SEM.

LKB1 farnesylation localizes kinase activity to the leading edge membrane to promote nascent adhesion site assembly and maturation

Our data suggests that LKB1 regulates membrane dynamics through FAK (Figures 2.8, 2.10). Since LKB1 farnesylation targets LKB1 to the membrane, and nascent adhesion (NA) sites form at or near the membrane of newly formed lamellipodia, we tested the hypothesis that LKB1 farnesylation serves as a targeting mechanism for placing NA sites at or near the membrane. Using mRuby-Paxillin to monitor adhesion site localization over time, we observed that empty GFP control cells contained NA sites throughout the lamellipodia, with an average NA site distance to the leading edge membrane of 4.0 μm and the closest site 3.0 μm from the membrane (Figure 2.12A-C). However, re-expressing wildtype LKB1 localizes the NA sites significantly closer to the leading edge of the membrane, with an average distance of 1.9 μm and the closest site 1.2 μm from the leading edge (Figure 2.12Ai, B, C). Disrupting kinase activity with the K78I mutant or CTD truncate did not impact NA site localization; however, when disrupting farnesylation with either the C430S or K78I-C430S mutations, the average distance to the membrane reverted back to 4.7 μm and 4.2 μm from the membrane and the closest NA sites to the membrane at 2.7 μm and 2.5 μm, respectively (Figure 2.12A-C). Together, these data suggest that LKB1 farnesylation is required for targeting of NA sites at or near the membrane of a newly-formed lamellipodia.

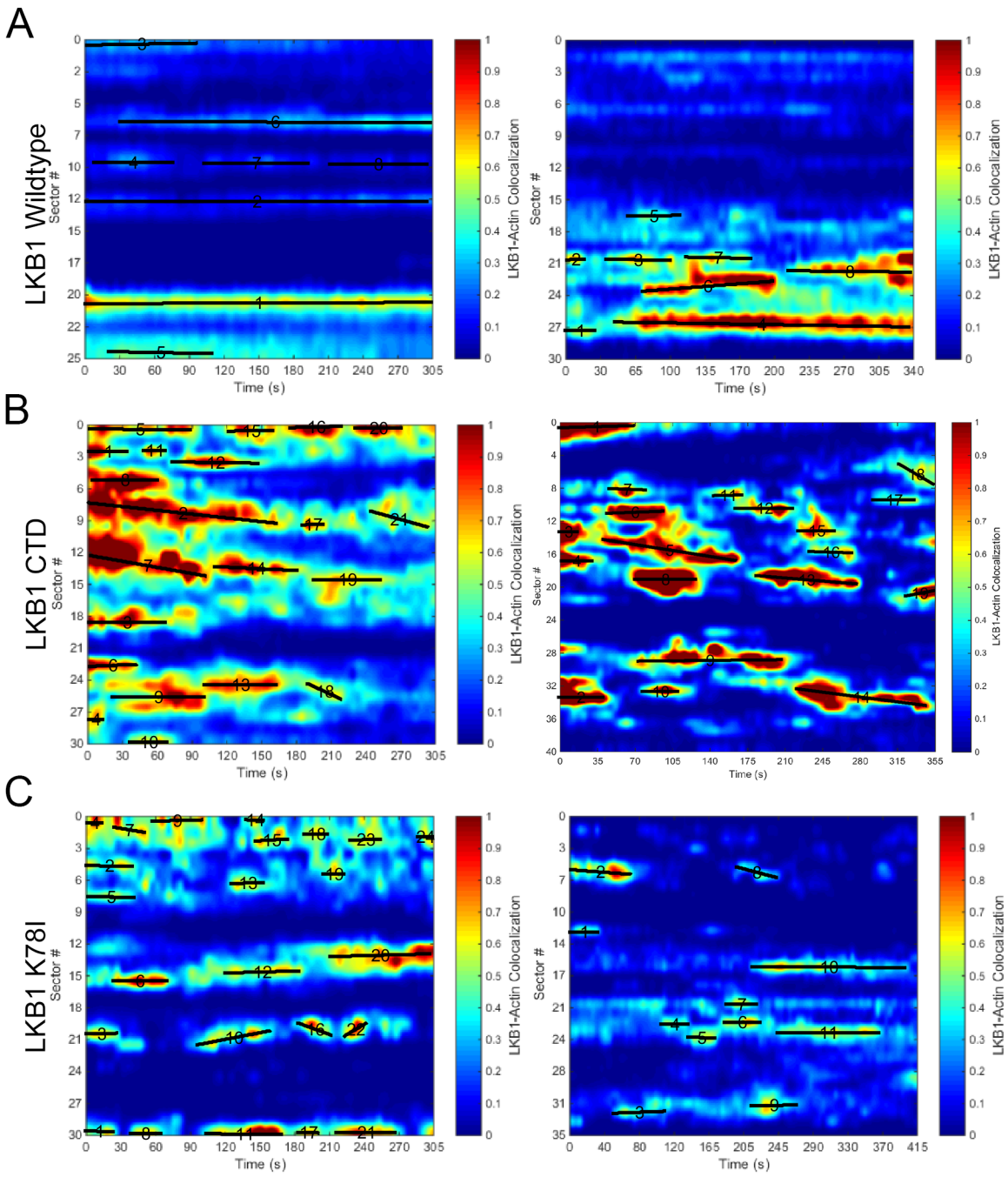

Figure 2.7: Further examples of persistence of LKB1-actin colocalization. (A) 2 examples, with colocalization events identified, of CADE analysis of HeLa cells re-expressing LKB1 wildtype. (B) 2 examples, with colocalization events identified, of CADE analysis of HeLa cells re-expressing LKB1 C-terminal domain. (C) 2 examples, with colocalization events identified, of CADE analysis of HeLa cells re-expressing LKB1 K78I.

NA site morphology was also quantified and we observed an increase in NA site area from 1.1 μm^2 with empty GFP control to 2.8 μm^2 with re-expressed wildtype LKB1 (Figure 2.12D). Additionally, re-expression of wildtype LKB1 promoted elongated NA sites of 3.1 μm in length, compared to 1.6 μm in empty GFP control (Figure 2.12E). We next probed how LKB1 kinase activity impacts NA site maturation, whereby both the K78I kinase inactive mutant and the CTD alone (lacking kinase activity) abrogated the increase in NA site area and elongation observed with wildtype LKB1 (Figure 2.12D, E). Interestingly, disrupting farnesylation with the C430S mutant also abrogated NA maturation, with NA site trends similar to empty GFP control and kinase dead mutants (Figure 2.12D, E). Together, these data indicate that LKB1 kinase activity and farnesylation are required to promote NA site maturation during cell motility.

Coordination of LKB1 farnesylation and kinase activity to direct cell motility

We next determined the impact of LKB1 status on cell motility. Using the panel of HeLa cells stably re-expressing LKB1 (Figure 2.1A), scratch wound assays were performed to monitor cell motility over time. When re-expressing wildtype LKB1 compared to empty GFP control, cells exhibited a higher meandering index during migration, suggesting wildtype LKB1 promotes directed migration during 2D motility (Figure 2.14A, B). This is consistent with previous data examining LKB1 function during 3D invasion[121]. Similarly, re-expressing a kinase-dead (K78I) LKB1 or the LKB1 CTD alone (also kinase dead) rescued the meandering index compared to empty GFP control, indicating that directed cell motility occurs independent of LKB1 kinase activity (Figure 2.14A, B). When LKB1 farnesylation is abrogated with the C430S, K78I-C430S, or CTD-C430S mutants,

cells have a lower meandering index (Figure 2.14A, B). Together, these data indicate that LKB1 promotes directional persistence in a farnesylation-dependent and kinase-independent manner.

We then determined how LKB1 impacts the rate of wound closure and observe that GFP:LKB1 promotes wound closure over time compared to empty GFP control at both 3 and 6 hours (Figure 2.13C, D). When farnesylation is abrogated with either a C430S mutation or the K78I-C430S double mutant, wound closure reverted back to empty GFP control levels (Figure 2.13C, D). Disrupting LKB1 kinase activity with a K78I mutation increased wound closure compared to both empty GFP control and wildtype LKB1, with 53% and 100% closure at 3 and 6 hours, respectively (Figure 2.13C, D). Together, these data show LKB1 farnesylation is required for directed migration, while kinase activity regulates migration rate.

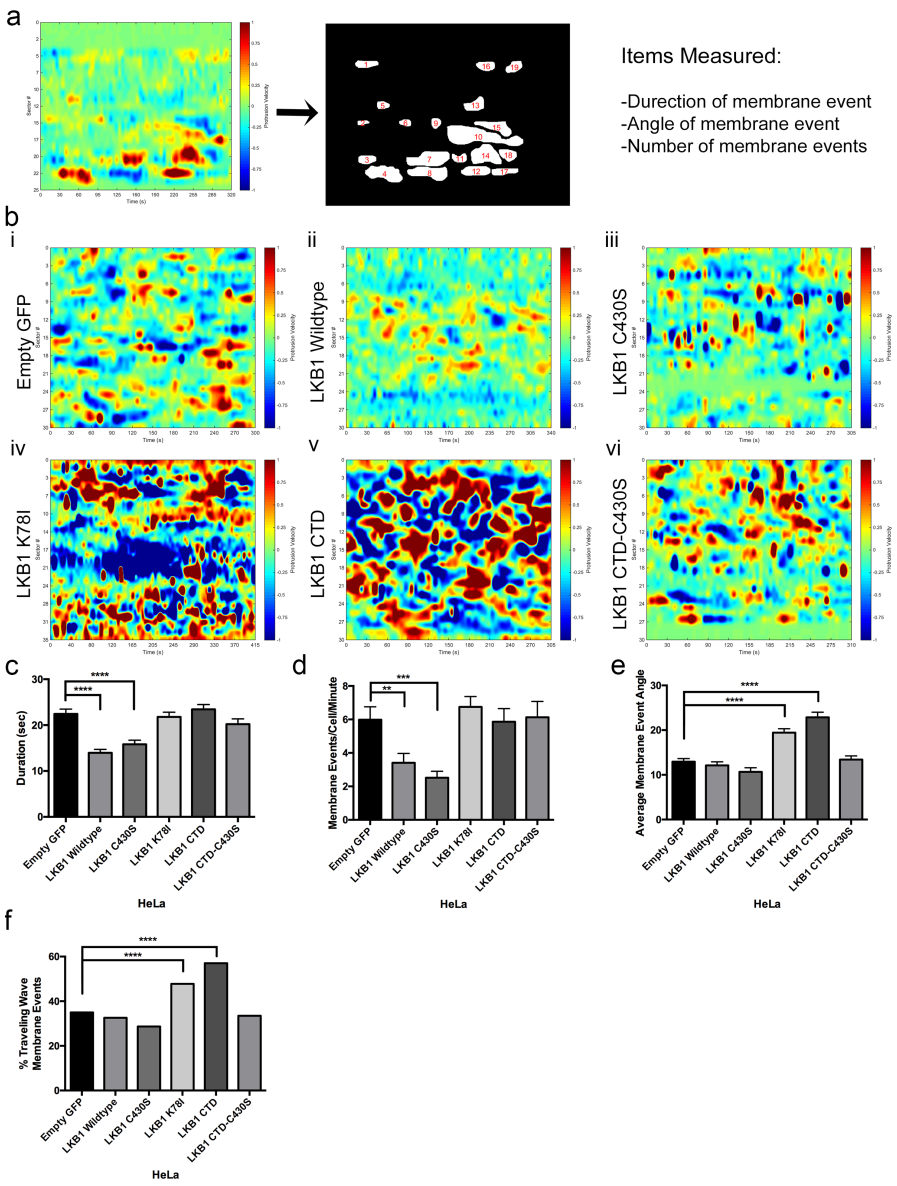

Figure 2.8: LKB1 kinase activity regulates cell membrane dynamics. (A) Membrane protrusion (red) and retraction (blue) events were measured around the cell periphery using the same CADE analysis as in Figure 3C. Cell boundary sectors are on y-axis, time is on x-axis. Protrusion and retraction events were manually identified and the duration, angle, and number of membrane events/cell/minute was quantified. (B) i) CADE analysis on empty GFP control cells. ii-vi) CADE analysis on LKB1 and the various LKB1 mutants. (C) Duration of membrane events (seconds). (D) Average number of membrane events/cell/minute. (E) Average membrane event angle. (F) Percent of membrane events exhibiting traveling waves, defined as an angle greater than 10^{o}. Significance was measured between comparisons in parts (C-E) using a 2-tailed unpaired t-test, while in part (F) using a 2-tailed Fisher's exact Chi-squared analysis, where **=$p \leq 0.01$; ***=$p \leq 0.001$; ****=$p \leq 0.0001$. N≥5 cells/condition. Error bars = SEM.

2.6 Discussion

LKB1 is an actin-colocalizing protein[105, 112] that primarily colocalizes with polymerizing cortical actin filaments adjacent to the cell membrane (Figures 2.5, 2.6). After polymerization, actin-associated LKB1 is rapidly translocated towards the cell interior presumably through retrograde flow[18, 138]. This actin association is farnesylation-dependent, since disrupting LKB1 farnesylation abolishes actin colocalization (Figures 2.5, 2.6) resulting in the loss of stress fibers (Figure 2.1), which suggests that LKB1 farnesylation is functionally linked to downstream actin stress fiber formation. Our data indicate that these events are at least in part due to RhoA-ROCK signaling, since a constitutively active RhoA rescues LKB1-farnesylation defects by restoring actin stress fibers (Figures 2.2, 2.3). Additionally, inhibition of the downstream RhoA kinase, ROCK[139], abolished LKB1-induced stress fiber formation (Figures 2.2, 2.3). This appears consistent with previous RhoA-ROCK pathways[104, 105, 112], placing LKB1 farnesylation and its actin colocalization upstream of canonical RhoA signaling pathways.

In contrast, LKB1 kinase activity is not required for the LKB1-actin association, since disrupting its kinase activity with a K78I mutation or completely removing the LKB1 kinase domain, does not impact actin colocalization. Though surprisingly, LKB1 kinase activity is important for the duration of the LKB1-actin association; specifically, in cells expressing a K78I point mutation in the kinase domain or removal of the kinase domain entirely (CTD alone), LKB1 still colocalizes with actin but these events are more frequent with significantly decreased durations compared to wildtype LKB1 (Figures 2.5, 2.6).

These data suggest that while its actin association *per se* is not kinase-dependent, its ability to maintain this colocalization over time is dependent on its kinase activity.

LKB1 serves as the upstream kinase for the AMPK family, which includes MARK1 and MARK4, and phosphorylates MARK1/4 to restrict FAK activity[116]. When LKB1 function is lost, pFAK-Y^{397} becomes hyperphosphorylated, resulting in cells with a higher adhesion that are able to remodel collagen more effectively in a 3D environment[115, 121, 140]. We observe in living motile cells that disrupting LKB1 kinase activity with either the K78I kinase mutant or the CTD alone resulted in increased membrane protrusion and retraction events, as well as an increase in membrane traveling waves, that lasted for a greater duration than cells re-expressing wildtype LKB1 (Figure 2.8). This would be consistent with the increased adhesion observed in LKB1-compromised cells[115, 116, 121] and supports a more stable and persistent lamellipodia due to regulated adhesion signaling. Additionally, pharmacologic inhibition of FAK signaling relieves these cells of dysregulated membrane activity (Figure 2.10), which supports the model that LKB1 kinase activity regulates lamellipodia adhesion through FAK. Specifically, disrupting LKB1 farnesylation significantly reduces NA area and elongation with sites mislocalized further from the membrane of lamellipodia as compared to wildtype LKB1. Interestingly, disrupting kinase activity also results in reduced NA area and elongation, although the immature NA sites remain proximal to the lamellipodial membrane.

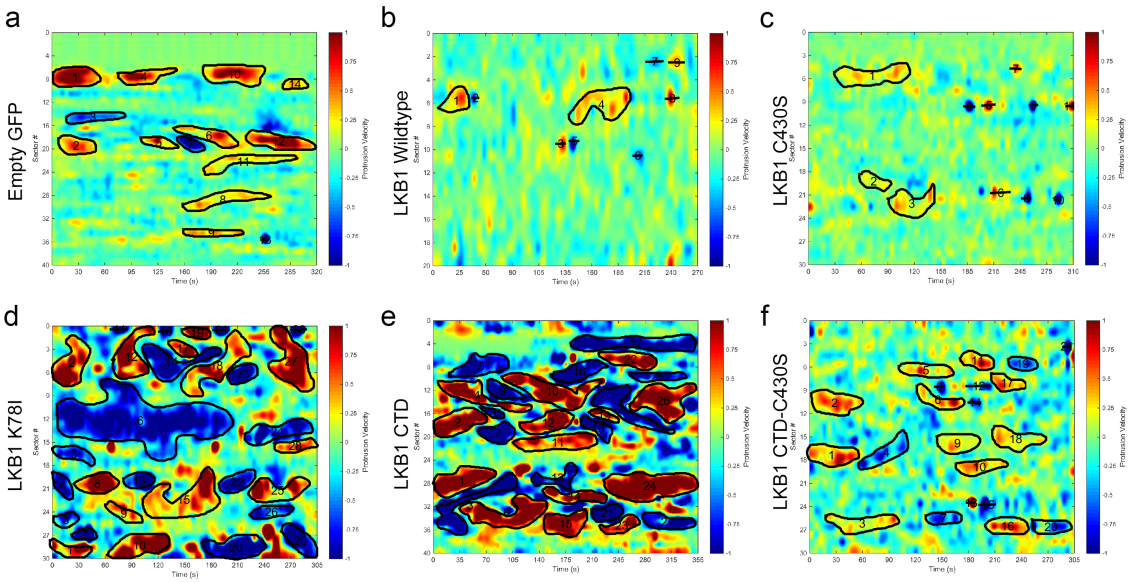

Figure 2.9: Further examples of cellular membrane dynamics. (A) Membrane analysis, with ROIs identified, of HeLa cells re-expressing empty GFP control. (B-F) Membrane analysis, with ROIs identified, of LKB1 wildtype and the various LKB1 constructs.

Taken together, we propose a model (Figure 2.14C, Table 1) whereby LKB1 kinase activity and farnesylation cooperate to regulate actin filament assembly, membrane activity, adhesion dynamics, and subsequent cell migration. First, LKB1 farnesylation allows LKB1 to localize to the membrane, where it colocalizes with actin and signals to the RhoA-ROCK pathway to promote downstream stress fiber assembly. This in turn leads to more directed migration, which is supported by our wound closure data (Figures 2.13, 2.14). Second, LKB1 kinase activity regulates FAK activity, resulting in repression of membrane dynamics and maturation of NA sites. Disrupting kinase activity also promotes increased wound closure rate suggesting that kinase activity alone is important for cell motility velocity, and we speculate could be related to the NA site defects. We hypothesize that this multi-step process begins with LKB1 farnesylation localizing it to the membrane, where its kinase activity then regulates FAK and subsequent NA formation and maturation. When this kinase activity is disrupted, increased adhesion and membrane dynamics ensue. However, our data suggests disrupting LKB1 farnesylation mislocalizes LKB1 kinase activity away from the membrane, thus impacting the ability of LKB1 kinase activity to regulate FAK and NA assembly. These data could be considered analogous to a previous report showing LKB1 farnesylation is critical for promoting AMPK phosphorylation by localizing LKB1 to the membrane for subsequent phosphorylation of AMPK[61]. The well-defined link between FAK and actin[127, 141-143] would suggest that the LKB1-actin function may be related to the LKB1-FAK function, given that its farnesylation appears to lie upstream of LKB1 kinase activity to regulate focal adhesion dynamics during cell motility. Together, these data suggest LKB1 farnesylation and kinase activity cooperatively function to promote cell motility.

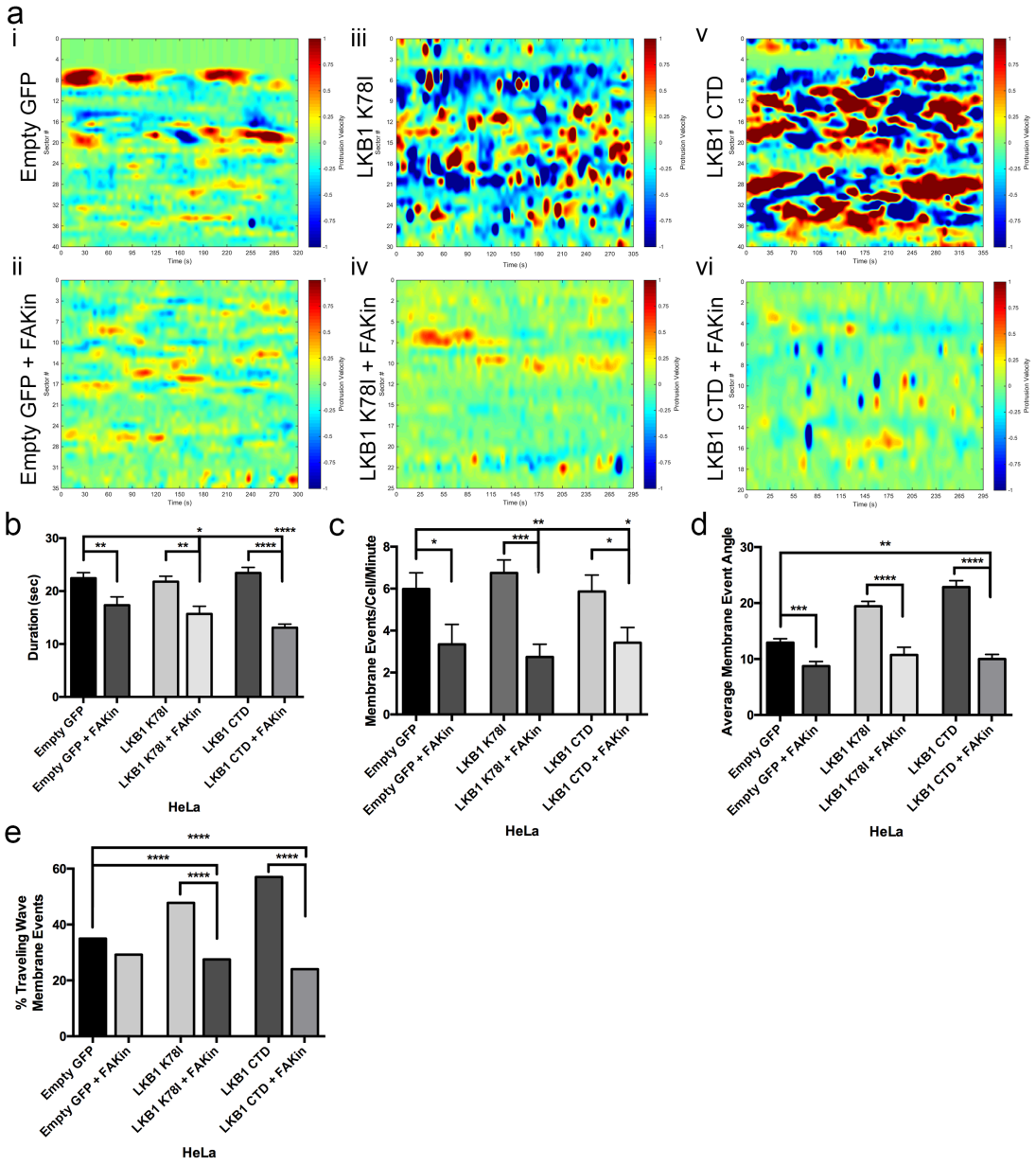

Figure 2.10: LKB1 signals to FAK to regulate cell membrane dynamics. (A) Cells were treated with 1 μM PF-562271 FAK inhibitor and imaged to examine membrane dynamics. i) CADE analysis on untreated empty GFP control cells exhibit basal level membrane events. ii) Analysis of empty GFP control with FAK inhibitor. iii) Untreated kinase dead LKB1 K78I. iv) LKB1 K78I with FAK inhibitor. v) Untreated LKB1 C-terminal domain. vi) LKB1 CTD with FAK inhibitor. (B) Duration of membrane events (seconds). (C) Average number of membrane events/cell/minute. (D) Average membrane event angle. (E) Percent of membrane events exhibiting traveling waves, defined as an angle greater than 10^{o}. Significance was measured between comparisons in parts (B-D) using a 2-tailed unpaired t-test, while in part (E) using a 2-tailed Fisher's exact Chi-squared analysis, where *=p≤0.05; **=p≤0.01; ***=p≤0.001; ****=p≤0.0001. N=5 cells/condition. Error bars = SEM.

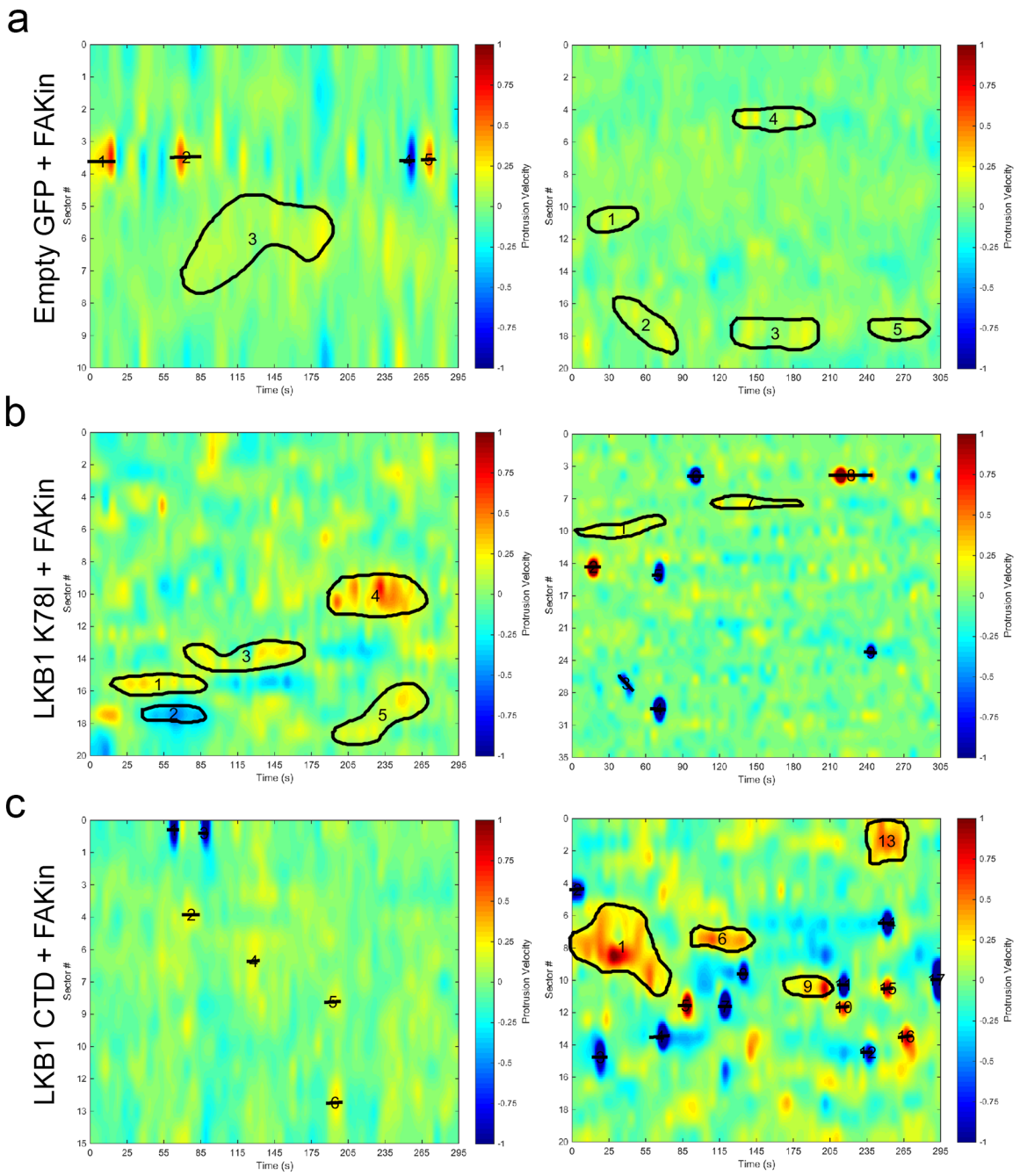

Figure 2.11: Further examples of cellular membrane dynamics on FAK inhibition. (A) 2 examples, with ROIs identified, of CADE analysis of HeLa cells re-expressing empty GFP control with 1 μM PF-562271 FAK inhibitor. (B) 2 examples, with ROIs identified, of CADE analysis of HeLa cells re-expressing LKB1 K78I with 1 μM PF-562271 FAK inhibitor. (C) 2 examples, with ROIs identified, of CADE analysis of HeLa cells re-expressing LKB1 CTD with 1 μM PF-562271 FAK inhibitor.

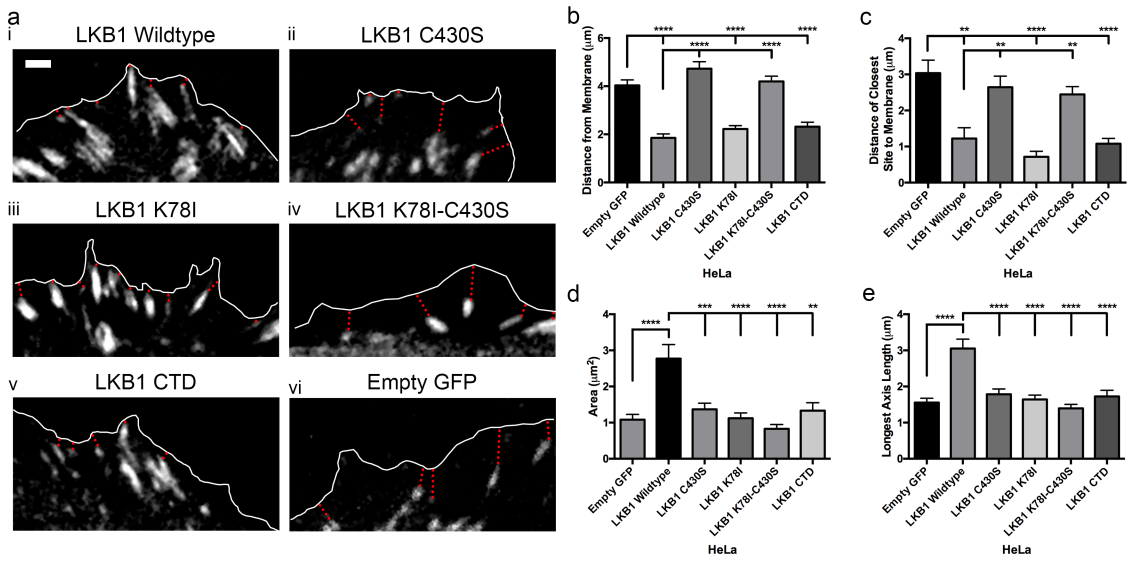

Figure 2.12: A combination of LKB1 farnesylation and kinase activity spatially regulates adhesion site development in emerging lamellipodia. (A) Live-cell imaging of mRuby-Paxillin within emerging lamellipodia identify nascent adhesion (NA) site development. White line indicates cell boundary; red dotted line indicates distance from adhesion site to membrane. i-v) Localization and size of paxillin sites in the various LKB1 constructs. vi) Localization and size of paxillin sites in empty GFP control. (B) Average NA site distance (μm) from the membrane. (C) Distance (μm) of the nearest NA site to the leading edge membrane. (D) Average NA site area (μm^2). (E) Average length (μm) of the longest axis in the NA sites. Significance was measured between comparisons using a 2-tailed unpaired t-test, where **=p≤0.01; ***=p≤0.001; ****=p≤0.0001. N=10 cells/condition. Scale bar: 2 μm. Error bars = SEM.

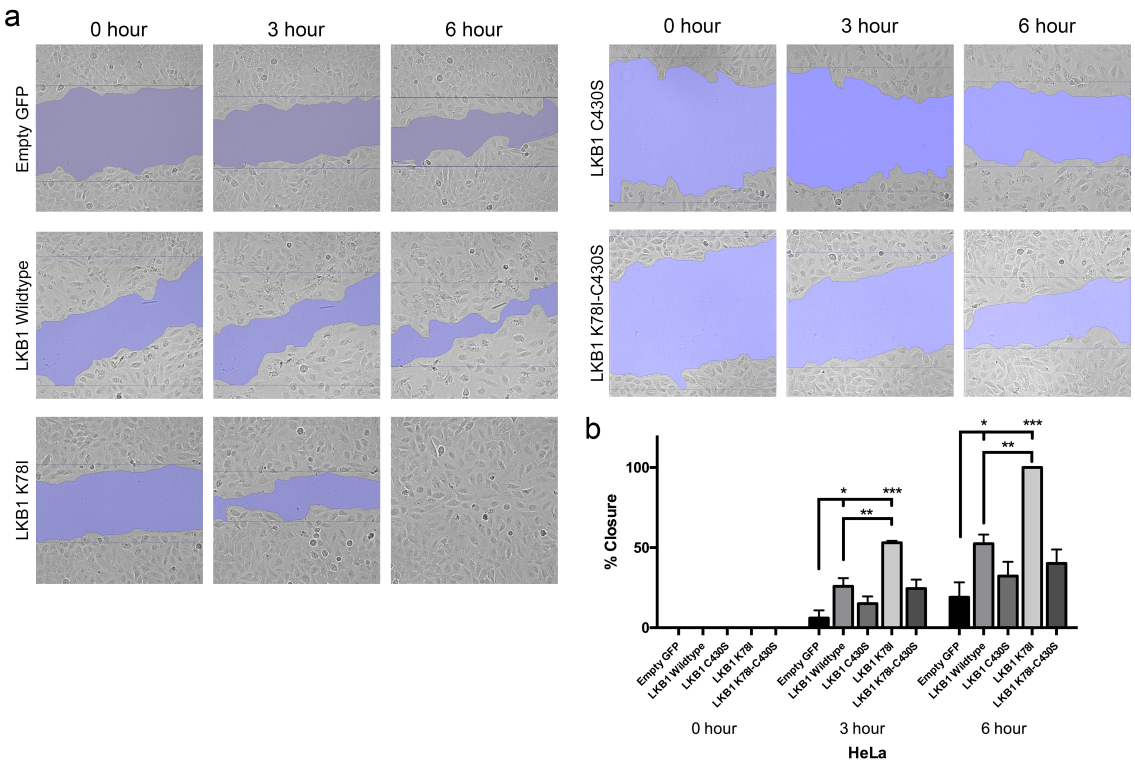

Figure 2.13: LKB1 farnesylation and kinase activity coordinate wound closure. (A) Live-cell imaging of scratch wound assays using HeLa cells stably expressing our panel of GFP-LKB1 plasmids. Area closed for each cell line at 0, 3, and 6 hours post-scratch. (B) The percentage of area closed at 0, 3, and 6 hours was calculated and shown as a bar graph. Significance was measured between comparisons using a 2-tailed unpaired t-test, where *=p≤0.05; **=p≤0.01; ***=p≤0.001; ****=p≤0.0001. N=30 cells/condition for meandering; N=3 scratches/condition for closure. Scale bar: 100 μm. Error bars = SEM.

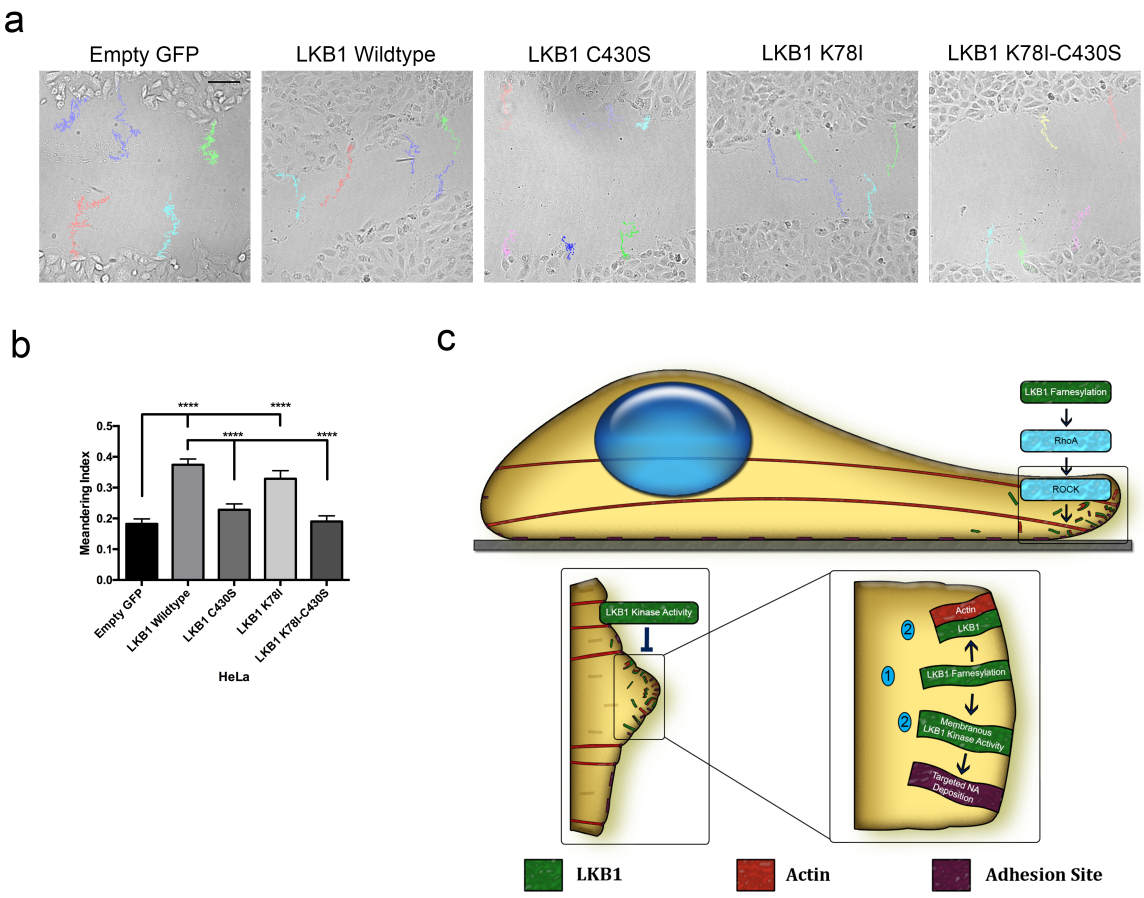

Figure 2.14: LKB1 farnesylation and kinase activity coordinate cell motility. (A) Live-cell imaging of scratch wound assays using HeLa cells stably expressing our panel of GFP-LKB1 plasmids. Representative meandering indices shown for each construct. (B) The meandering index for each cell line was calculated and shown as a bar graph. (C) Model: LKB1 farnesylation promotes its leading edge actin colocalization and signals via RhoA-ROCK to promote stress fiber formation, while LKB1 kinase activity regulates membrane dynamics. Together, LKB1 farnesylation localizes LKB1 to leading edge lamellipodia where LKB1 kinase activity can then regulate nascent adhesion formation and deposition. Significance was measured between comparisons using a 2-tailed unpaired t-test, where *=p≤0.05; **=p≤0.01; ***=p≤0.001; ****=p≤0.0001. N=30 cells/condition for meandering; N=3 scratches/condition for closure. Scale bar: 100 μm. Error bars = SEM.

2.7 Acknowledgements

This work was supported by grants R01CA142858 (A.I.M.), R01CA201340 (A.I.M.), 1R01CA194027 (AIM), U24CA180924 (J.S), U24CA194362 (LADC) and K22LM011576 (LADC). We would like to thank the Emory Integrated Cellular Imaging Core for their assistance with microscopy and the Emory Custom Cloning Core Facility for providing GFP-tagged plasmids. SW is supported by the National Institutes of Health under Ruth L. Kirschstein National Research Service Award 1F31CA200383-01 and was previously supported by a National Science Foundation Graduate Research Fellowship under Grant No. DGE-0940903. SW is partially supported by the Laney Graduate School. Research reported in this publication was supported in part by the Winship Cancer Institute and Emory Integrated Cellular Imaging Core and NIH/NCI under award number P30CA138292.

Tables

LKB1 Protein Domain Functions

	LKB1 Kinase Activity	LKB1 Farnesylation
Actin stress fiber assembly	+	++
Actin colocalization	-	+
Membrane Dynamics/Traveling Waves	+	-
Nascent Adhesion Area/Length	+	+
Nascent Adhesion Localization	-	+

Table 1: Differential effects of LKB1 protein domains on cell motility machinery LKB1 kinase activity impacts HeLa cell stress fiber assembly, represses traveling waves during membrane activity, and promotes nascent adhesion (NA) area and elongation. Conversely, LKB1 farnesylation is critical for stress fiber assembly, its actin colocalization, NA area and elongation, and NA localization to the leading edge membrane.

Chapter 3: LKB1 kinase-dependent and -independent defects disrupt polarity and adhesion signaling to drive collagen remodeling during invasion

3.1 Author's Contribution and Acknowledgement of Reproduction

This chapter is reproduced with minor edits from J Konen*, S Wilkinson*, B Lee, H Fu, W Zhou, Y Jiang, AI Marcus. *LKB1 kinase-dependent and -independent defects disrupt polarity and adhesion signaling to drive collagen remodeling during invasion*. *Mol. Biol. Cell*, 2016. 27(7): 1069-1084.

*These authors contributed equally to this work

JK and SW performed the experiments. SW performed cell polarization, Rho-GTPase assays, and pFAK staining (Figures 3.4-3.14, 3.22). JK, SW, and AIM conceived the initial idea for this study. BL performed quantification of collagen realignment. WZ, YJ, and AIM contributed to experimental design and analysis. SW, JK, and AIM wrote the manuscript with feedback from all authors.

3.2 Abstract

LKB1 is a serine/threonine kinase and a commonly mutated gene in lung adenocarcinoma. The majority of LKB1 mutations are truncations that disrupt its kinase activity and remove its C-terminal domain (CTD). Since LKB1 inactivation drives cancer metastasis in mice and leads to aberrant cell invasion *in vitro*, we sought to determine how compromised LKB1 function impacts lung cancer cell polarity and invasion. Using 3-D models, we show that LKB1 kinase activity is essential for focal adhesion kinase-mediated cell adhesion and subsequent collagen remodeling, but not cell polarity. Instead, cell polarity is overseen by the kinase-independent function of its CTD, and more specifically its farnesylation. This occurs through a mesenchymal-amoeboid morphological switch that signals through the Rho-GTPase RhoA. These data suggest that a combination of kinase-dependent and -independent defects by LKB1 inactivation create a uniquely invasive cell with aberrant polarity and adhesion signaling that drives invasion into the microenvironment.

3.3 Introduction

Liver kinase B1 (LKB1; also known as STK11) is a serine/threonine kinase that was identified as a tumor suppressor in the inherited autosomal-dominant disorder, Peutz-Jeghers Syndrome (PJS). PJS patients have LKB1 loss of heterozygosity resulting in gastrointestinal polyposis and a greater likelihood of developing sporadic tumors in the breast, gastrointestinal tract, and pancreas [144]. Somatic inactivation of LKB1 is observed in several cancer types including melanoma, lung, and cervical cancers [72, 125, 126, 145]. In lung adenocarcinoma, *LKB1* is the third most commonly mutated gene behind *KRAS* and *P53* [14, 15], though how *LKB1* mutations drive lung adenocarcinoma progression remains an area of intense interest.

LKB1 missense and truncating mutations in lung adenocarcinoma primarily occur within its central kinase domain [15]. LKB1 kinase activity was first linked to the canonical AMPK energy stress response pathway, where it serves as the upstream kinase of AMPK (5' AMP-activated protein kinase) [88, 89]. LKB1 also phosphorylates and activates 14 members of the AMPK family [94, 114, 146], including the microtubule affinity-regulating kinases (MARK1-4) [91, 94, 95], NUAK1/2 [96, 97] to control myosin contractility, SIK1 to oversee anoikis [92], and the BRSKs to promote axon differentiation [90, 93].

The LKB1 kinase domain is flanked by a short N-terminal domain and a longer C-terminal domain (CTD) containing a membrane-targeting farnesylation motif [60]**.** Predictably, LKB1 truncating mutations within its kinase domain disrupt kinase function and result in a truncated protein lacking the CTD, or a fully degraded transcript with complete protein

loss. This observation raises the intriguing question of how loss of kinase activity compared to loss of the CTD, impacts LKB1 function and cancer progression. One possible answer could be linked to its role in cell polarity; LKB1 serves as a master regulator of cell polarity across multiple species [122, 123]**.** In *C. elegans*, the LKB1 ortholog, PAR-4, is critical for establishing and maintaining an anterior-posterior (AP) axis during cell division [99]. Additionally, in *Drosophila*, LKB1 is essential for establishing the AP axis during oogenesis and for promoting an apical-basal polarity in eye and follicular cells [100, 101]. In single human intestinal epithelial cells, LKB1 re-expression leads to a fully polarized cell, even in the absence of cell-cell contacts [103]. LKB1 loss in epithelial cells also disrupts apical-basal polarity and basement membrane integrity, while promoting an epithelial to mesenchymal transition (EMT) [110, 111]. The role of LKB1 in regulating cell polarity and motility has linked LKB1 to the Rho family of small GTPases [17, 120]. Upon activation of cell motility in lung cancer cell lines, LKB1 rapidly translocates to the cellular leading edge where it binds to actin and associates with the small Rho-GTPase, cdc42 [112]. Additionally, in normal bronchial epithelial cells LKB1 coordinates with p114RhoGEF to regulate RhoA activity and maintain apical junctions [104, 105].

Complete LKB1 loss in a $Kras^{G12D}$-driven genetically engineered mouse model (GEMM) of lung cancer led to increased tumor burden, shortened survival time, and increased metastasis compared to $Kras^{G12D}$ mutant mice [87]. Despite these recent insights into LKB1 function, how LKB1 coordinates its kinase-dependent and -independent functions to regulate cell invasion remains poorly understood. Therefore, we sought to uncouple defects in CTD function from defects in kinase function during cancer cell invasion. Our data show

that the combination of defects in LKB1 kinase-dependent and -independent function creates a uniquely invasive cell that is unable to properly polarize and maintains an amoeboid shape; however, unlike classical amoeboid cells, LKB1 compromised cells maintain high FAK activity and still remodel collagen during 3-D invasion. Our studies show that FAK-driven cell adhesion and collagen remodeling are caused by defective kinase activity, whereas amoeboid cell shape occurs due to RhoA signaling defects caused by a lack of LKB1 CTD farnesylation. Given that LKB1 frequently undergoes truncating mutations in lung adenocarcinomas that predictably affect both farnesylation and kinase activity, this highlights the importance of this potent combination of defects that could impact cancer cell metastasis.

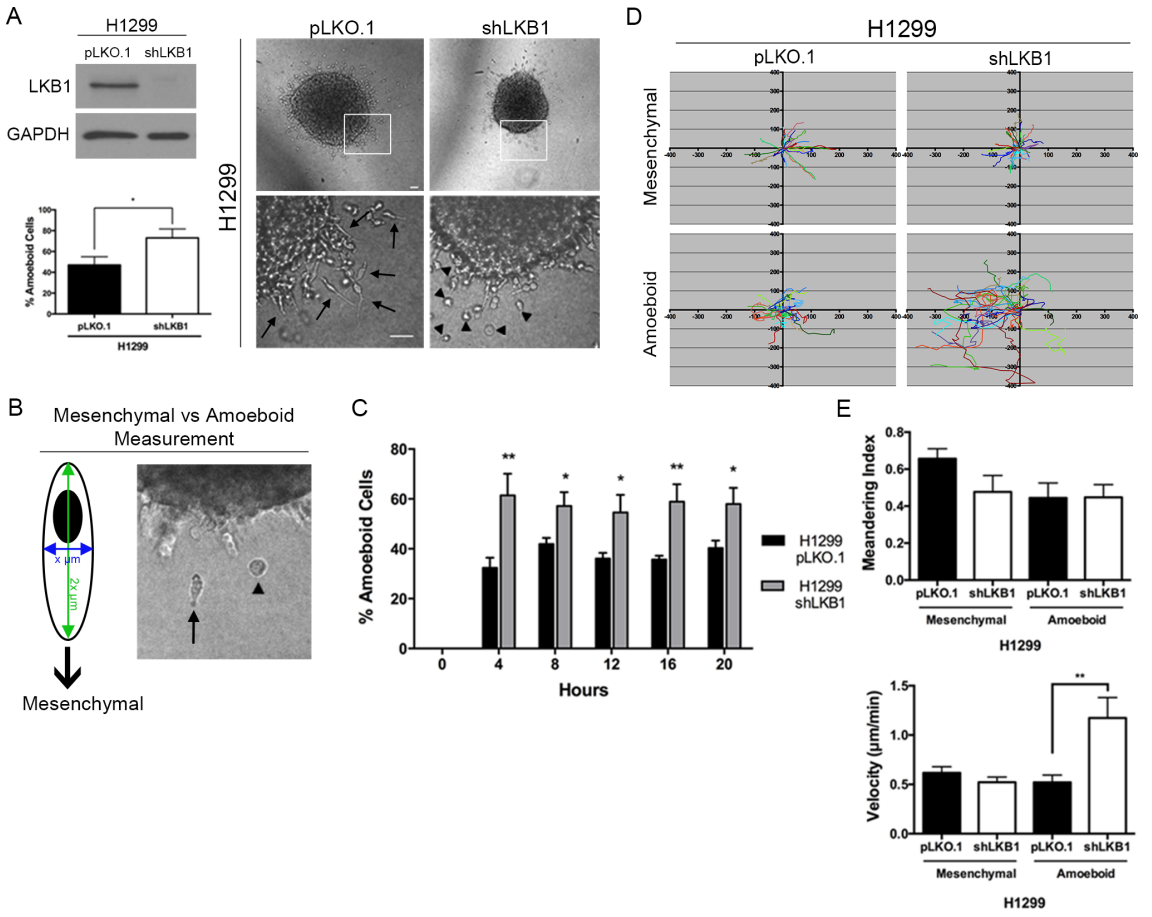

Figure 3.1: LKB1 induces a mesenchymal-amoeboid switch in 3-D invasive morphology. (A) Western blot (left) showing H1299 cells were stably depleted of LKB1 using a targeting shRNA lentivirus. Empty pLKO.1 vector was used as a control. Spheroids from H1299 pLKO.1 and shLKB1 cells were embedded in a collagen type I matrix and imaged at 24 hours post-embedding (right). Zoomed images are shown below. Amoeboid and mesenchymal cell morphologies were quantified as a percentage back to the total number of cells invaded in each spheroid. n = 3 spheroids. Scale = 50 µm. Arrows = mesenchymal cells, arrowheads = amoeboid cells. (B) Schematic illustrating how mesenchymal and amoeboid cells were quantified. Any cell whose length was greater than or equal to twice its width was considered a mesenchymal cell. Image on right shows an example of each cell morphology. Arrow = mesenchymal cell, arrowhead = amoeboid cell. (E-G) H1299 pLKO.1 and shLKB1 spheroids were embedded in a collagen matrix and imaged using live cell confocal. (E) Bar graph showing the percentage of amoeboid cells calculated over time in H1299 pLKO.1 and shLKB1 cells. N = 8 spheroids. (F) Cell tracks were plotted from a single point of origin in H1299 pLKO.1 and shLKB1 invasive amoeboid and mesenchymal cells. (G) Bar graph showing meandering index and velocity of H1299 shLKB1 and pLKO.1 subtypes. n = 11 cells. * = $p \leq 0.05$, ** $p \leq 0.01$, *** $p \leq 0.001$.

3.4 Materials and Methods

Cell culture and generating stable cells:

H1299, H1792 and H157 human NSCLC cells (ATCC, Manassas, VA) were cultured in Roswell Park Memorial Institute (RPMI-1640) media supplemented with 10% fetal bovine serum and 100 units/mL of penicillin/streptomycin, and maintained at 37°C and 5% CO_2. HeLa human cervical cancer cells (ATCC, Manassas, VA) were cultured in Dulbecco's Minimum Essential media supplemented with 10% fetal bovine serum and 100 units/mL of penicillin/streptomycin, and maintained at 37°C and 5% CO_2. Stable pLKO.1 vector control and LKB1-shRNA (shLKB1) H1299 and H1792 cells were created as previously described [115]. Briefly, these cells were created by lentiviral infection using specific shRNA constructs from Open Biosystems (Rockford, IL). Puromycin (2μg/ml, Sigma-Aldrich, St. Louis, MO) was used to select transduced cells and western analysis used to confirm knockdown.

To generate H157 and HeLa cells stably expressing LKB1 and constitutively active RhoA or cdc42, Wildtype LKB1 and the various LKB1 domains and mutations were cloned into a pEGFP-C1 vector. Empty GFP or the GFP-LKB1 constructs were then subcloned from the pEGFP-C1 vector into a pBabe-puro vector. Constitutively active RhoA (Q63L) and cdc42 (Q61L) were subcloned from a pCDNA3 vector into pBabe-Hygro. The pBabe constructs were then transfected into Phoenix-ampho cells with Lipofectamine 2000 and PLUS reagent (Invitrogen, Grand Island, NY). Cells expressing only empty GFP or GFP-LKB1 were selected with 1 μg/ml puromycin, while cells co-expressing the constitutively active RhoA or cdc42 mutants were selected with 1 μg/ml puromycin and 300 μg/ml

hygromycin (EMD Millipore, Billerica, MA). Proper expression of GFP-LKB1 was verified using IF and Western blot to confirm phenotype and molecular weight. Expression of constitutively active RhoA and cdc42 was confirmed using a Rho-GTPase activity assay comparing the constitutively active mutants to their isogenic partner lines.

Antibodies and stains:

Antibodies were used against pFAK^{Y397}, pPaxillin^{Y118}, MARK1, GAPDH, GFP (Cell Signaling, Boston, MA), LKB1 (Santa Cruz, Santa Cruz, CA), RhoA, and cdc42 (Cytoskeleton Inc, Denver, CO) for 3-D immunofluorescence, western blotting, and immunoprecipitation. Alexa Fluor® 555 Phalloidin, Alexa Fluor® 488, and Alexa Fluor® 555 goat-anti-rabbit (Invitrogen) and DAPI (4',6-diamidino-2-phenylindole, Invitrogen) were used for 3-D immunofluorescence. Horseradish peroxidase (HRP)-conjugated secondary antibodies (Jackson ImmunoResearch, West Grove, PA) were used for western blotting.

Transient transfection and Western blot:

For LKB1 rescue experiments, H157 cells were transfected with either pCDNA3 empty GFP control vector or pEGFP-C1 LKB1 WT using Lipofectamine 2000 (Invitrogen), per manufacturer's protocol. For silencing experiments, H1299 or H1792 cells were transfected with either a scrambled control siRNA or siRNA targeting MARK1 (Sigma) or LKB1 (Sigma) using Oligofectamine (Invitrogen), or with siRNA targeting FAK (Sigma) using Lipofectamine 2000 (Invitrogen), per manufacturer's protocol. 24 hours later, cells were harvested and lysed with TNES buffer (50 mM Tris pH 7.5, 100 mM NaCl, 2 mM

EDTA, 1% NP-40) supplemented with Roche Complete Protease Inhibitor Cocktail (Roche, Indianapolis, IN) and a phosphatase inhibitor cocktail (10 mM Sodium Fluoride, 2 mM Sodium Pyrophosphate, 2 mM β-Glycerophosphate, 200 nM Sodium Orthovanadate). Protein concentrations were determined using the bicinchoninic acid protein (BCA) assay kit (Pierce, Rockford, IL). 30 μg of lysates were boiled in Laemmli sample buffer, loaded onto 10% SDS-PAGE gels, transferred onto polyvinyldifluoride (PVDF) membranes, blocked in 10% milk for 1 hour at room temperature, probed overnight at 4^{o}C with primary antibodies diluted in either 5% BSA or non-fat dried milk, followed by appropriate horseradish peroxidase-conjugated secondary antibody and visualized using HyGlo Chemiluminescent HRP antibody detection (Denville, South Plainfield, NJ).

Generating 3-D tumor spheroids:

H1299 and H1792 cells with a stable or transient LKB1, MARK1, or FAK knockdown and corresponding controls, as well as H157 and HeLa cells stably expressing GFP-LKB1 or GFP-LKB1+constitutively active RhoA or cdc42, were grown to 70% confluency and then trypsinized, neutralized, and resuspended in complete RPMI (Invitrogen). To generate spheroids, 3000 cells in 200 μl (1.5 x 10^4 cells/ml) were added to a Spheron Nunclon 96 well plate (Thermo Scientific, Waltham, MA). 3 to 4 days later, compacted spheroids were collected and resuspended in 2.0 mg/ml Collagen Type I (Advanced Biomatrix, San Diego, CA), then plated in: a Lab-Tek 8 well borosilicate bottom plate (Thermo Scientific) for immunofluorescence; a 35 mm glass bottom dish (In Vitro Scientific, Sunnyvale, CA) for multiphoton microscopy; or a 6-well plate (Corning Inc, Corning, NY) for Rho-GTPase

activation assays. After the collagen solidified, complete RPMI was added to the top of the collagen matrix to provide a chemogradient for the spheroids.

Drug treatments:

Spheroids formed from H1299 shLKB1 or pLKO.1 control cells were generated as described earlier. While embedding spheroids in the 3-D collagen matrix, the FAK inhibitor PF-573228 (Sigma-Aldrich) was added at 1 μM or GM-6001 (Santa Cruz) was added at 20μM to both the collagen and complete RPMI media on top of the collagen matrix. Dimethyl sulfoxide (DMSO) was used as the vehicle control. Spheroids were incubated at 37^{o}C and 5% CO_2 for 16-20 hours to allow for invasion.

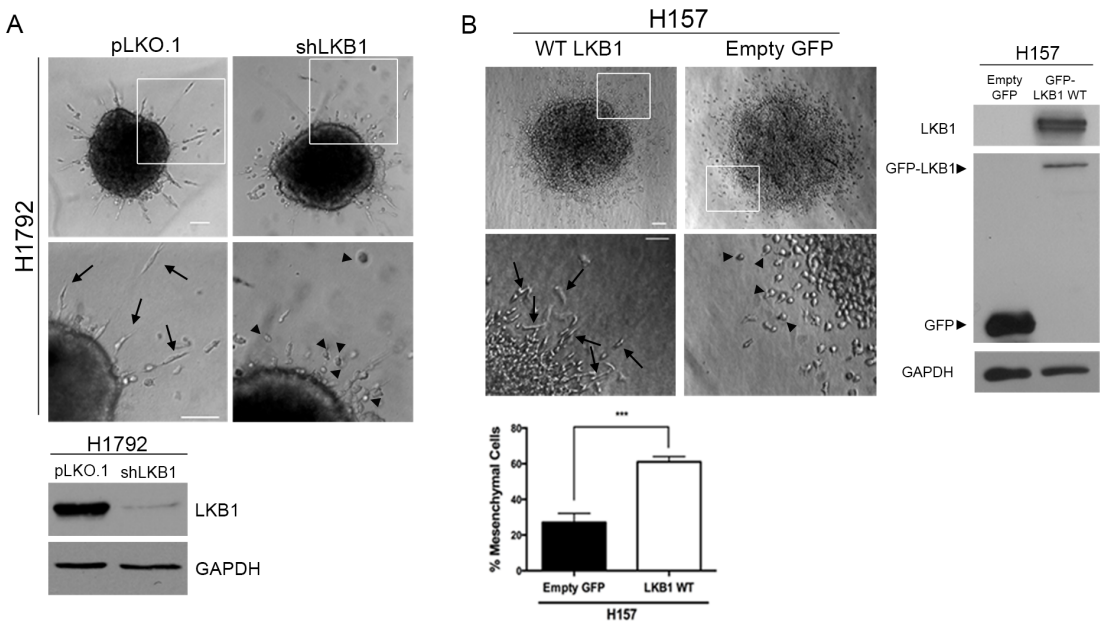

Figure 3.2: LKB1 induces a mesenchymal-amoeboid switch in 3-D invasive morphology across multiple cell types. (A) Experiment from Figure 3.1 was repeated in H1792 NSCLC cells. Western blot confirming LKB1 knockdown is shown below. (B) H157 cells (LKB1-null) were transiently transfected with either empty pcDNA3-GFP or pEGFP-C1 LKB1 WT vector. Spheroids were analyzed at 24 hours for invasive phenotypes. Western blot confirms expression of GFP-LKB1 (right). Bar graph showing the percentage of mesenchymal cells in empty GFP control and LKB1 transfected H157 cells is shown below.

Rho-GTPase activation assays:

Rho-GTPase activation assays were performed using H1299 and H157 cells, as previously described [112, 147]. In brief, H1299 shLKB1 and pLKO.1 control spheroids were embedded in a 3-D collagen matrix (2 mg/ml) as described earlier. At 0, 1, and 5 hours post-embedding, collagen was digested using collagenase (Sigma-Aldrich) at 37^{o}C. Spheroids were centrifuged and supernatant discarded. Remaining cell pellets were lysed using Rho-GTPase activity assay lysis buffer supplemented with 100x protease inhibitor cocktail (Cytoskeleton Inc). H1299 shLKB1 and pLKO.1, as well as H157 cells stably expressing empty GFP control or the various GFP-LKB1 constructs, as well as those co-expressing constitutively active RhoA or cdc42 were grown to 70% confluency. Cells were then trypsinized and 2.0 x 10^6 cells were plated on a 10 cm fibronectin coated plate (40 μg/ml). 24 hours later, cells were lysed using Rho-GTPase activity assay lysis buffer and 100x protease inhibitor (Cytoskeleton Inc). In all cases, total protein quantification was determined using a BCA protein assay kit (Pierce). 300 μg lysate was incubated with either GST-Rhotekin RBD beads (RhoA) or GST-PAK PBD beads (cdc42) for 1 hour at 4^{o}C. Pulldown and input samples (30 μg) were boiled in Laemmli sample buffer, loaded onto either 4-20% gradient (BioRad, Hercules, CA) or 12% SDS-PAGE gels, transferred onto PVDF membranes, blocked in 5% milk for 1 hour at room temperature, probed overnight at 4^{o}C with either mouse-RhoA (1:250 in TBST) or mouse-cdc42 (1:1000 in 0.1% milk) primary antibodies, followed by goat-anti-mouse horseradish peroxidase-conjugated secondary antibody (1:10,000 in TBST) and visualized using HyGlo Chemiluminescent HRP antibody detection (Denville).

3-D Spheroid Immunofluorescence:

Spheroids generated from either H1299 or H157 stable cells were embedded in a 3-D collagen matrix as previously described. 24 hours later, cells were fixed using 4% paraformaldehyde (Electron Microscopy Sciences, Hatfield, PA) for 20 minutes at room temperature and then quenched with 0.1 M glycine in PBS (Sigma-Aldrich) for 10 minutes. Spheroids were then permeabilized with 0.5% Triton-X (Promega, Madison, WI) for 1.5 hours, washed with PBS for 10 minutes, and blocked with 5% Normal Goat Serum (NGS, Jackson ImmunoResearch) for 1.5 hours. H1299 and H157 spheroids were probed with rabbit $pFAK^{Y397}$ (1:200 in PBS with 1% BSA and 1% NGS) overnight at 4^{o}C. Spheroids were then washed with PBS three times for 15 minutes each with vigorous shaking and probed with (H1299) Alexa Fluor® 488 goat-anti-rabbit or (H157) Alexa Fluor® 555 goat-anti-rabbit (1:750 in PBS with 1% NGS) for 1.5 hours with gentle shaking at room temperature. H1299 spheroids were also probed with rabbit $pPaxillin^{Y118}$ (1:200 in PBS with 1% NGS) and Alexa Fluor® 488 goat-anti-rabbit (1:750 in PBS with 1% NGS). After three PBS washes, all spheroids were then stained with 350 nM DAPI for 10 minutes followed by three more PBS washes.

For 40x representative images for cell polarization, H157 and HeLa cells were first fixed with 4% paraformaldehyde then quenched with 0.1 M glycine in PBS. Spheroids were then permeabilized with 0.5% Triton-X for 1.5 hours, washed with PBS for 10 minutes, stained with Alexa Fluor® 555 Phalloidin (1:100 in PBS) overnight at 4^{o}C, then washed with PBS three times for 15 minutes each with vigorous shaking before imaging.

Microscopy:

Widefield imaging

For cell polarity experiments, still images of H1299, H1792, H157, and HeLa spheroids were acquired at 0 and 24 hours using an Olympus IX51 at 4x (0.13 NA air), 10x (0.30 NA air) and 20x (0.45 NA air) using an Infinity2 CCD camera.

Confocal imaging

To quantify cell meandering and velocity, H1299 spheroids and H157 spheroids re-expressing GFP-LKB1 NTD, NTD-Kinase, Kinase Domain, and Kinase-CTD were imaged using a Perkin Elmer Ultraview spinning disk confocal microscope at 10x (Plan-Neofluar 0.30 NA) mounted onto a Zeiss Axiovert encased at 37^{o}C with 5% CO_2. Transmitted light images were acquired every 10 minutes for 20 hours with 10 um z-stack intervals using a Hamamatsu Orca ER CCD camera with 2X2 binning. H157 spheroids re-expressing Empty GFP control, GFP-LKB1: Wildtype, C430S, K78I, K78I-C430S, CTD, and CTD-C430S were imaged using a Leica TCS SP8 inverted confocal microscope with live cell chamber at 10x (HC Plan Fluotar 0.30 NA), acquiring images every 10 minutes for 24 hours with 5 μm z-stack intervals using a 488 nm argon laser under resonance scanning (8 KHz, 32 averaging). Representative images for H157 cell polarization were acquired using a Leica SP8 inverted confocal microscope at 40x (HP PL APO 1.30 NA oil) using a 514 nm argon laser.

For 3-D immunofluorescence imaging, H1299 spheroids were imaged using the FV1000 inverted confocal mounted on an Olympus IX81 inverted microscope (40x 0.90 NA, Water

PlanApo) with 1.3 μm z-stack intervals and sequential scanning (405 nm, 488 nm). H157 spheroids were imaged with the Leica TCS SP8 inverted confocal microscope (40x oil HC PL APO, 1.30 NA) using 1.3 μm z-stack intervals and sequential scanning (405 nm DMOD Flexible, 488 nm argon, 514 nm argon) at 600 hz with 4 averaging.

Multiphoton imaging

Spheroids of H1299 shLKB1 and pLKO.1 or H157 stable cells were dyed using 1μM of Red CellTracker (Invitrogen). The H1299 stable spheroids were imaged at 0, 6, and 24 hours post-invasion, and H157 stable spheroids were imaged at 0 and 24 hours post-invasion, using a standard upright Zeiss Axio Examiner Z1 microscope with 20x water immersion objective (1.0 NA DIC (UV) VIS-IR). The second harmonic generation (SHG) signal was obtained using a bandpass 380-430 nm cube. To image the cells stained with Red CellTracker, a bandpass of 570-610nm cube with a long pass of 550 nm. Images were taken with a Coherent Chameleon Verdi laser at 790 nm wavelength. Z-stack images were taken with a 1μm interval.

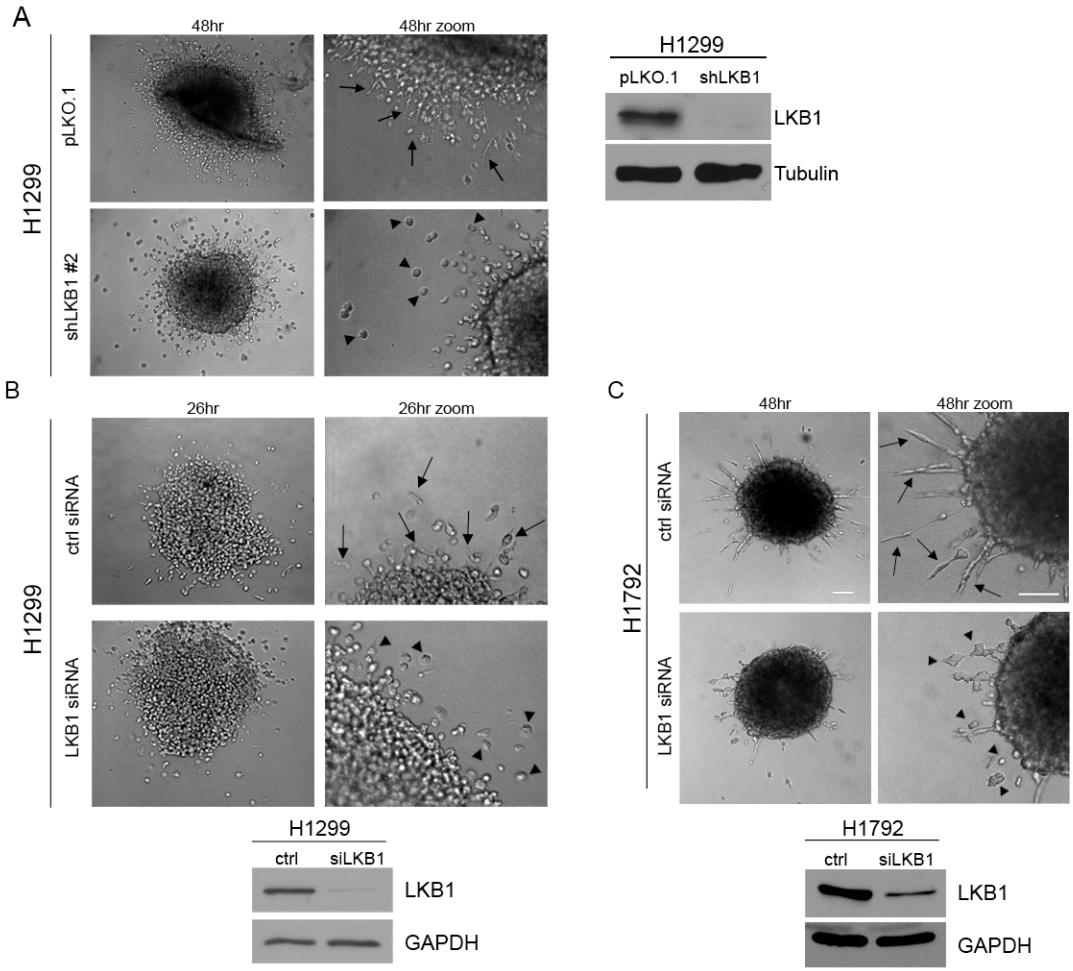

Figure 3.3: Knockdown of LKB1 causes a mesenchymal to amoeboid transition in invasive morphology in H1299 and H1792 cells. (A) LKB1 was stably depleted in H1299 cells using a second targeted shRNA. A spheroid invasion assay was performed and images taken at 48 hours. Western blot confirms LKB1 knockdown. Arrows=mesenchymal cells, arrowheads=amoeboid cells. (B) LKB1 was knocked down via targeted siRNA in H1299 cells with scrambled siRNA used as a control, and a spheroid invasion assay was performed as previously described. Invading cells were imaged after 26 hours of invasion time. Zoomed images are shown to the right. Western blot shows efficiency of the knockdown, and GAPDH was used as a loading control. (C) Experiment from B was repeated in H1792 (LKB1 wildtype) cells. Images were taken at 48 hours post-embedding. Scale = 100 μm.

Image Analysis:

Cell polarity was calculated using ImageJ/Fiji (NIH, Bethesda, MD), where an invading cell was considered to have a mesenchymal polarity if their length was greater than or equal to 2 times their width [148, 149]. Polarity of H1299 shLKB1 was compared to pLKO.1 control, as was polarity of H1299 stable cells in response to FAK inhibition, using the 2-tailed Student's t-test with a p-value of 0.05. Each H157 and HeLa GFP-LKB1 cell line was compared to the respective empty GFP control lines and also to its farnesylation mutant partner (WT vs C430S, K78I vs K78I-C430S, CTD vs CTD-C430S) using Fisher's exact test with a p-value of 0.05. * ≤0.05; ** ≤0.01; *** ≤0.001; **** ≤0.0001

For H1299 cells, Volocity (Perkin Elmer, Waltham, MA) image analysis software and manual tracking was used to quantify total invasion (FAK inhibitor experiment), cell velocity, and meandering index (displacement/distance) as a means of determining directional persistence. The total number of cells invaded in response to FAK inhibition was compared between H1299 shLKB1 and pLKO.1 control, as was the difference in velocity of mesenchymal and amoeboid cells from H1299 shLKB1 and pLKO.1 control cells upon FAK inhibition. For H157 cells, 30 cells for each condition were tracked using automated tracking through the Spots function with Brownian motion, with a maximum distance of 20 μm and a gap size of 2. Cell velocity and meandering of H1299 shLKB1 was compared to pLKO.1 control using the 2-tailed Student's t-test with a p-value of 0.05. Each H157 GFP-LKB1 cell line was compared to both the H157 empty GFP control line and its respective farnesylation mutant (as described above), while cell lines co-expressing constitutively-active RhoA or cdc42 were compared to their isogenic partner line and

empty GFP control cells using the 2-tailed Student's t-test with a p-value of 0.05. * ≤0.05; ** ≤0.01; **** ≤0.0001.

Phospho-FAK and phospho-paxillin levels were analyzed with the vesicle tracking feature in Imaris Cell (Bitplane, South Windsor, CT). Phospho-FAK sites in H1299 pLKO.1 and shLKB1 cells were quantified with quality ranging from 438 to 1201 (16-bit imaging) and the minimum region threshold of 25. In H1299 MARK1 siRNA and siRNA control cells, pFAK sites were quantified with quality ranging from 297 to 1073 (16-bit imaging), and the minimum region threshold of 14.5. H157 cells' pFAK sites were thresholded with the quality ranging from 54.3 to 255 (8-bit imaging) and the minimum region threshold of 70.12. pPaxillin sites in H1299 pLKO.1 and shLKB1 cells were quantified with thresholding ranging from 333 to 1335 (16-bit imaging) and the minimum region threshold of 33.1. Mean pFAK and pPaxillin intensity and number of sites/cell of H1299 shLKB1 was compared to pLKO.1 control, while each H157 GFP-LKB1 cell line was compared to H157 empty GFP control cells using the 2-tailed Student's t-test with a p-value of 0.05. * ≤0.05; **** ≤0.0001

Quantification of collagen alignment:

A novel local alignment coefficient was used to quantify the heterogeneous alignment patterns. The collagen fibers in microscopy images were extracted using the CT-FIRE (curvelet transform fiber extraction) software [150]. All fibers were quantized with a 5-pixel length. For every pixel in X and Y axis of all Z-stack images, the local alignment coefficient was measured (Figure 3.18 explains definition of the local alignment coefficient

and the choice of optimal measurement parameters). A local alignment value of 0 means that the fiber angular distribution is isotropic with no bias in any orientation, or the number of fibers in a local circular bin is below a threshold and considered too few to count. A local alignment value of 1 means all the fibers are perfectly aligned. Histograms of local alignment coefficients, surface plots, and contour plots were generated. When comparing between different time points, we normalized to the 0 hour measurements, and plotted the difference in histograms to show the changes in the alignment distribution.

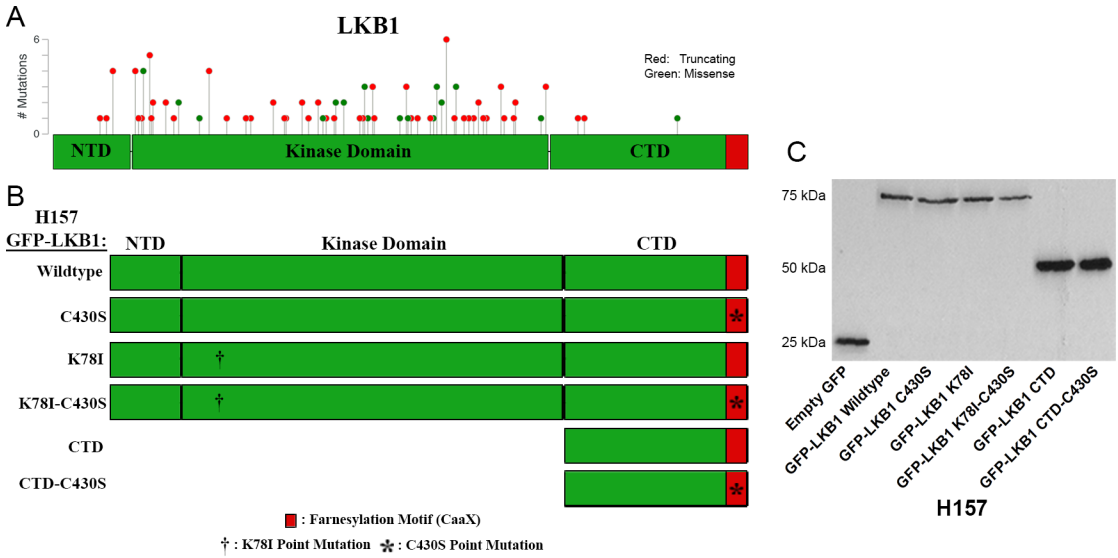

Figure 3.4: LKB1 mutations are found throughout the gene. (A) LKB1 consists of a central kinase domain with a C-terminal farnesylation motif. Schematic of LKB1 mutations in lung adenocarcinoma patients; data adapted from cBioPortal. Red are truncating mutations, green are missense. (B) Schematic showing H157 (NSCLC, LKB1-null) cells that were generated stably expressing GFP-tagged: wildtype LKB1, a C430S mutation to disrupt farnesylation, a K78I kinase dead mutation, a double mutation with both K78I and C430S, the C-terminal domain (CTD) alone, or the CTD alone with a C430S mutation. (C) Western blot probed with a GFP antibody verifying expression of the H157 stable cells.

3.5 Results

LKB1 loss induces a morphological switch during 3-D invasion to create a unique amoeboid cell population

To probe the role of LKB1 in regulating 3-D invasion, LKB1 was stably depleted in H1299 non-small cell lung cancer cells (LKB1 wildtype) and compared to isogenic parental vector control cell pLKO.1 (Figure 3.1A). Stable knockdown of LKB1 resulted in cells switching from a mesenchymal morphology to an amoeboid morphology (Figure 3.1A). In the pLKO.1 cells, 47% of the invasive cells showed an amoeboid morphology, as compared to 73% in the shLKB1 cells. Mesenchymal cells were defined as those cells that had a length greater than two times its width as previously described [148, 149] (Figure 3.1B). A similar transition was observed in H1792 cells (LKB1 wild-type NSCLC), with stable LKB1 depletion (Figure 3.2A). Similarly, a second LKB1 targeted shRNA in H1299 cells, as well as transient knockdown of LKB1 in H1299s and H1792s using siRNA, also had similar effects, resulting in amoeboid-like morphology during invasion (Figure 3.3). To confirm this was an LKB1-dependent effect on cell invasion, the reverse experiment was performed and H157 non-small cell lung cancer cells (LKB1-null) expressing either GFP-tagged full length (WT) LKB1 or empty GFP control vector were used to analyze invasive morphology. Re-expression of WT LKB1 caused invaded cells to switch from an amoeboid-like morphology to an elongated mesenchymal-like morphology (Figure 3.2B). Of the invasive cells expressing LKB1, 61% of the cells were mesenchymal in morphology, as compared to 27% in the LKB1-null parental cells.

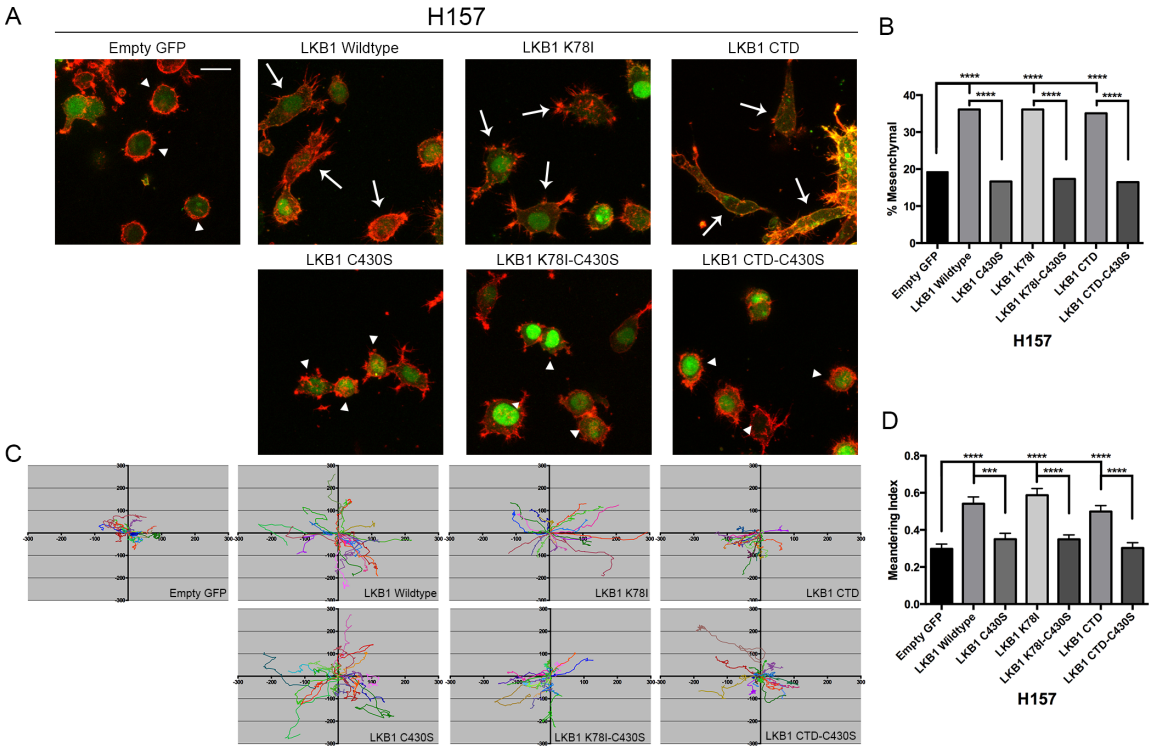

Figure 3.5: LKB1 regulates cellular polarization through its C-Terminal Domain in a farnesylation-dependent manner. (A) Immunofluorescence of H157 spheroids embedded in collagen and stained with phalloidin. Amoeboid and mesenchymal morphologies (described in Figure 3.1) were quantified as a percentage back to the total number of cells invaded in each spheroid. n=4 spheroids. Scale=20 μm. Arrows=mesenchymal cells, arrowheads=amoeboid cells. (B) The percentage of mesenchymal cells was quantified for each cell line at 24 hours post-embedding. (C) Each cell line was tracked over time. Cell tracks were plotted from a single point of origin. (D) Meandering index was calculated using the cell tracks from C. Meandering index is defined as the linear distance divided by the total path length. n=30 cells ***=p≤0.001, ****=p≤0.0001.

Live cell imaging of H1299 pLKO.1 control and shLKB1 spheroids was performed to determine the percentage of amoeboid cells present in the total invasive population over time. These data confirm that LKB1 loss induces a switch to amoeboid morphology compared to control cells, and this switch was stable across all time points measured (Figure 3.1C). Single cell track plots show that LKB1-depleted amoeboid cells move greater distances from their point of origin compared to mesenchymal cells found in the LKB1-depleted population and even other amoeboid cells found in pLKO.1 control cells (Figure 3.2D, bottom right panel). While no difference in cell directionality was seen with LKB1 loss as measured by meandering index (Figure 3.2E, left), LKB1-depleted amoeboid cells show a significantly increased velocity compared to all other cell types (Figure 3.2E, right), including amoeboid cells found in LKB1 wild-type pLKO.1 controls. These data suggest that amoeboid cell morphology alone cannot solely explain the increase in velocity and distance from origin observed in the LKB1-depleted amoeboid cells.

The LKB1 C-terminal domain, and specifically its farnesylation, regulate cellular polarity and directional persistence.

Since the majority of LKB1 mutations in lung cancer patients are truncations [15] (Figure 3.4A), we made a series of stable cells re-expressing GFP-tagged LKB1 mutants and domain truncates (Figure 3.4B, C) to determine if they could induce mesenchymal invasion in both H157 LKB1-null human lung cancer cells and HeLa (LKB1-null cervical cancer) cells. Using 3-D invasion assays of spheroids embedded in collagen, a full length wildtype LKB1 induced mesenchymal polarization during invasion as compared to empty GFP control (Figure 3.5A, B, Figure 3.6), confirming the data seen with the transient

transfections (Figure 3.2B). Similarly, H157 cells re-expressing an LKB1 K78I kinase dead mutant (Figure 3.7) also exhibit a mesenchymal polarity, indicating that kinase activity is not required for promoting mesenchymal polarization. In contrast, a C430S farnesylation mutant or a K78I and C430S double mutant were unable to significantly restore mesenchymal polarization over empty GFP control, highlighting the role of LKB1 farnesylation in promoting mesenchymal polarization during invasion in a kinase-independent manner.

We then tested the hypothesis that the C-terminal domain of LKB1 alone can restore mesenchymal polarization during invasion, since this contains the C430 farnesylation site. The LKB1 CTD alone is sufficient to promote mesenchymal polarization, highlighting a kinase-independent promotion of mesenchymal polarity. Furthermore, mutation of the C430 site abolishes the ability of the CTD to promote mesenchymal polarity, in both H157 and HeLa cells (Figure 3.5A, B, Figure 3.6). Additionally, the LKB1 N-terminal domain (NTD) alone and kinase domain alone both are unable to promote this mesenchymal polarization during invasion (Figure 3.8). Overall, these data suggest that the LKB1 C-terminal domain and specifically its farnesylation promote mesenchymal polarity during invasion and, importantly, this occurs independently of LKB1 kinase activity.

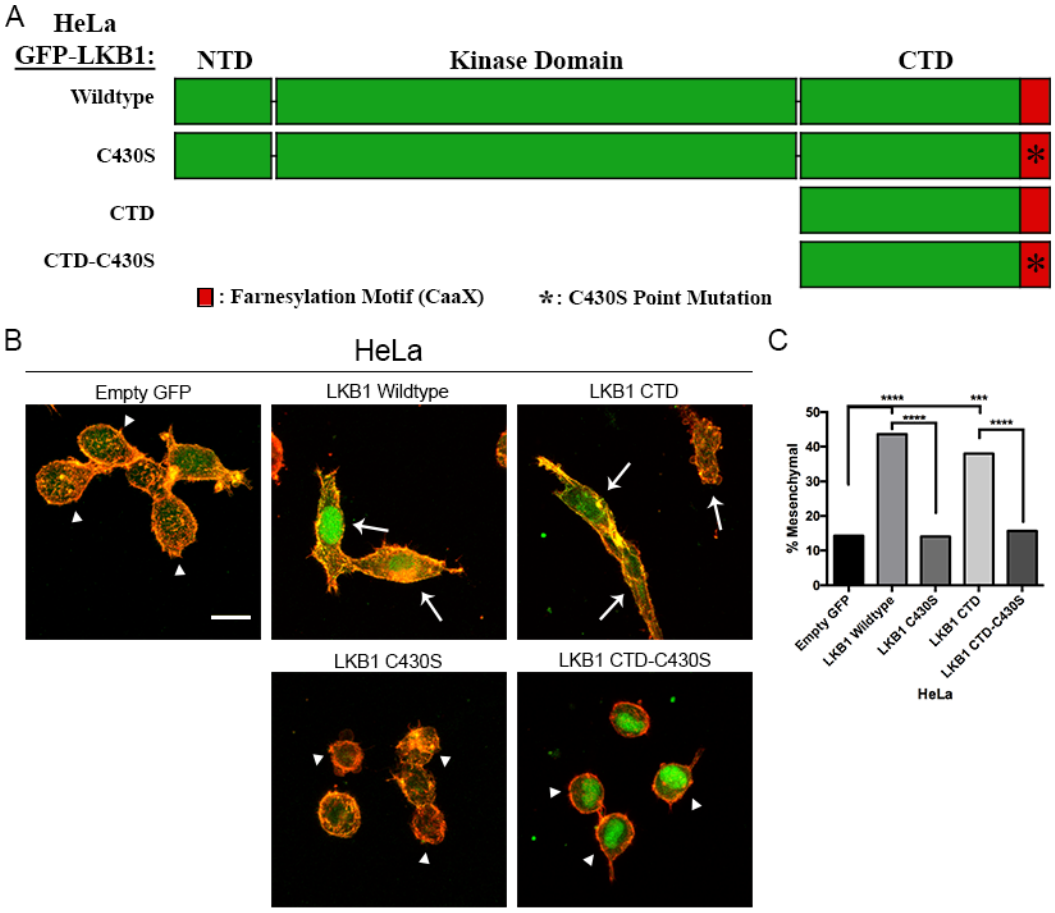

Figure 3.6: LKB1 regulates cellular polarization through its C-Terminal Domain in a farnesylation-dependent manner in HeLa cells. (A) Schematic showing HeLa (cervical carcinoma, LKB1-null) cells that were generated stably expressing GFP-tagged: wildtype LKB1, a C430S mutation to disrupt farnesylation, the C-terminal domain (CTD) alone, or the CTD alone with a C430S mutation. (B) Immunofluorescence of HeLa spheroids embedded in collagen and stained with phalloidin. Amoeboid and mesenchymal morphologies (described in Figure 3.1) were quantified as a percentage back to the total number of cells invaded in each spheroid. n=4 spheroids. Scale=20 μm. Arrows=mesenchymal cells, arrowheads=amoeboid cells. (C) The percentage of mesenchymal cells was quantified for each cell line at 24 hours post-embedding. ***=$p \leq 0.001$, ****=$p \leq 0.0001$.

Our data show that the CTD and farnesylation, promote mesenchymal polarization during invasion, therefore we examined the role of LKB1 in regulating directional migration. Full length wildtype LKB1, the LKB1 K78I kinase dead mutant, and the LKB1 CTD alone significantly restore directional persistence over empty GFP control (Figure 3.5C, D). Upon mutation of the C430 farnesylation site in wildtype LKB1, LKB1 K78I, and the LKB1 CTD there is an abrogation of directional persistence as compared to their respective wildtype farnesylation construct. Taken together, these data highlight the importance of LKB1 farnesylation, independent of its kinase activity, and specifically the CTD in regulating directed cell invasion.

LKB1 differentially regulates Rho-GTPases through its CTD and farnesylation

We next sought to understand the mechanism by which LKB1 regulates this amoeboid-mesenchymal invasion switch. Since amoeboid invasive motility is driven through a balance of RhoA and cdc42 activity [26, 36, 151], we probed the activity of these GTPases in 3-D spheroids. A time course of H1299 (wildtype LKB1) pLKO.1 control cells shows a robust activation of both RhoA and cdc42 at the 5 hour timepoint (Figure 3.9A-D); however, the isogenic shLKB1 cells have reduced active cdc42 and RhoA. To enrich for motile cells, GTPase activation assays were performed in 2-D. The data show that H1299 cells activate both RhoA and cdc42 but this activation is severely attenuated upon LKB1 loss (Figure 3.9E-H). These data are consistent with previous reports showing that LKB1 depletion reduces cdc42 and RhoA activity in motile cells [104, 105, 112], and suggests that LKB1-depleted cells do not rely on canonical Rho-GTPase activity.

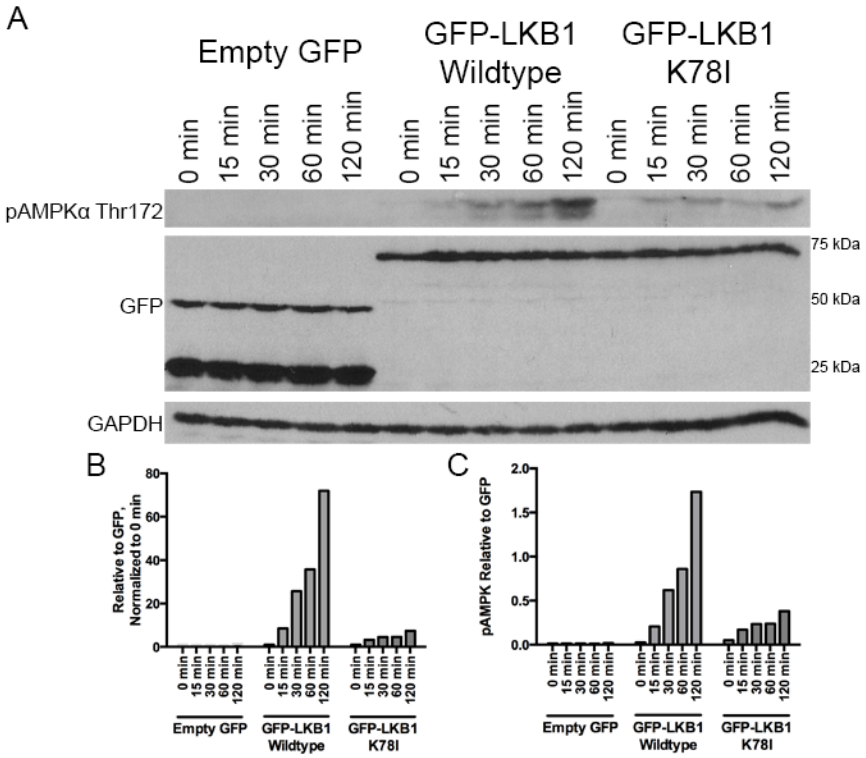

Figure 3.7: LKB1 K78I kinase dead exhibits reduced phosphorylation of AMPK. (A) Western blot show pAMPKα Thr172 expression at 0, 15, 30, 60, and 120 minutes of glucose deprivation in H157 cells re-expressing: Empty GFP, GFP-tagged LKB1 Wildtype, or GFP-tagged LKB1 K78I (kinase-dead mutant). (B) Densitometry of pAMPKα Thr172 normalized to GFP expression. (C) Densitometry of pAMPKα Thr172 normalized to GFP expression and 0 minute time point for each cell line.

Since the LKB1 CTD and specifically its farnesylation are critical for promoting mesenchymal motility, we examined the role of these domains in regulating Rho-GTPase activity. RhoA activity is enhanced upon re-expression of wildtype LKB1 relative to the empty GFP control (Figure 3.9I, J), confirming that LKB1 is responsible for promoting RhoA activity. Similarly, the LKB1 CTD alone is sufficient for promoting RhoA activity, although inhibiting LKB1 farnesylation within the CTD completely abrogates RhoA activation (Figure 3.9I, J*)*. Taken together, these data suggest that LKB1 regulates RhoA activity through its CTD and specifically through its farnesylation.

The role of LKB1 in regulating cdc42 activity was then probed further, since we have previously shown that depletion of LKB1 impacts cdc42 in human lung cancer cell lines in 2-D [112]. We show that wildtype LKB1 promotes cdc42 activity, and that this occurs through the LKB1 CTD (Figure 3.9K, L). Interestingly, LKB1 farnesylation has no impact on the activity of cdc42, as the full-length farnesylation mutant is able to activate cdc42 at levels similar to wildtype LKB1. These data suggest that while LKB1 regulates cdc42 activity through its C-terminal domain, this activation is farnesylation-independent, unlike the farnesylation-dependent activation of RhoA (Figure 3.9K, L).

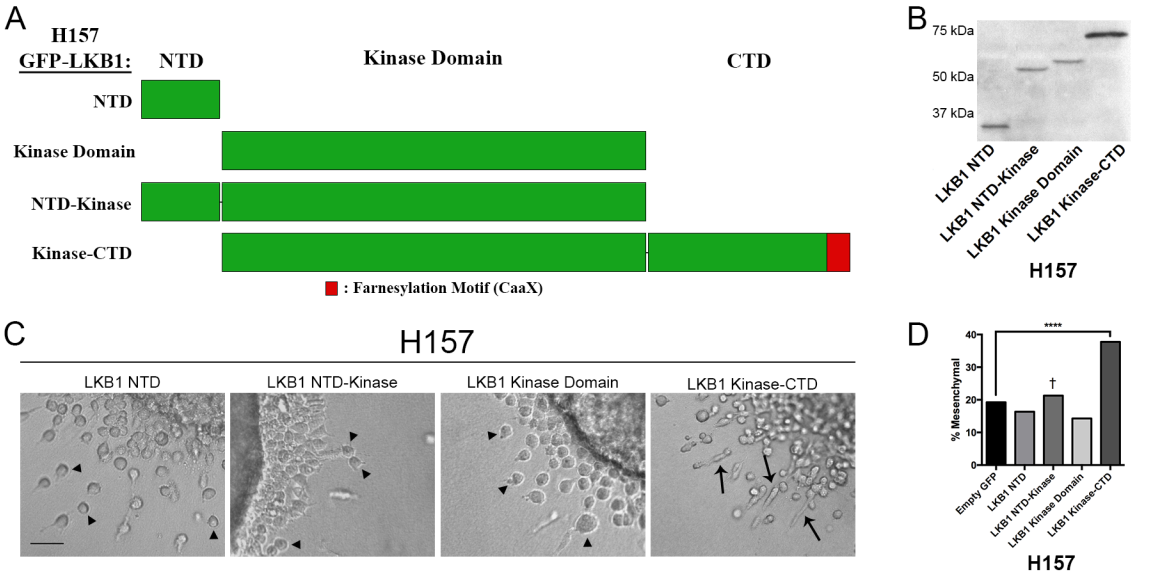

Figure 3.8: LKB1 N-terminal and kinase domains do not restore mesenchymal polarization. (A) Schematic showing H157 (NSCLC, LKB1-null) cells that were generated stably expressing GFP-tagged: LKB1 N-terminal domain (NTD), N-terminal and kinase domains (NTD-Kinase), kinase domain, and kinase domain and C-terminal domain (Kinase-CTD). (B) Western blot probed with a GFP antibody verifying expression of the H157 stable cells. (C) Bright field imaging of H157 spheroids embedded in collagen. Amoeboid and mesenchymal morphologies were quantified as a percentage back to the total number of cells invaded in each spheroid. n=4 spheroids. Scale=50 μm. Arrows = mesenchymal cells, arrowheads = amoeboid cells. (D) The percentage of mesenchymal cells was quantified for each cell line at 24 hours post-embedding. †: H157 cells re-expressing LKB1 NTD-Kinase largely exhibited collective invasion. Quantifications of polarity are for the cells that invaded individually. ****=p≤0.0001.

LKB1 farnesylation activates RhoA to promote mesenchymal polarity

The current data show the LKB1 CTD, and specifically its farnesylation, promote both mesenchymal cell polarity and RhoA activity, we next sought to determine whether LKB1 promotes mesenchymal polarization through RhoA signaling. We created double stable cells expressing either empty GFP or GFP-LKB1 wildtype or a C430S farnesylation mutant, and the constitutively active form of either RhoA (Q63L) or cdc42 (Q61L) (Figure 3.10A). Cells re-expressing wildtype LKB1 and either constitutively active RhoA or cdc42 maintain a mesenchymal polarization similar to cells re-expressing wildtype LKB1 alone (Figure 3.10B, C). Similarly, rescuing cdc42 activity in farnesylation-mutant cells results in a predominantly amoeboid phenotype, similar to LKB1 farnesylation-mutant cells alone (Figure 3.10B, C), suggesting that LKB1 does not signal to cdc42 to promote mesenchymal polarization. However, upon rescuing RhoA activity in LKB1 farnesylation-mutant cells, cells re-acquire a mesenchymal polarization during 3-D invasion (Figure 3.10B, C). Importantly, this result is consistent with mesenchymal polarization in cells re-expressing wildtype LKB1. Restoring either RhoA or cdc42 activity in empty GFP control cells fails to restore this mesenchymal polarization (Figure 3.10B, C). Given that our previous data highlight the role of LKB1 farnesylation in promoting mesenchymal polarity, these data suggest this occurs through LKB1 signaling to RhoA, as rescuing RhoA activity in farnesylation-compromised cells restores mesenchymal polarity.

This data was expanded by examining directional migration in these cells expressing constitutively active RhoA or cdc42. Similar to cells re-expressing wildtype LKB1, cells re-expressing constitutively active RhoA or cdc42 maintain a strong directional persistence

(Figure 3.11A, B). Additionally, cells re-expressing constitutively active cdc42 in LKB1 farnesylation-mutant cells have poor directional persistence similar to farnesylation-mutant cells alone, suggesting that cdc42 signaling is not responsible for promoting directionality. However, upon rescuing RhoA activity in these farnesylation-compromised cells, cells restore their directional persistence similar to cells re-expressing wildtype LKB1 (Figure 3.11A, B). Similar to mesenchymal polarization, restoring RhoA or cdc42 activity in empty GFP control cells fails to restore directional persistence. Together, these data highlight a LKB1 farnesylation-RhoA pathway to promote mesenchymal polarity and strong directional persistence during 3-D invasion.

The regulation of FAK activity by LKB1 is kinase dependent.

Our current data show that the LKB1 CTD is responsible for controlling this amoeboid-mesenchymal switch during 3-D invasion. We and others have also shown that LKB1 loss results in an increase in adhesion signaling, most notably through hyperactive focal adhesion kinase (FAK) signaling [87, 115-117]. Thus, we sought to determine if this amoeboid-mesenchymal switch is related to adhesion signaling by using our panel of H157 stable cells (Figure 3.4B) to assess $pFAK^{397}$ activity. Compared to empty GFP control cells, H157 cells expressing wildtype LKB1 showed repression of the total number of $pFAK^{397}$ sites using immunofluorescence (Figure 3.12A, B). This result is consistent with previous findings that LKB1 is a pFAK repressor in lung cancer cells [115, 116]. Interestingly, this repression was not dependent on LKB1 farnesylation, as mutation of the LKB1 C430 farnesylation motif had no impact on the ability of LKB1 to repress $pFAK^{397}$ (Figure 3.12A, B). In contrast, when re-expressing either the K78I kinase dead mutant or

the K78I-C430S double mutant LKB1, $pFAK^{397}$ expression was not repressed and remained at similar levels as empty GFP control cells (Figure 3.12A, B). While LKB1 served to repress total number of $pFAK^{397}$ sites/cell, the mean intensity of each pFAK site was similar across all cell lines (Figure 3.13). These data suggest that the kinase activity of LKB1, but not farnesylation, is necessary for LKB1 to repress FAK during 3-D invasion.

To further probe the mechanism by which LKB1 regulates FAK, we analyzed the role of the downstream target of LKB1 kinase activity, MARK1, which represses FAK through an LKB1-MARK1 pathway [116]. Immunofluorescence staining of $pFAK^{Y397}$ in MARK1 siRNA-depleted cells show that MARK1 loss increases pFAK expression when compared to scrambled siRNA control (Figure 3.12C), thus phenocopying the loss of LKB1. Quantification of $pFAK^{Y397}$ staining confirms that MARK1 loss increases the number of pFAK sites per cell (Figure 3.12D), with a slight increase in the intensity of each pFAK site (Figure 3.13). Western blot analysis of three LKB1 wildtype lung cancer lines (H1792, H1299, and H157 + GFP-LKB1) also shows an increase in $pFAK^{Y397}$ with MARK1 knockdown (Figure 3.12E); however, MARK1 knockdown had no significant impact on cell morphology (Figure 3.14), which is consistent with our data that cell polarity during 3-D invasion is independent of its kinase function.

LKB1-depleted amoeboid cells require FAK activation to navigate through a collagen matrix

We next wanted to determine the impact of LKB1 loss specifically on the amoeboid population as these cells showed a significant increase in velocity during invasion, even

more so than amoeboid cells in the wildtype population (Figure 3.1D). We first assessed if FAK was hyperactive in LKB1 depleted cells. Western blot confirms an increase in $pFAK^{Y397}$ in H1299 and H1792 LKB1-depleted cells as compared to controls (Figure 3.15A); however, this only provided information on the whole population. Therefore, we then analyzed single invasive cells for their pFAK status based upon morphology in H1299 pLKO.1 and shLKB1 spheroids via immunofluorescence. We confirmed that LKB1 loss resulted in $pFAK^{Y397}$ hyperactivation compared to pLKO.1 control cells (Figure 3.15B). The mean intensity of each individual pFAK site significantly increased from 748 in pLKO.1 cells to 1751 in shLKB1 cells (6C, left), and the total number of pFAK sites per cell showed a significant increase from 3 to 72 sites per cell with LKB1 depletion (Figure 3.15C, right). This increase in $pFAK^{Y397}$ also resulted in increased downstream adhesion signaling, since both the mean phospho-paxillin ($pPax^{Y118}$) site intensity and total number of $pPax^{Y118}$ sites per cell significantly increases (Figure 3.15D, E).

We next examined $pFAK^{Y397}$ expression specifically in mesenchymal and amoeboid cells of pLKO.1 and shLKB1 cells to determine if shLKB1 amoeboid cells have unique FAK activity compared to wild-type LKB1 amoeboid cells. These data show that LKB1 loss increases $pFAK^{Y397}$ expression in both mesenchymal and amoeboid cells that lack LKB1 (Figure 3.15F); however, the amoeboid populations within shLKB1 cells express significantly higher levels of pFAK when compared to amoeboid cells in pLKO.1 control cells (Figure 3.15F), showing that this pFAK activity does not solely arise from amoeboid morphology.

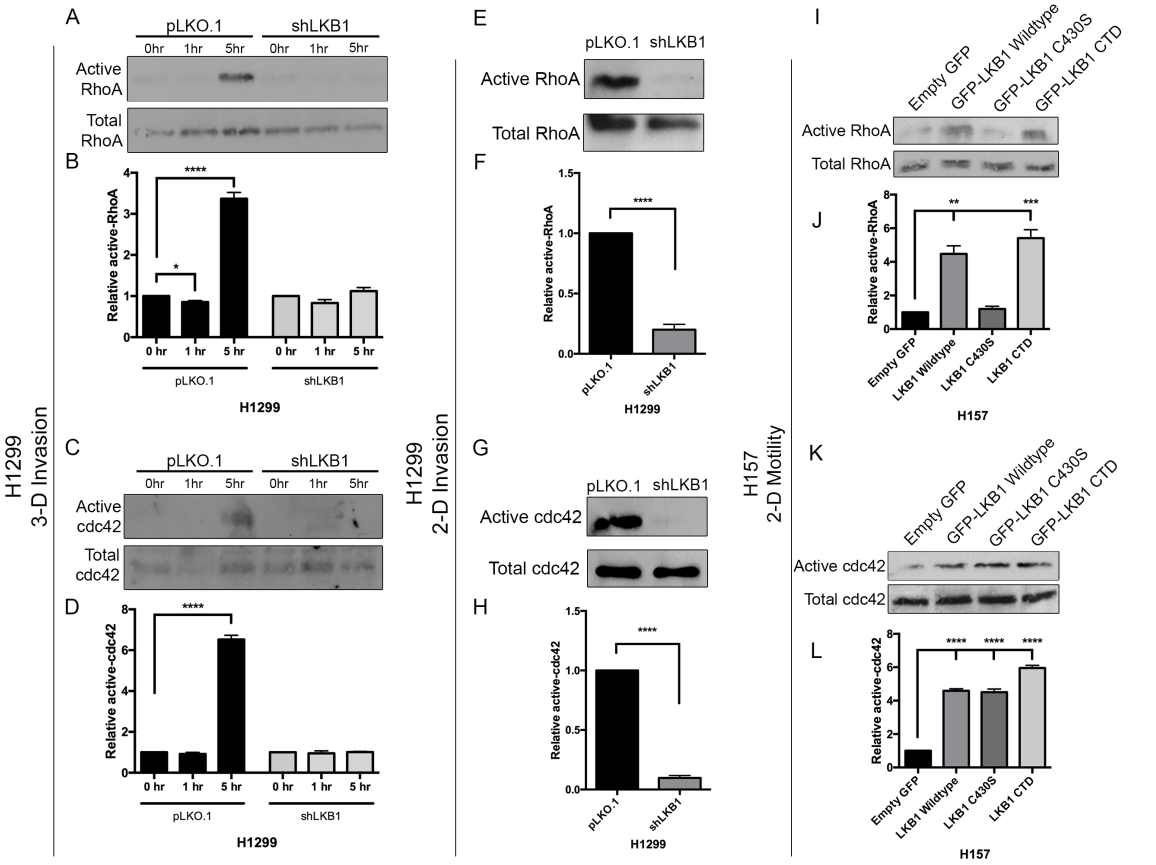

Figure 3.9: LKB1 differentially regulates RhoA and cdc42. (A) Representative western blot showing RhoA activity assay over time in pLKO.1 and shLKB1 H1299 cells embedded in a collagen type I matrix. (B) Densitometry of western blot from (A) normalized to total RhoA levels. (C) Representative western blot of a cdc42 activity assay over time in pLKO.1 and shLKB1 H1299 cells embedded in a collagen type I matrix. (D) Densitometry of western blot from (C), normalized to total cdc42 levels. (E) Representative western blot showing RhoA activity assay in 2-D in pLKO.1 and shLKB1 H1299 cells. (F) Densitometry of western blot from (E), normalized to total RhoA levels. (G) Representative western blot showing cdc42 activity assay in 2-D in pLKO.1 and shLKB1 H1299 cells. (H) Densitometry of western blot from (G), normalized to total cdc42 levels. (I) Representative RhoA activity assay of H157 cells stably expressing either empty GFP control or GFP-tagged: wildtype LKB1, LKB1 C430S, or the LKB1 C-terminal domain. (J) Densitometry of western blot from (I), normalized to total RhoA levels. (K) Representative western blot showing a cdc42 activity assay of H157 cells stably expressing either empty GFP control or GFP-tagged: wildtype LKB1, LKB1 C430S, or the LKB1 C-terminal domain. (L) Densitometry of western blot from (K), normalized to total cdc42. n=3 experiments. *=p≤0.05, **=p≤0.01, ***=p≤0.001, ****=p≤0.0001.

To further probe this finding, we tested the hypothesis that inhibition of FAK activity will specifically inhibit shLKB1 amoeboid cell invasion due to the aberrantly active $pFAK^{Y397}$ levels. We first transiently knocked down FAK via targeted siRNA and found that FAK knockdown completely abolished invasion in the H1299 shLKB1 cells (Figure 3.14). To address how FAK activity alters cell morphology and motility specifically in LKB1-depleted cells, we pharmacologically inhibited FAK. H1299 pLKO.1 and shLKB1 spheroids were exposed to 1μM of FAK inhibitor PF-573228 and assayed for invasion over time using live cell imaging. Inhibition of FAK did result in a significant decrease in the total shLKB1 cells invaded when compared to DMSO control, decreasing from about 65 cells/spheroid to 35 cells/spheroid after 16h of invasion (Figure 3.16A). In contrast, the FAK inhibitor had no significant impact on the total cells invaded in pLKO.1 spheroids (Figure 3.16A), suggesting these cells are less dependent on adhesion during invasion. Importantly, using 1μM FAK inhibitor did not completely abolish invasion in the shLKB1 cells as siRNA treatment did, thus allowing for further analysis of cell motility features in the presence of inhibitor. Interestingly, it was specifically the velocity of LKB1-depleted amoeboid cells that was significantly inhibited by exposure to FAK inhibitor (Figure 3.15B). The velocity of shLKB1 amoeboid cells in the presence of PF-573228 was equivalent to the velocity of pLKO.1 amoeboid cells, suggesting that increased FAK activity provides LKB1-depleted amoeboid cells an advantage of faster motility during invasion. Additionally, while FAK inhibition specifically impacts the velocity of shLKB1 amoeboid cells, it had no significant impact on cell shape (Figure 3.16C). These data taken together suggest that amoeboid cells lacking LKB1 expression represent an atypical

population of rounded cells that utilize adhesion signaling for invasion through the collagen gel.

LKB1 loss causes an increase in collagen remodeling during 3-D invasion

Since we show that LKB1 loss results in a unique amoeboid cell population, we wanted to determine if this provides an invasive advantage while navigating the microenvironment. To do this we performed multiphoton imaging on H1299 pLKO.1 and shLKB1 spheroids to visualize collagen remodeling and its relationship to cell type and invasive potential. LKB1 loss resulted in an increase in collagen alignment at 6 and 21 hours (Figure 3.17A). We used a novel local alignment coefficient to quantify the heterogeneous alignment patterns. CT-FIRE (curvelet transform fiber extraction) software was utilized to extract collagen fibers (7Bi,ii). All fibers were quantized with a 5-pixel length. Then for every pixel, we measured the local alignment coefficient parameter for every pixel by selecting all fiber segments within a circular neighborhood of 20 pixels (Figure 3.17Biii) to generate the alignment field (Figure 3.18 explains optimization of local alignment coefficient calculation). Using this parameter, histograms of local alignment coefficients, surface plots, and contour plots are generated to quantify alignment (Figure 3.17C). Using this quantification of the local alignment coefficient and comparing back to the 0 hour baseline value, we found that at 6 hours, shLKB1 cells show an increase in collagen alignment, which is further accentuated at 21 hours; on the other hand, pLKO.1 control cells result in a decrease in the number of aligned fibers over time (Figure 3.17D), suggesting that LKB1 may actually negatively regulate remodeling during invasion. Thus, LKB1-depleted cells are more efficient at re-aligning collagen fibers as they invade. Interestingly, this

realignment of the collagen matrix seems to be occurring via a matrix metalloproteinase (MMP)-independent mechanism. When treated with the pan-MMP inhibitor GM6001, shLKB1 show no significant change in invasion when compared to vehicle control (Figure 3.19). These data suggest that LKB1 loss promotes collagen remodeling in an MMP-independent manner.

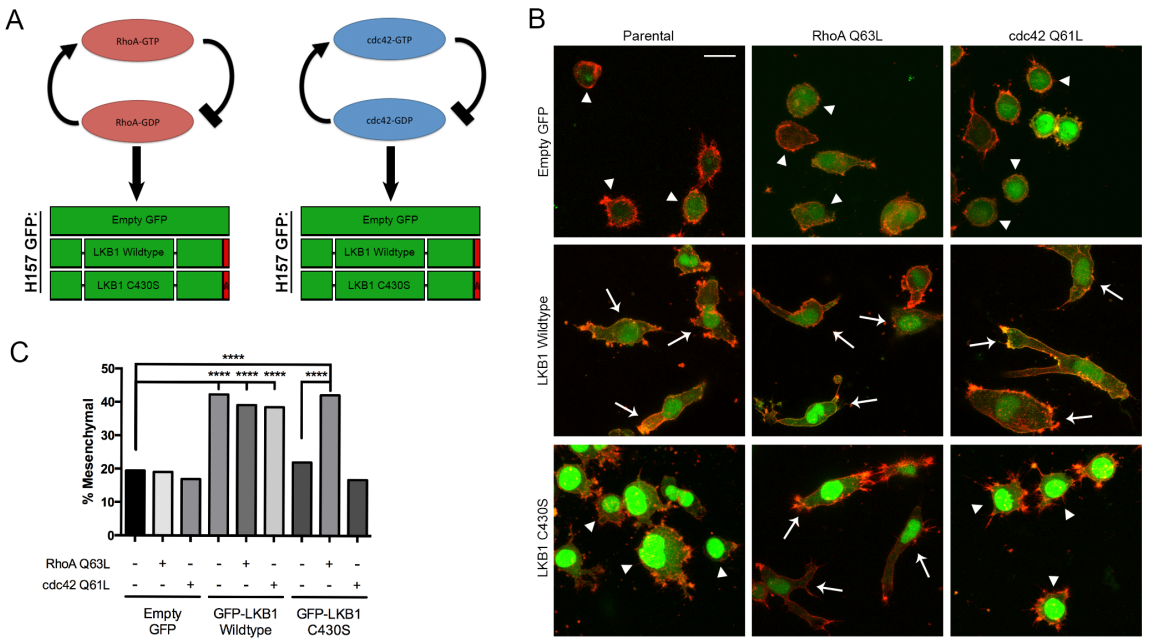

Figure 3.10: Constitutively active RhoA restores mesenchymal polarity in LKB1 farnesylation-mutant cells. (A) Schematic of double-stable cell lines expressing either empty GFP control or GFP-tagged: wildtype LKB1 or LKB1 C430S, with constitutively active RhoA (Q63L) or cdc42 (Q61L). (B) Spheroids of H157 cells expressing either empty GFP control or GFP-tagged: wildtype LKB1 or LKB1 C430S, and spheroids of these cells also expressing constitutively active RhoA or cdc42, were embedded in a collagen type I matrix. 24 hours post-embedding cells were fixed and stained with phalloidin. Amoeboid and mesenchymal morphologies (described in Figure 1) were quantified as a percentage back to the total number of cells invaded in each spheroid. n=4 spheroids. Scale=20 μm. Arrows=mesenchymal cells, arrowheads=amoeboid cells. n=30 cells. ****=p≤0.0001

LKB1 kinase activity represses collagen remodeling through regulation of FAK activity

We next wanted to test the hypothesis that LKB1 kinase activity represses collagen remodeling, therefore we assessed collagen remodeling and invasion in the H157 cells stably expressing various LKB1 domains or mutants. At 24 hours, H157 empty GFP invading cells show epicenters of significant collagen alignment (Figure 3.20Ai), whereas cells expressing either LKB1 wildtype or LKB1 C430S show significantly less alignment (Figure 3.20Aii, iii). However, cells expressing either the K78I kinase dead LKB1 or the K78I-C430S double mutant LKB1 fail to repress alignment (Figure 3.20Aiv,v), suggesting that kinase activity is required for collagen remodeling. Quantification of alignment shows that empty GFP, LKB1 K78I, and LKB1 K78I-C430S cells have increased alignment coefficients when compared to those cells expressing LKB1 wildtype or C430S (Figure 3.20B).

MARK1 was then transiently knocked down via siRNA in H157 LKB1 wild-type cells to determine if LKB1 kinase activity signals through MARK1 to repress FAK activity. Cells lacking MARK1 phenocopy LKB1-depleted cells, showing increased remodeling when compared to scrambled siRNA control (Figure 3.21A). This remodeling can be inhibited by treating H1299 shLKB1 cells with PF-573228 FAK inhibitor (Figure 3.19), supporting the concept that FAK activity is required for the increase in manipulation of the collagen gel. These data point to the LKB1-MARK1-FAK pathway for regulating collagen remodeling as cells invade.

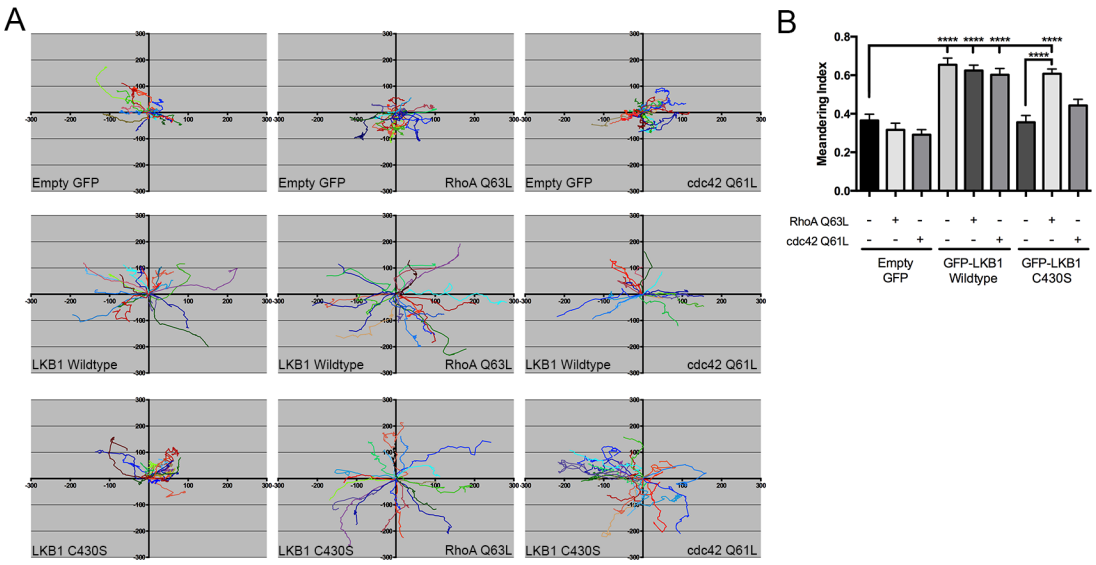

Figure 3.11: Constitutively active RhoA restores directional persistence in LKB1 farnesylation-mutant cells. (A) Each cell line from Figure 3.10B was tracked over time. Cell tracks were plotted from a single point of origin. (B) Meandering index was calculated using the cell tracks from (A). Meandering index is defined as the linear distance divided by the total path length. n=30 cells. ****=$p \leq 0.0001$

We next reasoned that since the LKB1-depleted amoeboid cells have high levels of FAK activity, even compared to wild-type amoeboid cells, perhaps these cells also can remodel collagen. This would be unlike typical amoeboid cells, which in general do not remodel collagen [152, 153]. To test this, we acquired images of single amoeboid cells within the H157 cells expressing different LKB1 domains and mutants. Surprisingly, H157 empty GFP invading amoeboid cells were associated with high collagen alignment (Figure 3.21B, arrows). In contrast, H157 amoeboid cells with wild-type LKB1 do not show local collagen alignment. The LKB1 K78I mutant was similar to the GFP control, indicating that LKB1 kinase activity is required to suppress local collagen alignment. Re-expression of the LKB1 C430S mutant was similar to LKB1 wildtype cells and showed no local alignment in amoeboid cells, again indicating that LKB1 kinase activity but not farnesylation is important for collagen remodeling. These data show that amoeboid cells lacking LKB1 kinase activity boast the invasive advantage of remodeling a 3-D collagen matrix, which does not typically occur in amoeboid motile cells.

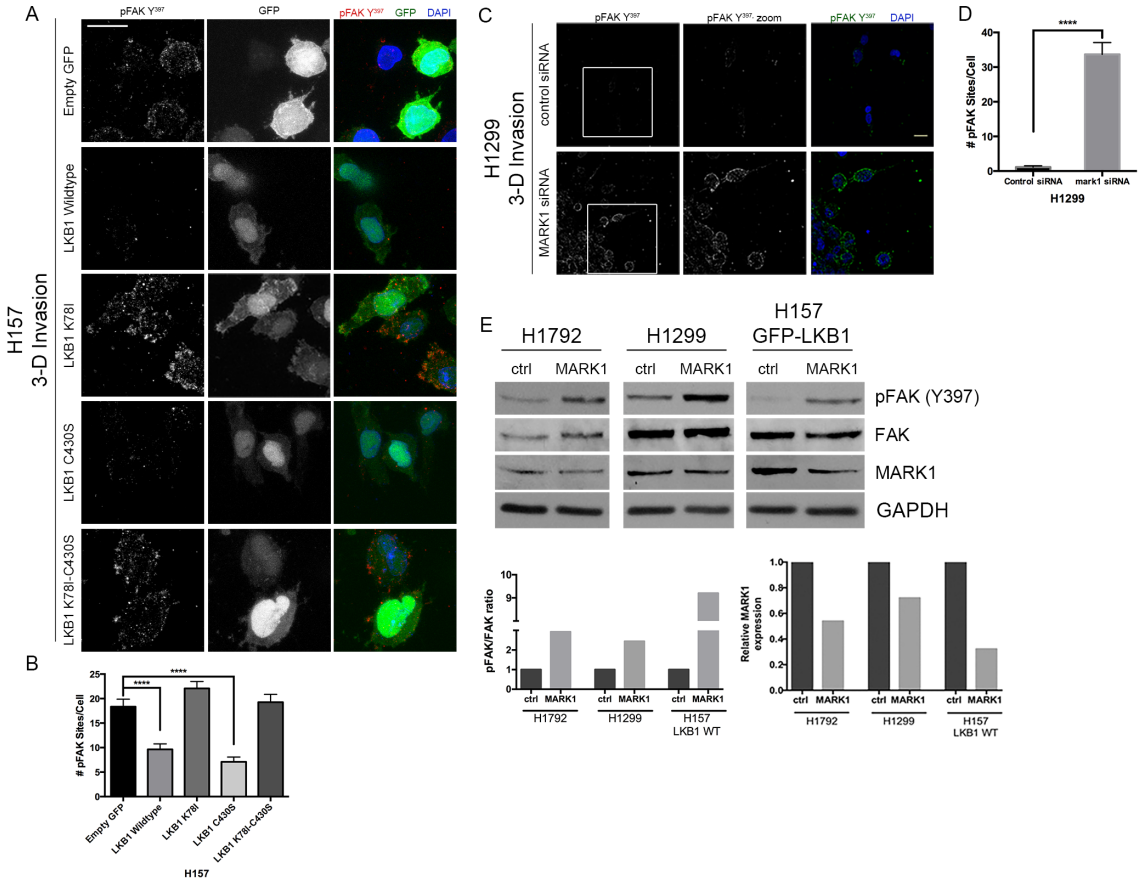

Figure 3.12: LKB1 regulates pFAK activity through its kinase domain. (A) Spheroids of H157 cells stably expressing either empty GFP control or GFP-tagged LKB1 constructs embedded in a collagen type I matrix. After 24 hours, cells were fixed and stained by immunofluorescence for pFAK^{Y397}, GFP, and DAPI. (B) Total number of pFAK^{Y397} sites for each experimental group in (A) were quantified. (C) Expression of pFAK^{Y397} was examined by immunofluorescence of spheroids after 24hrs of invasion. DAPI was used to stain the nuclei of the cells. (D) The total number of pFAK^{Y397} sites per cell was quantified from the images obtained in (C). ****=p≤0.0001. (E) Western blot showing pFAK^{Y397} expression after MARK1 siRNA depletion in H1792, H1299, and H157 LKB1 WT cells compared to scrambled control siRNA. GAPDH was used as a loading control. Densitometry analysis of phospho to total FAK ratio (left) and relative MARK1 expression (right) in control siRNA and MARK1 siRNA treated cells are shown below.

3.6 Discussion

The functional diversity of LKB1 has been attributed to it phosphorylating 14 members of the AMPK family of proteins, which, when activated, go on to regulate a diverse set of biological processes [94, 114, 146]. However, multiple reports show a kinase-independent function of LKB1 that is linked to cell polarity [123, 154]. Since a majority of the truncating mutations [15] (~72% of *LKB1* mutations in lung adenocarcinoma patients, Figure 3.4A) would predictably disrupt its kinase activity and remove its C-terminal domain, we sought to uncouple defects in CTD function from defects in kinase function in the context of cancer cell invasion. These results support an overall model whereby the LKB1 CTD regulates cell polarization through a mesenchymal-amoeboid cell switch, while the kinase domain regulates FAK-based cell adhesion during invasion. These results would suggest that when both kinase activity and CTD function are compromised, both aberrant cell polarity and adhesion programs would ensue. Our data indicates that this is indeed the case; complete LKB1 depletion creates a uniquely invasive, amoeboid shaped cell that, in contrast to typical amoeboid cells [23, 155, 156], maintains a hyperactive FAK-based cell adhesion program and remodels collagen. We speculate that truncating mutations in *LKB1* mutant patients may create a similar scenario (Figure 3.22), where both CTD and kinase function is disrupted, leading to increased invasiveness by creating an agile cell that can be amoeboid, adherent, and able to navigate the tumor microenvironment.

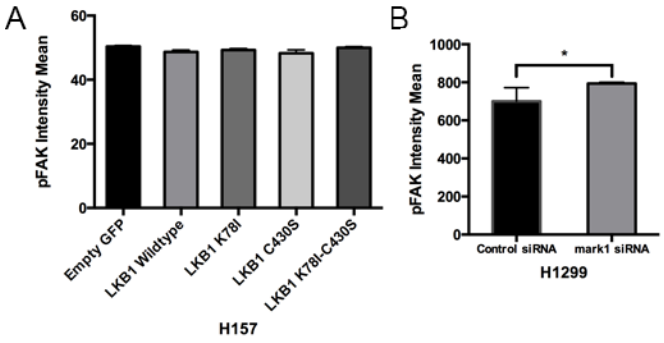

Figure 3.13: Individual pFAK site intensity mean exhibits little to no difference between LKB1 domains and a MARK1 knockdown phenocopying of these domains. (A) Individual pFAK site intensity mean in H157 cells re-expressed empty GFP control or GFP-tagged LKB1. (B) Individual pFAK site intensity mean in H1299 cells after MARK1 knockdown. *=$p \leq 0.05$.

Our results show that specifically LKB1 CTD farnesylation is required for proper polarization during invasion, such that when farnesylation is intact, cells are more mesenchymal, while cells revert to an amoeboid morphology upon loss (Figure 3.5A, B). This suggests that LKB1 membrane localization drives proper cell polarization and controls a mesenchymal-amoeboid morphological switch. Since LKB1 loss leads to inactivation of the small Rho-GTPases RhoA and cdc42 [104, 105, 112] (Figure 3.9A-H), we probed this observation and show that while the LKB1 CTD alone is capable of activating both RhoA and cdc42, LKB1 farnesylation is critical only for the activation of RhoA (Figure 3.9I-L), suggesting a prenylation-independent regulation of cdc42. Similarly, a constitutively active RhoA, but not cdc42, can rescue mesenchymal polarization upon LKB1 farnesylation defects (Figure 3.10B), again supporting a role for RhoA but not cdc42 in promoting mesenchymal polarization. Interestingly, it appears a region of LKB1 is necessary to rescue polarity defects in these cells, as restoring RhoA activity in empty GFP control cells fails to restore mesenchymal polarity. Previous studies show that LKB1 regulates p114RhoGEF to promote RhoA activity (Xu et al., 2013), and thus we propose that LKB1 CTD farnesylation anchors LKB1 into the membrane to promote this activity. It has always remained unclear as to why LKB1 loss would inactivate RhoA and cdc42 signaling [104, 105, 112], since it would be expected that LKB1 loss, which causes increased invasion [124, 157], would instead hyperactivate RhoA and cdc42. However, recent studies show RhoA loss-of-function driver mutations in gastric cancer [158, 159], suggesting that inactivation of RhoA, and perhaps cdc42, could in fact be drivers of tumor progression.

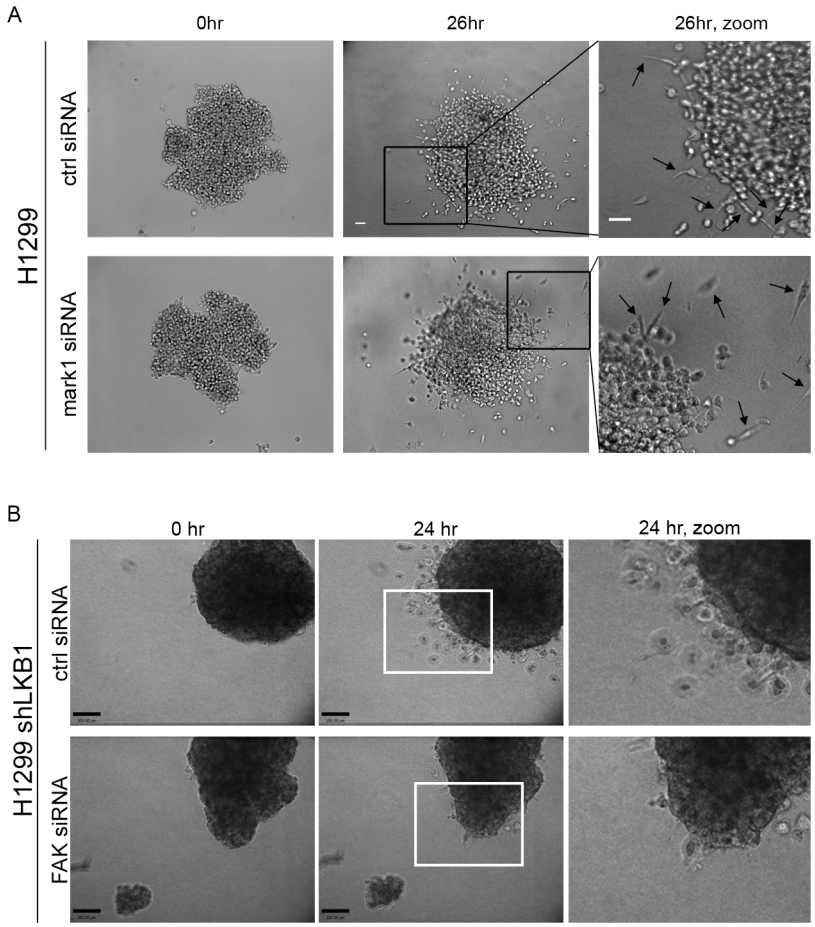

Figure 3.14: MARK1 knockdown does not impact invasive morphology, while FAK knockdown abolishes invasion in LKB1-depleted cells. (A) MARK1 was knocked down via targeted siRNA in H1299 cells (LKB1 wildtype). Scrambled siRNA was used as a negative control. Spheroids formed from control or MARK1 siRNA were embedded in a collagen matrix and imaged after 0 and 26 hours of invasion time. Zoomed images are shown on the right. Scale = 50μm. Arrows = mesenchymal cells. (B) H1299 shLKB1 cells were treated with either scrambled siRNA control or FAK targeted siRNA. Spheroids formed from these cells were then embedded in a collagen matrix and imaged at 0 and 24 hours post-embedding. Zoomed images are shown on the right. Scale = 100 μm.

We show that LKB1 is a repressor of adhesion signaling and collagen remodeling where intact kinase activity is required to maintain normal FAK levels (Figures 3.12, 3.15, 3.16, 3.17, 3.20, 3.21). Restoration of LKB1 kinase activity in LKB1-deficient cells is sufficient to repress FAK-positive adhesion sites and collagen remodeling (Figure 3.12A, B). Depletion of the LKB1 kinase target, MARK1, is sufficient to phenocopy this finding (Figure 3.12D, E), and these data are consistent with previous findings that highlight LKB1 as a FAK repressor [115, 117] through its kinase-dependent activation of MARK1 [116]; though our previous data also suggest that the LKB1 NTD alone can also repress FAK, suggesting a potential dual mechanism for interacting with and controlling FAK activity. Our data also builds on the LKB1-MARK1 signaling pathway by showing that it regulates collagen remodeling during invasion in a FAK-dependent manner (Figures 3.20, 3.21). LKB1 regulates lysyl oxidase (LOX), a collagen crosslinking enzyme, through the mTOR/HIF-1α signaling pathway [140], where LKB1 loss leads to increased LOX expression and collagen deposition [140, 160]. Potentially, these two pathways are linked or related through FAK, since LOX is responsible for hypoxic human cancer cell invasion through FAK activity and cell-matrix adhesion [161].

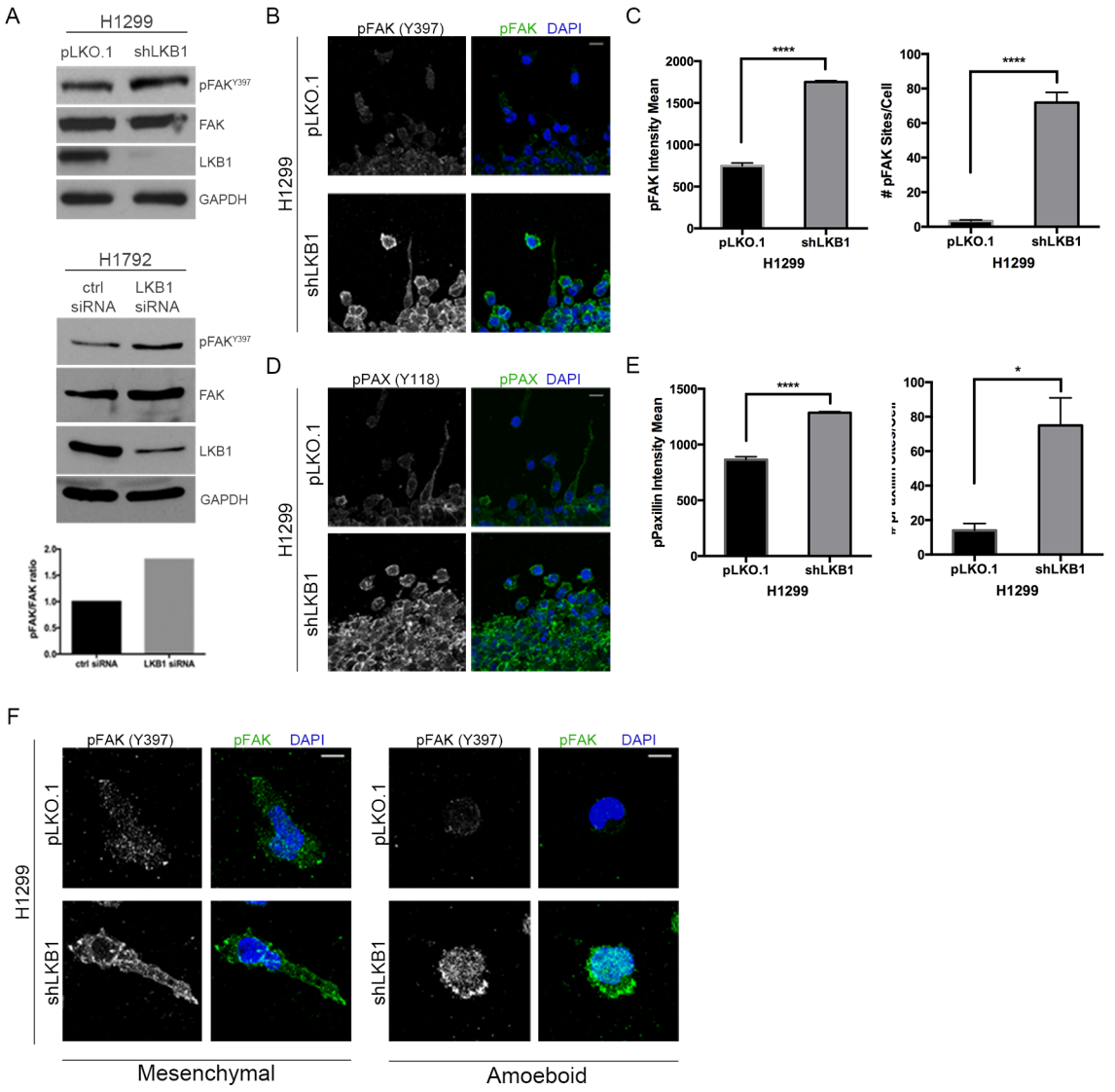

Figure 3.15: LKB1-depleted amoeboid cells are dependent on pFAK during invasion. (A) Western analysis of pFAK^{Y397} expression in H1299 pLKO.1 and shLKB1 cells (top). A similar experiment was performed in H1792 LKB1 siRNA treated cells (below). Bar graph shows densitometry of the phospho to total FAK ratio in the H1792 LKB1 knockdown cells as compared to control siRNA. (B) H1299 pLKO.1 and shLKB1 spheroids were analyzed for expression of pFAK^{Y397} using immunofluorescence imaging. Scale=20 μm. (C) Quantification of pFAK^{Y397} site intensity (left) and total number of pFAK^{Y397} sites per cell (right). (D) Activity of downstream FAK signaling was analyzed using immunofluorescence imaging of pPAX^{Y118} in H1299 pLKO.1 and shLKB1 spheroids. Scale=20 μm. (E) Quantification of pPAX^{Y118} site intensity (left) and total number of pPAX^{Y118} sites per cell (right). (F) Zoomed images of pFAK immunofluorescence imaging (described in B). Mesenchymal and amoeboid cell types in H1299 pLKO.1 and shLKB1 are shown. Scale=10 μm. n=5-6 spheroids. *=p≤0.05, ***=p≤0.001, ****=p≤0.0001.

In contrast to classical amoeboid cell motility, LKB1-depleted amoeboid cells lack Rho-GTPase activity, have high FAK activity, and still remodel collagen (Figures 3.9, 3.12, 3.15, 3.16, 3.17, 3.20, 3.21). Classical amoeboid cells do not generally make sustained contacts with the extracellular matrix and do not remodel collagen fibers as they move; instead, their motility is dependent upon squeezing through and deforming the matrix during invasion [23, 152, 155, 156, 162]. Additionally, RhoA is frequently implicated in amoeboid invasion by promoting ROCK-mediated myosin light chain (MLC) phosphorylation to promote actomyosin contractility required for cell blebbing during invasion [107, 108, 163-165]. In contrast, amoeboid cells lacking LKB1 activity have reduced RhoA activity, and instead, restoring RhoA in LKB1-depleted cells promotes a mesenchymal, polarized cell (Figure 3.10B, C). Therefore, we propose that LKB1 inactivation in both its kinase domain and CTD disrupts cell polarity and adhesion signaling, resulting in a uniquely invasive cell that is adhesive, amoeboid in shape, and remodels collagen, but may only represent an amoeboid cell in shape rather than the underlying molecular biology.

In vivo studies highlight the importance of LKB1 as a metastasis suppressor. In a seminal publication, LKB1 function was assessed using a *Kras*^{G12D}-driven genetically engineered mouse model (GEMM) of lung cancer [87]. In this model, *Lkb1* inactivation in mutant *Kras* tumors led to increased tumor burden, shortened survival time, and increased metastasis compared to *Kras* mutant-only mice. Furthermore, these mice have hyperactive FAK [117], similar to that described in our 3-D model here. It remains difficult to assess polarity during invasion in an *in vivo* model to determine if these cells have polarity defects

as well; however, future imaging of living lung tissue slices could shed light on this. Additionally, given that LKB1 serves as the upstream regulator of AMPK (5' AMP-activated protein kinase) in the energy stress response pathway [89], the interplay between defects in metabolic signaling, adhesion, and cell polarity remains unclear in the context of lung cancer metastasis.

Taken together, our data support a model whereby LKB1 kinase-dependent and -independent functions have separate roles in regulating various cellular processes during cancer cell invasion that when lost, synergize to create an uniquely-invasive cell. Thus, we speculate that loss of both LKB1 kinase activity and the CTD, which predictably occurs in lung adenocarcinoma patients with LKB1 truncating mutations, results in an aberrantly polarized and adhesive cell population that is superior at navigating the microenvironment during invasion.

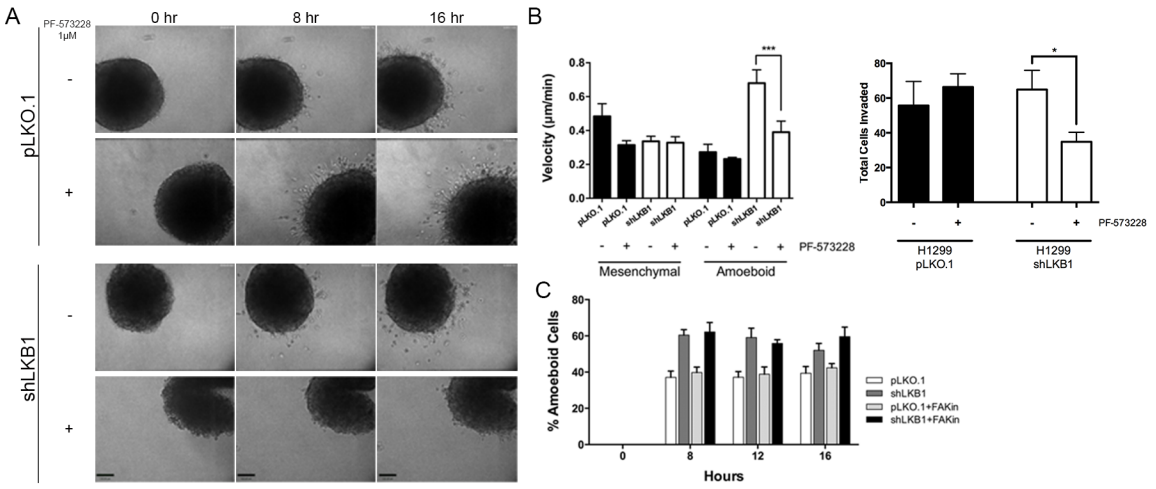

Figure 3.16: FAK inhibition in LKB1-depleted cells disrupts invasion. (A) Still images of the live cell imaging experiment were taken every 8hrs. Quantification of total cells invaded shown below shows significantly decreased cells invaded in shLKB1 cells treated with FAK inhibitor. Scale=100 μm (B) Cell tracks from the FAK inhibitor experiment showed that LKB1-depleted amoeboid cells have a significantly decreased velocity during invasion as compared to vehicle control. n=8-15 cells. (C) The percentage of amoeboid cells in the live cell FAK inhibitor experiment was assessed at 0, 8, 12, and 16 hours. n=5-6 spheroids. *=$p \leq 0.05$, ***=$p \leq 0.001$, ****=$p \leq 0.0001$.

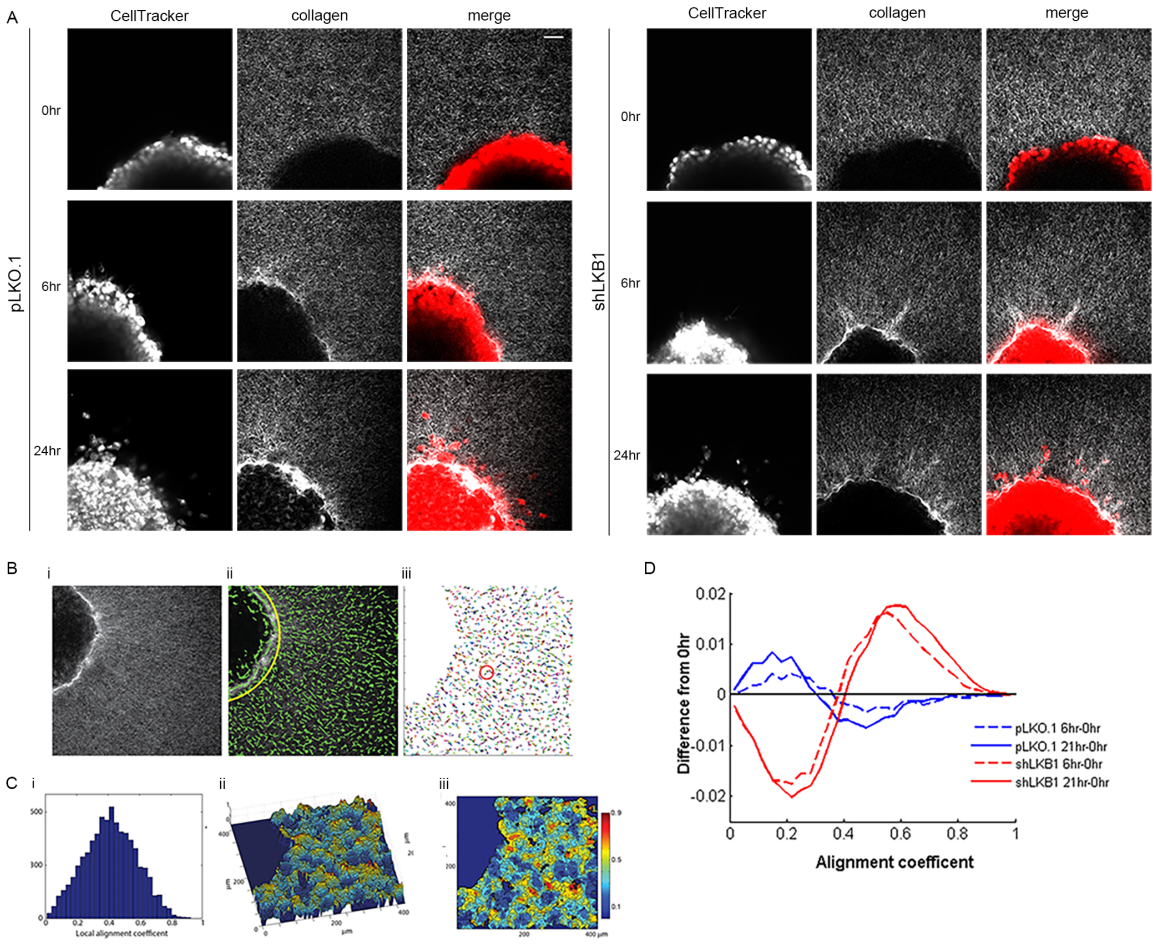

Figure 3.17: Loss of LKB1 results in increased collagen remodeling during invasion. (A) H1299 pLKO.1 and shLKB1 spheroids and the collagen matrix were imaged using second harmonic generation microscopy. Spheroids were dyed using CellTracker Red in order to visualize cells during invasion. Images were obtained at 0, 6, and 21 hours post-embedding. Scale=50 μm. (B) Images from A were quantified using collagen alignment analysis. A single z-stack image (i) is used in CT-FIRE software to extract collagen fibers (green, ii). The software automatically determines various fiber lengths in the image, represented as different line colors (iii). Yellow line represents the manually selected tumor boundary. (C) i) Example histogram generated via CT-FIRE analysis of collagen alignment coefficients. ii) Surface and iii) contour plots of local alignment show topography of alignment patterns. (D) Alignment analysis was performed as described in B,C for H1299 pLKO.1 (blue) and shLKB1 (red) spheroids at 6 and 21 hours, with the 0 hour baseline alignment subtracted to remove any initial bias.

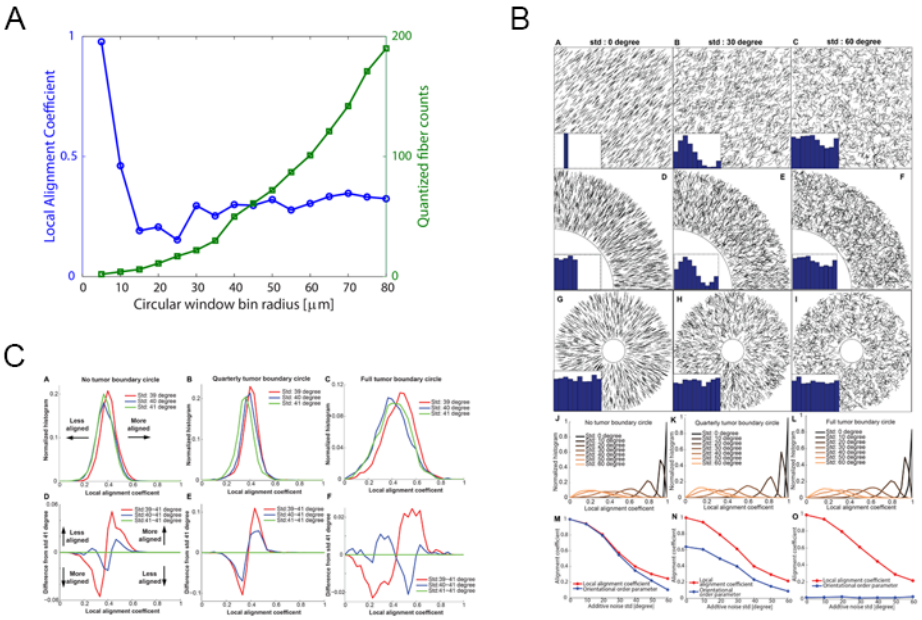

Figure 3.18: Optimization of the local alignment coefficient for quantifying heterogeneous collagen alignment. (A) Local alignment coefficient and quantized fiber counts for various circular window bin using figure 7Biii. (B) For each simulation, a line presents a fiber. Three different test cases were considered: collagen fibers without any tumor boundary (A-C), with a quarterly tumor boundary circle, located at the lower left corner of the box (D-F), with a tumor boundary circle, located at the center of the box (G-I). Inset figures show fiber angular histogram from 0-180^o (A-C, G-I) or 0-90^o (D-F). Aligned fibers are disturbed by adding an angle, sampled from normal distribution, where the mean is zero and standard deviation (std) is 30^o (B, E, H), and 60^o (C, F, I). Local alignment coefficient distribution for 7 std degree values for no tumor boundary circle (J), quarterly tumor boundary circle (K), and full tumor boundary circle (L). The average value of the local alignment coefficient and the orientational order parameter value for 7 std degree values for no tumor boundary circle (M), quarterly tumor boundary circle (N), and full tumor boundary circle (O), as compared to the orientational order parameter. (C) The local alignment coefficient distribution for 3 std degree values (39^o, 40^o, 41^o) for no tumor boundary circle (A), quarterly tumor boundary circle (B), and full tumor boundary circle (C). The difference curve of local alignment coefficient distribution from the baseline distribution curve (std 41^o) for three different std degree values for no tumor boundary circle (D), quarterly tumor boundary circle (E), and full tumor boundary circle (F).

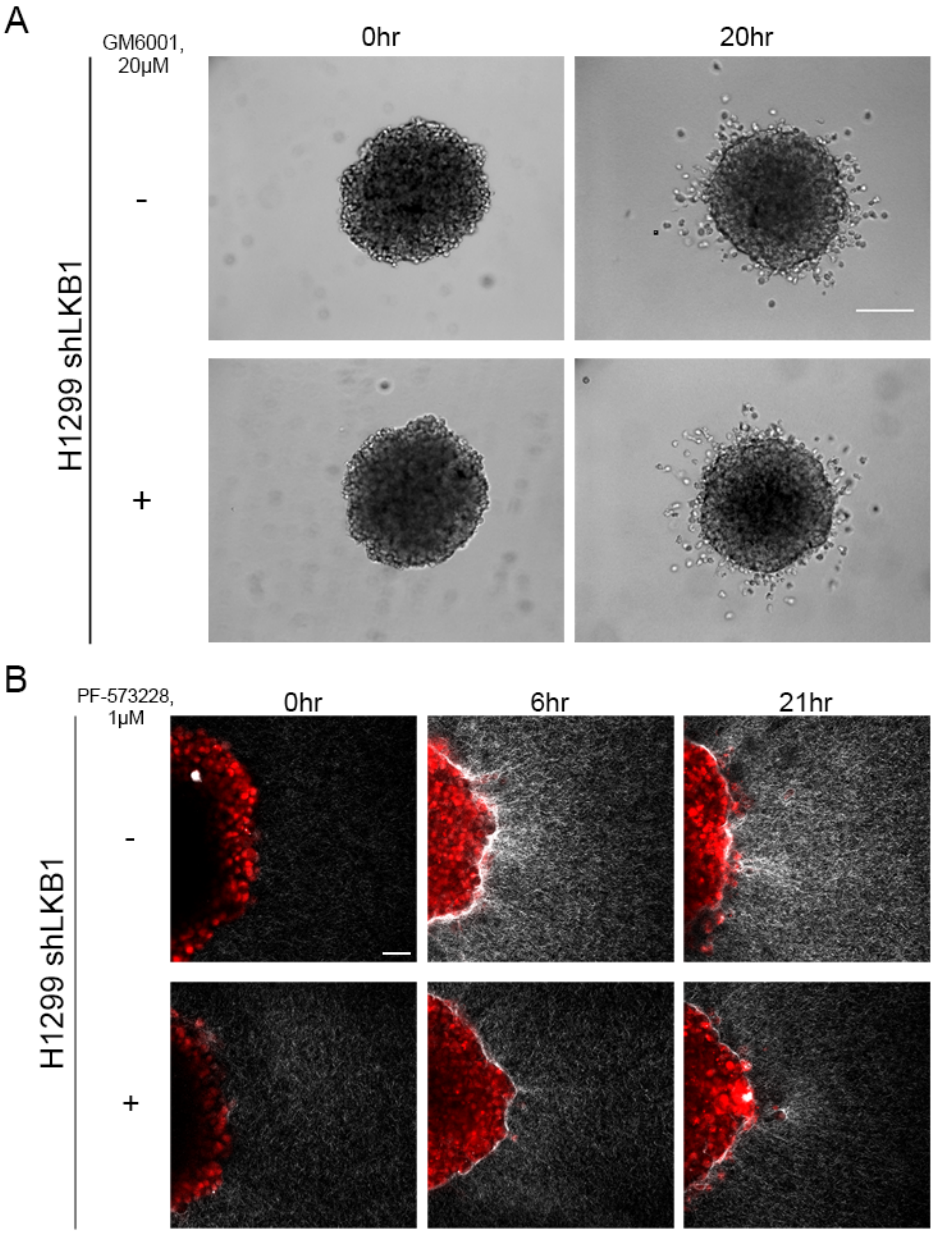

Figure 3.19: Pharmacological inhibition of MMPs does not impact collagen invasion, whereas FAK inhibition decreases collagen remodeling in LKB1-depleted cells. (A) H1299 shLKB1 spheroids were embedded in collagen in the presence of either DMSO control or 20μM of the pan-MMP inhibitor GM6001. Images were taken at 0 and 20 hours post-embedding. Scale = 100μm. (B) H1299 shLKB1 spheroids were dyed with CellTracker Red to visualize invading cells and embedded in a collagen matrix. The spheroids were imaged using SHG imaging in the presence of either DMSO vehicle control or 1μM FAK inhibitor PF-573,228. Images were taken at 0, 6, and 21 hours. Scale=50 μm.

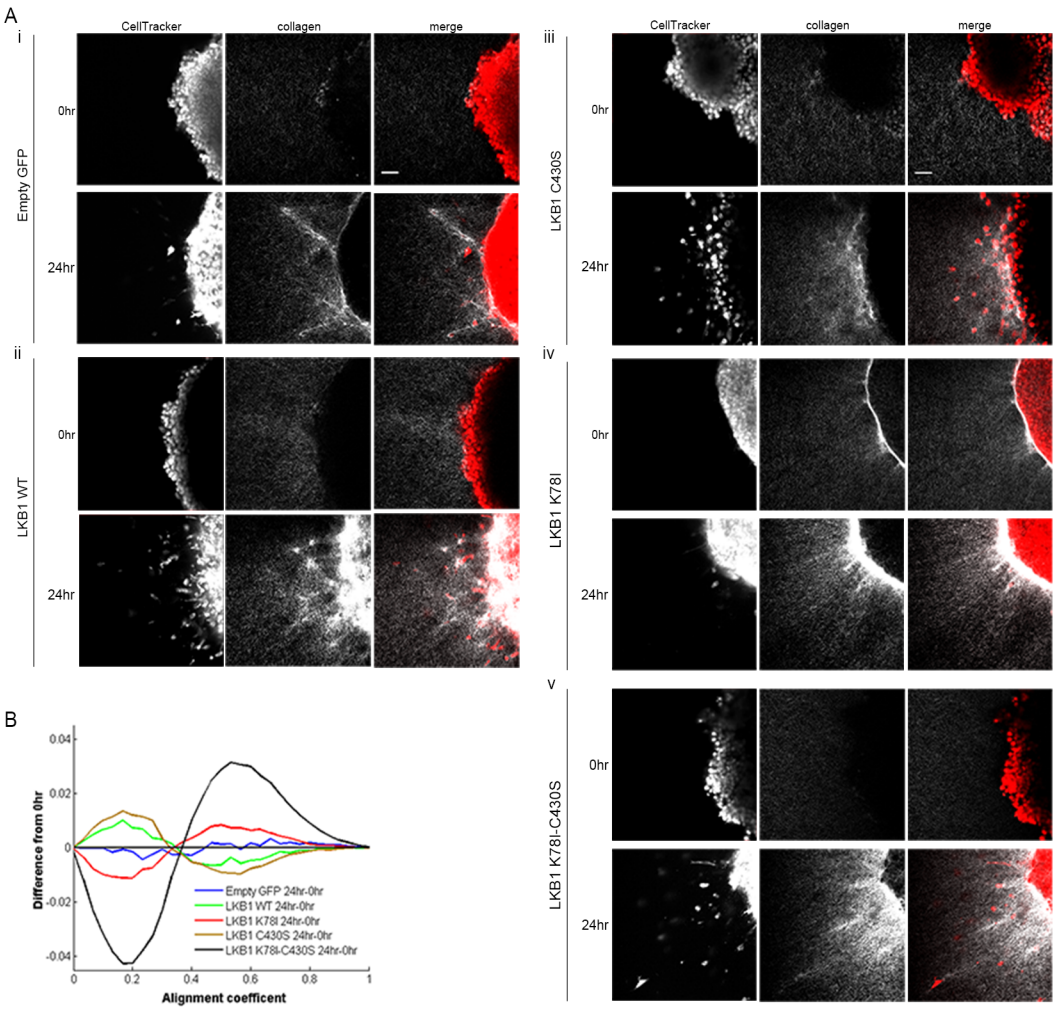

Figure 3.20: Kinase activity of LKB1 represses collagen remodeling. (A) Multiphoton imaging was performed at 0 and 24 hours to visualize collagen using H157 stables with the following LKB1 constructs: Empty GFP control, LKB1 WT, LKB1 C430S (farnesylation mutant), LKB1 K78I (kinase dead), and LKB1 K78I-C430S. (B) Images obtained in A were quantified for collagen alignment using CT-FIRE image analysis. Arrow = amoeboid cell that remodels collagen, arrowhead = amoeboid cell that does not remodel collagen. Scale = 50 μm.

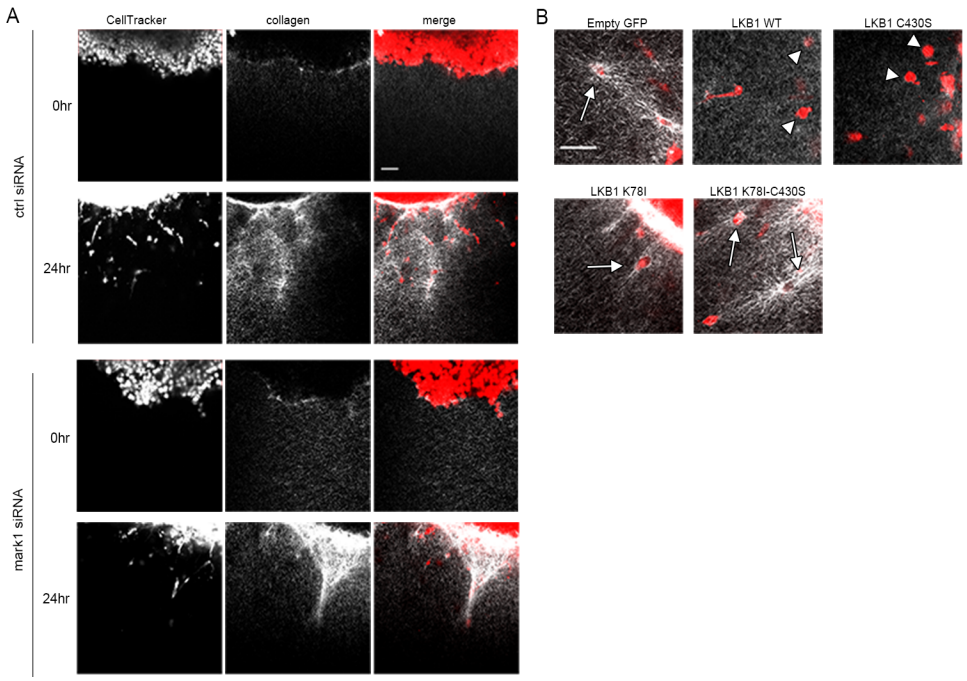

Figure 3.21: Kinase activity of LKB1 represses collagen remodeling over multiple cell types. (A) Collagen SHG imaging of MARK1 siRNA depleted H157 LKB1 wildtype stable cells compared to scrambled siRNA. (B) Zoomed images showing collagen and single invading cells. Arrow = amoeboid cell that remodels collagen, arrowhead = amoeboid cell that does not remodel collagen. Scale = 50 μm.

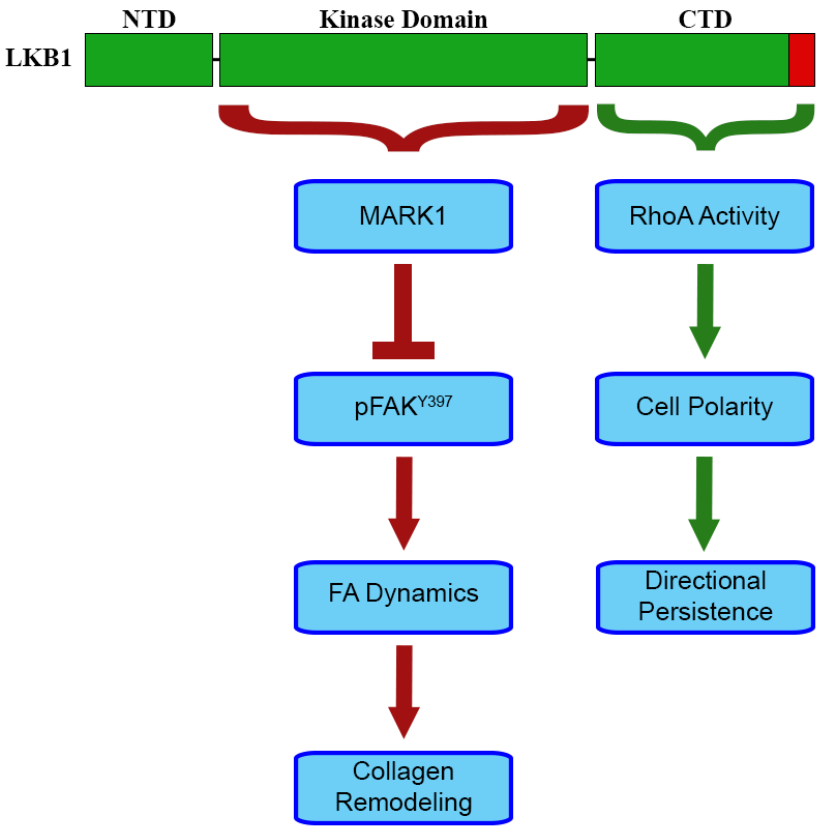

Figure 3.22: Model Figure. LKB1 provides kinase-dependent and -independent mechanisms of regulating cell polarity during invasion. Through the LKB1 C-terminal domain (CTD) and its farnesylation, LKB1 activates the Rho-GTPase RhoA to promote mesenchymal polarization and strong directional persistence during invasion. Independent of its CTD, LKB1 kinase activity phosphorylates MARK1 to repress the active form of focal adhesion kinase (pFAK), leading to regulation of focal adhesion dynamics and collagen remodeling during 3-D invasion.

3.7 Acknowledgements

We thank Stefan Kaluz for his assistance with cloning, the Emory Integrated Cellular Imaging Core for their assistance with microscopy, and the Emory Custom Cloning Core Facility for providing GFP-tagged plasmids. JK is supported by the National Institutes of Health under Ruth L. Kirschstein National Research Service Award 1F31CA180511. SW is supported by the National Institutes of Health under Ruth L. Kirschstein National Research Service Award 1F31CA200383-01. SW was previously supported by a National Science Foundation Graduate Research Fellowship under Grant No. DGE-0940903. SW and JK are partially supported by Laney Graduate School. BL and YJ are supported partially by NIH/NCI: 1U01CA143069. WZ is supported by the National Cancer Institute (R01CA140571). This work was supported by the National Cancer Institute (1R01CA1428580, 1R01CA201340, 1R01CA194027) awarded to AIM. Research reported in this publication was supported in part by the Winship Cancer Institute and Emory Integrated Cellular Imaging Core and NIH/NCI under award number P30CA138292.

Chapter 4: General Discussion and Future Directions

Despite the immense time and resources contributed by scientists across the world for decades, cancer remains a disease that inspires fear across the globe. Although survival rates have increased over the last several decades[166], cancer still remains the second leading cause of death in the United States[1]. Further, while some cancers, including stomach and colorectal cancer, have seen increased survival rates over the past decade, other cancers, including liver and pancreatic cancer, are experiencing worsening survival trends over the past decade[166]. These data, together, indicate that while our understanding of the biological basis of cancer and how to treat it continues to grow, much work remains in understanding the intricate nuances of tumor development, ranging from signaling pathways to early steps in cell motility and invasion to factors inducing a disseminated metastatic lesion.

4.1 LKB1 in Lung Cancer

LKB1 is a dynamic tumor suppressive kinase that regulates multiple pathways in cellular metabolism, polarization, and motility. Early studies in Peutz-Jeghers Syndrome patients revealed mutations scattered throughout the entire gene, with a majority of mutations resulting in an abrogation of LKB1 kinase function[145, 167]. Since that time, LKB1 was identified as the upstream kinase of AMPK in the AMPK energy sensing pathway[69, 89, 94], and has since been identified as the upstream kinase for the 14 members of the AMPK family. Through its kinase function, LKB1 serves to regulate cellular metabolism, polarization, growth, and motility[168]. Independent of its kinase activity, LKB1 also drives actin stress fiber assembly[105] and cell polarization[100, 121]. Given the many

roles of LKB1 in regulating normal cellular function, the fact that LKB1 is frequently lost in non-small cell lung cancer (NSCLC)[15] presents a scenario in which these cancers would be expected to be more invasive and metastatic.

Although LKB1 appears to serve as a master tumor suppressor kinase, mice with LKB1 mutations alone do not form tumors[168], suggesting that LKB1 loss must coordinate with another frequently mutated gene to drive tumor growth. Similarly, when normal Kras function is disrupted with a G12D mutation, tumors form in the lung but with no metastatic lesions[169-171]. However, when LKB1 loss is combined with $Kras^{G12D}$, lung tumors form with a much more invasive phenotype, with a high tumor multiplicity and 61% of mice exhibiting distal metastases[87]. Together, these data indicate that LKB1 loss alone does not drive tumor development and invasion, but that its loss combined with that of the Kras oncogene activation coordinates to drive a more invasive cancer. Given that Kras is the second most commonly mutated gene in NSCLC[15], the combination of LKB1 loss and Kras mutation presents immense challenges to the successful treatment of lung cancer patients.

4.2 LKB1 Localization

LKB1 contains two nuclear localization signals (NLS) and one nuclear export signal (NES) to drive its subcellular localization. Upon its interaction with STRADα, LKB1 undergoes a conformational shift to expose its NES and export into the cytoplasm[60]. Previous studies examining Peutz-Jeghers Syndrome patients show mutations that disrupt the LKB1-STRADα interaction, resulting in a nuclear LKB1 that loses its kinase activity[80,

172]. We show that LKB1 farnesylation also appears to anchor its cytoplasmic localization, as disrupting the farnesylation results in a more nuclear LKB1 signal (Figure 2.4). Thus, LKB1 must interact with STRADα to export from the nucleus, but also must maintain its farnesylation to anchor into the membrane and maintain its cytoplasmic localization. Given that a majority of the LKB1 mutations seen in lung cancer are truncations[15], this would result in a loss of farnesylation and subsequent translocation to the nucleus, where LKB1 would no longer interact with STRADα and MO25 and theoretically exhibit reduced kinase activity[68], thus inhibiting several LKB1-mediated tumor suppression pathways in these cancer cells.

4.3 LKB1 and Actin Dynamics During Cell Motility

LKB1 has been shown to drive cell motility through a variety of different systems. In human epithelial cells, LKB1 re-expression is able to induce acinar actin caps in non-adherent cells[67], while in motile cells LKB1 rapidly translocates to the leading edge to associate with lamellipodial actin[112]. Further, LKB1 also promotes actin stress fiber assembly in a kinase-independent manner[105], again highlighting LKB1 as a regulator of actin dynamics. Although a clear connection has been made between LKB1 and the actin cytoskeleton, the functional significance of this association and consequences of LKB1 mutation in lung cancer remained largely unstudied.

Using HeLa cells, which are LKB1-null, we examined the role of LKB1 in associating with actin and regulating membrane dynamics. In Chapter 2, we further examined the role of LKB1 in promoting actin stress fiber assembly, and show that LKB1 promotes this

assembly through its C-terminal domain (CTD) in a farnesylation-dependent and kinase-independent manner (Figure 2.1). When examining this mechanism further, we identified that LKB1 activates RhoA, which then signals to ROCK to drive this stress fiber phenotype (Figures 2.2, 2.3). Importantly, when disrupting ROCK function with a ROCK inhibitor, the stress fiber phenotype is abrogated, placing LKB1 upstream of the RhoA-ROCK stress fiber pathway. These studies align strongly with other studies examining LKB1 in stress fiber development[105]. Given that stress fiber assembly and contraction in motile cells directly correlates with cellular motility, the loss of LKB1 in NSCLC would thus disrupt the LKB1-RhoA-ROCK pathway, suggesting this loss would result in disruption of regulated cell motility. Indeed, we identify that loss of either LKB1 farnesylation or kinase activity does alter regulated cell motility (Figures 2.13, 2.14), suggesting that the interaction between LKB1 and actin filament dynamics is critical for regulating directed motility. Although stress fibers exist in only a 2D environment rather than a more complex environment such as *in vivo* systems, this phenotype has a strong implication in tumor development. Stress fibers are historically thought to represent actomyosin contractility in *in vivo* systems. Thus, the loss of LKB1 in NSCLC patients would theoretically disrupt regulated actomyosin contractility during cell motility, potentially driving aberrant contraction and increased invasion throughout the tumor.

Our data on LKB1 regulating actin dynamics also highlighted the role of LKB1 in mediating membrane dynamics. Although LKB1 farnesylation drives its actin colocalization and stress fiber assembly, farnesylation appears to have limited impact on cellular membrane dynamics. Cellular membrane ruffling in two dimensions correlates

with adhesion and motility in more complex systems, allowing us to again examine the impact of LKB1 in regulating normal cellular function. When re-expressing either wildtype or farnesyl-mutant LKB1, we witness a repression of membrane ruffling (Figure 2.8), which was previously shown to drive cancer cell motility and invasion[173, 174]. Strikingly, disruption of LKB1 kinase activity appears to abrogate this repression of membrane ruffling, indicating that LKB1 is phosphorylating a downstream target to repress this ruffling. Interestingly, disruption of LKB1 kinase activity also appeared to drive traveling waves along the membrane, which has previously been shown to correlate with defects in lamellipodial adhesion during motility[128, 131, 134, 175-177]. Indeed, when using a FAK inhibitor to disrupt FAK activity, we witness an abrogation of these traveling waves (Figure 2.9), indicating that LKB1 kinase activity is signaling to FAK to promote adhesion and thus repress traveling waves. These data correlate with tumor samples, whereby LKB1 loss results in hyperactive FAK and more adhesive and thus more invasive tumors[87]. Given that previous studies show LKB1 signaling to MARK1 to regulate FAK activity, this data would appear to indicate that LKB1-mediated adhesion sites are critical for maintaining normal cell function. Yet again, this loss of LKB1 in NSCLC patients would theoretically again drive aberrant invasion through this inability to properly regulate membrane dynamics and localized adhesion.

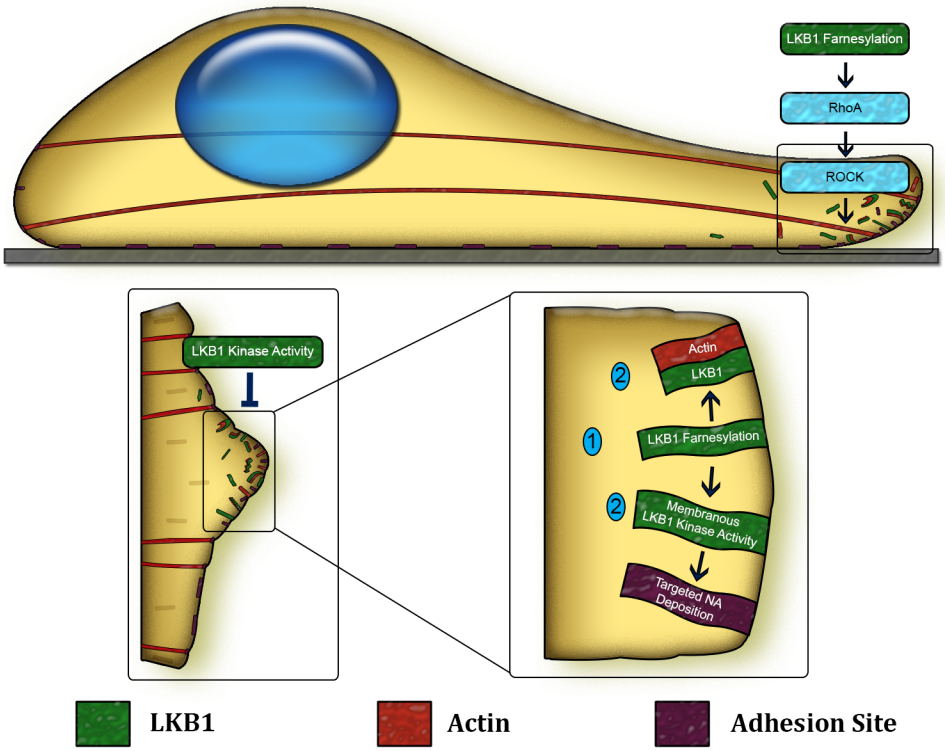

Figure 4.1: Model Figure LKB1 farnesylation targets it to the leading edge membrane. At the membrane, farnesylated LKB1 associates with leading edge actin and drives stress fiber assembly in 2D, and activates RhoA to drive mesenchymal polarization and directional persistence in 3D invasion. LKB1 kinase activity also targets focal adhesion site assembly at the leading edge to regulate lamellipodia formation in 2D and invadopodia in 3D invasion. Together, the combination of LKB1 farnesylation and kinase activity coordinates to regulate cell motility in 2D and cell invasion in 3D.

Figure adapted from Wilkinson et al 2016 in revision at *Scientific Reports*, also from Figure 2.14.

4.4 LKB1 Drives Cellular Polarization During Invasion

Several studies in the early 2000s highlighted LKB1 as a critical driver of embryonic differentiation and formation of the Anterior-Posterior (AP) axis in *D. melanogaster* and *C. elegans*[99, 100]. Further, research has also shown that in humans, re-expressing LKB1 can induce normal epithelial polarization in non-adherent epithelial cells, with formation of apical and basolateral junctions and acinar actin caps[103]. LKB1 was also shown to activate RhoA in normal epithelial cells, through activation of the RhoA GEF p114RhoGEF[104]. In motile cells, our lab also showed that in motile cells, LKB1 rapidly translocates to the cellular leading edge to associate with the Rho-GTPase cdc42 to drive Golgi reorientation and cell polarity[112]. Although these events highlight LKB1 as a master regulator of both apical-basal and unidirectional polarity, the functional significance of LKB1 mutation or loss on this polarization profile remained largely unstudied.

A majority of studies examining actin and polarization use planar polarity in 2 dimensions to examine Golgi reorientation. However, we sought to more closely replicate *in vivo* conditions and thus chose to examine polarization and adhesion in 3 dimensions using a spheroid model. Now, rather than simply reorienting Golgi, we are able to directly monitor an elongated polarization by examining mesenchymal and amoeboid morphologies. This provides a huge benefit over traditional 2D assays, as we can now monitor the ability of the cell to interact with the extracellular matrix (ECM) through secretion of matrix metalloproteinases (MMPs) to degrade the matrix, as well as the ability of the cell to physically interact with and sense the ECM during invasion. Although these spheroid

invasion models do have certain limitations (one cell type, no tumor stroma), this model has allowed us to progress our understanding of polarization in a much stronger context than previously available with 2D studies.

When beginning to examine the role of LKB1 in regulating 3D polarization, we initially showed, similar to other studies, that re-expressing wildtype LKB1 promotes a mesenchymal polarization as compared to empty GFP control (Figures 3.1-3.6). However, when examining polarization in response to LKB1 status, we show that LKB1 drives this mesenchymal polarization through its CTD farnesylation, in a kinase-independent manner (Figures 3.4-3.6). These cells also exhibit a strong directional persistence, suggesting that LKB1 farnesylation is driving this mesenchymal phenotype to promote interaction with the ECM and directed invasion. Importantly, the mesenchymal phenotype described here appears to align with LKB1 signaling to RhoA to drive stress fiber expression. Similar to that, we also show that LKB1 drives this mesenchymal polarization through its activation of RhoA in a farnesylation-dependent but kinase-independent manner (Figures 3.9-3.11), again suggesting the LKB1-RhoA interaction is critical for driving normal cellular function. Although RhoA is infrequently mutated in cancer, recent studies have identified novel RhoA mutations in gastric cancer[158, 159, 178]. Importantly, LKB1 is infrequently mutated in gastric cancers, suggesting that LKB1 and RhoA mutation could occur independent of each other but phenocopy the same disease progression.

Interestingly, we show that when re-expressing the LKB1 N-terminal domain (NTD) and kinase domain (NTD-kinase) but truncating the gene prior to the CTD, these cells appear

to undergo a reversion to an epithelial phenotype and invade in a sheet-like manner with re-expression of E-Cadherin (Figure 3.8). These data suggest that the LKB1 CTD, and specifically its farnesylation, drive mesenchymal cellular polarization during invasion, although the NTD-kinase truncate appears to shift the cells to an epithelial phenotype. Given that a majority of the mutations seen in the clinic are truncations, this would suggest that patients with LKB1 mutation would have tumors which exhibit aberrant polarization and the inability to properly interact with the tumor microenvironment during regulated motility. Again, the advent of 3D model systems has allowed us to expand our understanding beyond the canonical polarization markers, such as Golgi and centrosome alignment, instead allowing us to examine cell morphology and invasion patterns that are oftentimes undetectable in a 2D system.

4.5 LKB1 Regulates Adhesion Signaling

Knowing that LKB1 associates with actin to regulate cell motility and drives mesenchymal polarization during 3D invasion, we wanted to question how LKB1 status impacted focal adhesion deposition, duration, and localization, and whether this also contributed to cell motility. Several studies have highlighted LKB1 as a selective FAK repressor through phosphorylating MARK1[115, 116, 121], and thus we questioned whether this FAK regulation drove focal adhesion dynamics. Our data indicate that a combination of LKB1 farnesylation and kinase activity are critical for regulating both nascent adhesions (NA) and mature focal adhesions. When disrupting LKB1 farnesylation, cells exhibit extremely limited lamellipodia formation, with any focal adhesion sites located distal to the cellular leading edge as compared to cells re-expressing wildtype LKB1, where cells exhibit broad

lamellipodia with adhesions proximal to the leading edge membrane (Figure 2.12). When we disrupt LKB1 kinase activity, focal adhesions still appear proximal to the leading edge membrane, but the size and elongation of the adhesions are significantly reduced (Figure 2.12), highlighting LKB1 kinase activity as critical for driving focal adhesion deposition. Importantly, LKB1 farnesylation appears to guide the kinase activity to the leading edge membrane, which is similar to other reports indicating LKB1 farnesylation promotes AMPK phosphorylation at the membrane[61].

Although the data on focal adhesion localization was studied in 2D motility, we wanted to again bring this closer to an *in vivo* environment and examined focal adhesions in our 3D spheroid model. While examining these focal adhesions, we found similar trends in focal adhesion signaling as what we show in 2D. Specifically, LKB1 kinase activity remains critical for repressing active FAK, although in 3D this localization appears independent of LKB1 farnesylation (Figures 3.12, 3.13, 3.15, 3.16). Of note, we identified that LKB1 does not repress the level of FAK^{Y397}, but instead represses the number of focal adhesion sites in a kinase-dependent manner. This data correlates with earlier studies from our lab, where we show that LKB1 spatially represses FAK activity at the cellular leading edge[115]. Importantly, while LKB1 is regulating FAK activity during invasion, it also appears to be driving collagen remodeling to facilitate invasion. When LKB1 is lost, these invasive amoeboid cells exhibit the ability to pull on collagen to induce collagen realignment to drive invasion (Figures 3.17-3.21). However, re-expressing wildtype LKB1 appears to abrogate this collagen realignment. This data would seem to suggest that LKB1-expressing

mesenchymal do not rely on collagen alignment to drive invasion, and perhaps invade instead through the secretion of MMPs.

Given that a large majority of LKB1 mutations are truncations that would predictably disrupt farnesylation, these data suggest that in NSCLC patients with LKB1 loss, tumor cells have aberrant focal adhesion and lamellipodia dynamics, potentially driving increased invasion. We would thus hypothesize that in those patients with LKB1 loss, tumors will exhibit hyperactive focal adhesion signaling, which would then lead to increased integrin-ECM interaction. Integrins have been shown to interact with and realign collagen matrices[179-181], and thus LKB1 loss could indirectly activate integrins to drive collagen remodeling to facilitate amoeboid cell invasion and metastasis. Future studies will fully examine the role of both LKB1 farnesylation and kinase activity in metastasis suppression using *in vivo* models to monitor tumor growth in response to LKB1 status.

4.6 Conclusions

A cancer diagnosis within the United States and across the globe continues to represent a disease with a very poor prognosis and difficult treatment. Although treatments have improved and survival rates are beginning to rise, the systematic understanding of cancer cell biology remains an area ripe with speculation and hypotheses. Thus far, cancer treatments rely largely on surgery, radiation, and global chemotherapy in the hopes of killing cancerous cells before killing healthy ones. Although targeted treatments are beginning to arise, the sheer volume of cancer mutations makes this treatment avenue one full of promise for future research. However, before being able to target specific proteins

or pathways in cancer treatment, we must first understand the biology behind the cancer cell.

This research has focused on the role of LKB1, a tumor suppressor kinase frequently mutated in non-small cell lung cancer (NSCLC), in regulating multiple cellular functions. Ranging from driving normal membrane dynamics and actin structures to promoting mesenchymal polarization and focal adhesion signaling during 3D invasion, we have strived to explain the molecular mechanisms underlying LKB1-mediated tumor suppression. By further exploring these avenues driving normal cell motility, we have identified how LKB1 loss can contribute to a more invasive cancer cell. Together, we now propose a model whereby a combination of LKB1 farnesylation and kinase activity promote cell polarization and actin dynamics to regulate cell motility during invasion (Figure 4.1). First, LKB1 farnesylation targets it to the membrane where it can colocalize with leading edge actin, induce stress fiber assembly in 2D, and drive mesenchymal polarization and cell-ECM interactions during 3D invasion. Conversely, the LKB1 kinase activity drives regulation of FAK activity and subsequent lamellipodial adhesion and membrane dynamics in 2D motility, as well as focal adhesion assembly during 3D invasion. Together, we now propose a model whereby farnesylation localizes LKB1 kinase activity to the membrane, thus coordinating to regulate adhesion site assembly, turnover, and RhoA-mediated polarization to regulate cell motility during invasion.

This research has provided insights into domain-specific consequences of LKB1 loss during tumor development. While our research highlights a role of LKB1 in regulating cell invasion using *in vitro* models, future directions will examine the translational aspect of

these consequences further. Xenograft models of our panel of H157 cells stably re-expressing the GFP-LKB1 constructs will help to identify whether farnesylation and/or kinase activity are critical for tumor or metastasis suppression *in vivo*. If tumor burden was greater in response to disruption of either farnesylation or kinase activity (or both), we would be able to state that a combination of LKB1 farnesylation and kinase activity coordinate to drive tumor suppression.

Further, although a majority of LKB1 mutations in lung adenocarcinoma patients are truncations that result in loss of farnesylation, not all mutations would predictably also disrupt kinase activity. As such, future research could use computer modeling to predict whether specific point mutations would disrupt kinase activity, which could then be verified in the lab. Additionally, a systematic approach to analyzing specific mutations in lung adenocarcinoma samples would involve examining changes in amino acid structure, charge, and phobicity, and then examining whether any of these changes would predictably alter kinase status or folding to disrupt farnesylation. Finally, future research should also directly examine the most common point mutants in lung adenocarcinoma patients by performing similar techniques to stably express these mutants in lung cancer cells and then monitor the impact on polarization, adhesion, and invasion using both *in vitro* and *in vivo* systems. Although the research presented in this dissertation informs us of domain-specific functions of LKB1, many questions regarding the function of LKB1 loss remain less well studied. By combining these data with the future directions, this research provides one more step in understanding cancer cell biology to progress the research community forward towards our ultimate goal of a cancer cure.

Chapter 5: References

1. *Cancer Facts & Figures 2016*. 2016: American Cancer Society.
2. Fidler, I.J., *The pathogenesis of cancer metastasis: the 'seed and soil' hypothesis revisited.* Nat Rev Cancer, 2003. 3. (6): p. 453-8.
3. Lee, M. and V. Vasioukhin, *Cell polarity and cancer – cell and tissue polarity as a non-canonical tumor suppressor.* Journal of Cell Science, 2008. 121. (8): p. 1141-1150.
4. Thiery, J.P., H. Acloque, R.Y.J. Huang, and M.A. Nieto, *Epithelial-Mesenchymal Transitions in Development and Disease.* Cell, 2009. 139. (5): p. 871-890.
5. Acloque, H., M.S. Adams, K. Fishwick, M. Bronner-Fraser, and M.A. Nieto, *Epithelial-mesenchymal transitions: the importance of changing cell state in development and disease.* J Clin Invest, 2009. 119. (6): p. 1438-49.
6. Kalluri, R. and E.G. Neilson, *Epithelial-mesenchymal transition and its implications for fibrosis.* J Clin Invest, 2003. 112. (12): p. 1776-84.
7. Tiwari, N., A. Gheldof, M. Tatari, and G. Christofori, *EMT as the ultimate survival mechanism of cancer cells.* Semin Cancer Biol, 2012. 22. (3): p. 194-207.
8. Yilmaz, M. and G. Christofori, *EMT, the cytoskeleton, and cancer cell invasion.* Cancer Metastasis Rev, 2009. 28. (1-2): p. 15-33.
9. Hanahan, D. and R.A. Weinberg, *Hallmarks of cancer: the next generation.* Cell, 2011. 144. (5): p. 646-74.
10. Lafrenie, R.M., M.R. Buchanan, and F.W. Orr, *Adhesion molecules and their role in cancer metastasis.* Cell Biophys, 1993. 23. (1-3): p. 3-89.

11. Lafrenie, R.M., C.A. Buckner, and M.A. Bewick, *Cell adhesion and cancer: is there a potential for therapeutic intervention?* Expert Opin Ther Targets, 2007. 11. (6): p. 727-31.

12. Vega, F.M. and A.J. Ridley, *Rho GTPases in cancer cell biology.* FEBS Lett, 2008. 582. (14): p. 2093-101.

13. Kalluri, R. and R.A. Weinberg, *The basics of epithelial-mesenchymal transition.* J Clin Invest, 2009. 119. (6): p. 1420-8.

14. Ding, L., G. Getz, D.A. Wheeler, E.R. Mardis, M.D. McLellan, K. Cibulskis, C. Sougnez, H. Greulich, D.M. Muzny, M.B. Morgan, L. Fulton, R.S. Fulton, Q. Zhang, M.C. Wendl, M.S. Lawrence, D.E. Larson, K. Chen, D.J. Dooling, A. Sabo, A.C. Hawes, H. Shen, S.N. Jhangiani, L.R. Lewis, O. Hall, Y. Zhu, T. Mathew, Y. Ren, J. Yao, S.E. Scherer, K. Clerc, G.A. Metcalf, B. Ng, A. Milosavljevic, M.L. Gonzalez-Garay, J.R. Osborne, R. Meyer, X. Shi, Y. Tang, D.C. Koboldt, L. Lin, R. Abbott, T.L. Miner, C. Pohl, G. Fewell, C. Haipek, H. Schmidt, B.H. Dunford-Shore, A. Kraja, S.D. Crosby, C.S. Sawyer, T. Vickery, S. Sander, J. Robinson, W. Winckler, J. Baldwin, L.R. Chirieac, A. Dutt, T. Fennell, M. Hanna, B.E. Johnson, R.C. Onofrio, R.K. Thomas, G. Tonon, B.A. Weir, X. Zhao, L. Ziaugra, M.C. Zody, T. Giordano, M.B. Orringer, J.A. Roth, M.R. Spitz, Wistuba, II, B. Ozenberger, P.J. Good, A.C. Chang, D.G. Beer, M.A. Watson, M. Ladanyi, S. Broderick, A. Yoshizawa, W.D. Travis, W. Pao, M.A. Province, G.M. Weinstock, H.E. Varmus, S.B. Gabriel, E.S. Lander, R.A. Gibbs, M. Meyerson, and R.K. Wilson, *Somatic mutations affect key pathways in lung adenocarcinoma.* Nature, 2008. 455. (7216): p. 1069-75.

15. The Cancer Genome Atlas Research, N., *Comprehensive molecular profiling of lung adenocarcinoma.* Nature, 2014. 511. (7511): p. 543-550.

16. Schabath, M.B., E.A. Welsh, W.J. Fulp, L. Chen, J.K. Teer, Z.J. Thompson, B.E. Engel, M. Xie, A.E. Berglund, B.C. Creelan, S.J. Antonia, J.E. Gray, S.A. Eschrich, D.T. Chen, W.D. Cress, E.B. Haura, and A.A. Beg, *Differential association of STK11 and TP53 with KRAS mutation-associated gene expression, proliferation and immune surveillance in lung adenocarcinoma.* Oncogene, 2015.

17. Etienne-Manneville, S., *Cdc42--the centre of polarity.* J Cell Sci, 2004. 117. (Pt 8): p. 1291-300.

18. Nabi, I.R., *The polarization of the motile cell.* J Cell Sci, 1999. 112 (Pt 12). p. 1803-11.

19. Etienne-Manneville, S., *Polarity proteins in migration and invasion.* Oncogene, 2008. 27. (55): p. 6970-80.

20. Ridley, A.J. and A. Hall, *The small GTP-binding protein rho regulates the assembly of focal adhesions and actin stress fibers in response to growth factors.* Cell, 1992. 70. (3): p. 389-99.

21. Lauffenburger, D.A. and A.F. Horwitz, *Cell migration: a physically integrated molecular process.* Cell, 1996. 84. (3): p. 359-69.

22. Narumiya, S., *The small GTPase Rho: cellular functions and signal transduction.* J Biochem, 1996. 120. (2): p. 215-28.

23. Friedl, P., K.S. Zanker, and E.B. Brocker, *Cell migration strategies in 3-D extracellular matrix: differences in morphology, cell matrix interactions, and integrin function.* Microsc Res Tech, 1998. 43. (5): p. 369-78.

24. Tomar, A., S.-T. Lim, Y. Lim, and D.D. Schlaepfer, *A FAK-p120RasGAP-p190RhoGAP complex regulates polarity in migrating cells.* Journal of Cell Science, 2009. 122. (11): p. 1852-1862.

25. Liu Y, L.-P.C., *The Regulation of Cell Polarity in the Progression of Lung Cancer.* Journal of Cancer Research and Therapeutics, 2013. 9. (5): p. 80-85.

26. Parri, M. and P. Chiarugi, *Rac and Rho GTPases in cancer cell motility control.* Cell Commun Signal, 2010. 8. p. 23.

27. Roberts, P.J., N. Mitin, P.J. Keller, E.J. Chenette, J.P. Madigan, R.O. Currin, A.D. Cox, O. Wilson, P. Kirschmeier, and C.J. Der, *Rho Family GTPase modification and dependence on CAAX motif-signaled posttranslational modification.* J Biol Chem, 2008. 283. (37): p. 25150-63.

28. Benard, V., B.P. Bohl, and G.M. Bokoch, *Characterization of rac and cdc42 activation in chemoattractant-stimulated human neutrophils using a novel assay for active GTPases.* J Biol Chem, 1999. 274. (19): p. 13198-204.

29. Chou, J., N.A. Burke, A. Iwabu, S.C. Watkins, and A. Wells, *Directional motility induced by epidermal growth factor requires Cdc42.* Exp Cell Res, 2003. 287. (1): p. 47-56.

30. Liu, B.P. and K. Burridge, *Vav2 activates Rac1, Cdc42, and RhoA downstream from growth factor receptors but not beta1 integrins.* Mol Cell Biol, 2000. 20. (19): p. 7160-9.

31. Rohatgi, R., H.Y. Ho, and M.W. Kirschner, *Mechanism of N-WASP activation by CDC42 and phosphatidylinositol 4, 5-bisphosphate.* J Cell Biol, 2000. 150. (6): p. 1299-310.

32. Rohatgi, R., L. Ma, H. Miki, M. Lopez, T. Kirchhausen, T. Takenawa, and M.W. Kirschner, *The interaction between N-WASP and the Arp2/3 complex links Cdc42-dependent signals to actin assembly.* Cell, 1999. 97. (2): p. 221-31.

33. Chrzanowska-Wodnicka, M. and K. Burridge, *Rho-stimulated contractility drives the formation of stress fibers and focal adhesions.* J Cell Biol, 1996. 133. (6): p. 1403-15.

34. Nakaya, Y. and G. Sheng, *Epithelial to mesenchymal transition during gastrulation: an embryological view.* Dev Growth Differ, 2008. 50. (9): p. 755-66.

35. Bewick, M.A. and R.M. Lafrenie, *Adhesion dependent signalling in the tumour microenvironment: the future of drug targetting.* Curr Pharm Des, 2006. 12. (22): p. 2833-48.

36. Huang, Y.W., R. Baluna, and E.S. Vitetta, *Adhesion molecules as targets for cancer therapy.* Histol Histopathol, 1997. 12. (2): p. 467-77.

37. Varelas, X., P. Samavarchi-Tehrani, M. Narimatsu, A. Weiss, K. Cockburn, B.G. Larsen, J. Rossant, and J.L. Wrana, *The Crumbs complex couples cell density sensing to Hippo-dependent control of the TGF-beta-SMAD pathway.* Dev Cell, 2010. 19. (6): p. 831-44.

38. Fanjul, M., V. Gmyr, C. Sengenes, G. Ratovo, M. Dufresne, B. Lefebvre, J. Kerr-Conte, and E. Hollande, *Evidence for epithelial-mesenchymal transition in adult human pancreatic exocrine cells.* J Histochem Cytochem, 2010. 58. (9): p. 807-23.

39. Meng, F. and G. Wu, *The rejuvenated scenario of epithelial-mesenchymal transition (EMT) and cancer metastasis.* Cancer Metastasis Rev, 2012. 31. (3-4): p. 455-67.

40. Brabletz, T., F. Hlubek, S. Spaderna, O. Schmalhofer, E. Hiendlmeyer, A. Jung, and T. Kirchner, *Invasion and metastasis in colorectal cancer: epithelial-mesenchymal transition, mesenchymal-epithelial transition, stem cells and beta-catenin.* Cells Tissues Organs, 2005. 179. (1-2): p. 56-65.

41. Jung, A., M. Schrauder, U. Oswald, C. Knoll, P. Sellberg, R. Palmqvist, G. Niedobitek, T. Brabletz, and T. Kirchner, *The invasion front of human colorectal adenocarcinomas shows co-localization of nuclear beta-catenin, cyclin D1, and p16INK4A and is a region of low proliferation.* Am J Pathol, 2001. 159. (5): p. 1613-7.

42. Hirohashi, S., *Inactivation of the E-cadherin-mediated cell adhesion system in human cancers.* Am J Pathol, 1998. 153. (2): p. 333-9.

43. Jiang, P., A. Enomoto, and M. Takahashi, *Cell biology of the movement of breast cancer cells: intracellular signalling and the actin cytoskeleton.* Cancer Lett, 2009. 284. (2): p. 122-30.

44. Macara, I.G. and L. McCaffrey, *Cell polarity in morphogenesis and metastasis.* Philos Trans R Soc Lond B Biol Sci, 2013. 368. (1629): p. 20130012.

45. Stengel, K. and Y. Zheng, *Cdc42 in oncogenic transformation, invasion, and tumorigenesis.* Cell Signal, 2011. 23. (9): p. 1415-23.

46. Gomez del Pulgar, T., S.A. Benitah, P.F. Valeron, C. Espina, and J.C. Lacal, *Rho GTPase expression in tumourigenesis: evidence for a significant link.* Bioessays, 2005. 27. (6): p. 602-13.

47. Alblazi, K.M. and C.H. Siar, *Cellular protrusions--lamellipodia, filopodia, invadopodia and podosomes--and their roles in progression of orofacial tumours: current understanding.* Asian Pac J Cancer Prev, 2015. 16. (6): p. 2187-91.

48. Price, L.S., J. Leng, M.A. Schwartz, and G.M. Bokoch, *Activation of Rac and Cdc42 by integrins mediates cell spreading.* Mol Biol Cell, 1998. 9. (7): p. 1863-71.

49. Rottner, K., A. Hall, and J.V. Small, *Interplay between Rac and Rho in the control of substrate contact dynamics.* Curr Biol, 1999. 9. (12): p. 640-8.

50. Zamir, E. and B. Geiger, *Molecular complexity and dynamics of cell-matrix adhesions.* J Cell Sci, 2001. 114. (Pt 20): p. 3583-90.

51. Zamir, E., M. Katz, Y. Posen, N. Erez, K.M. Yamada, B.Z. Katz, S. Lin, D.C. Lin, A. Bershadsky, Z. Kam, and B. Geiger, *Dynamics and segregation of cell-matrix adhesions in cultured fibroblasts.* Nat Cell Biol, 2000. 2. (4): p. 191-6.

52. Mitra, S.K. and D.D. Schlaepfer, *Integrin-regulated FAK-Src signaling in normal and cancer cells.* Curr Opin Cell Biol, 2006. 18. (5): p. 516-23.

53. Nagano, M., D. Hoshino, N. Koshikawa, T. Akizawa, and M. Seiki, *Turnover of focal adhesions and cancer cell migration.* Int J Cell Biol, 2012. 2012. p. 310616.

54. Krause, M. and A. Gautreau, *Steering cell migration: lamellipodium dynamics and the regulation of directional persistence.* Nat Rev Mol Cell Biol, 2014. 15. (9): p. 577-590.

55. Pollard, T.D., *Regulation of actin filament assembly by Arp2/3 complex and formins.* Annu Rev Biophys Biomol Struct, 2007. 36. p. 451-77.

56. Geiger, B., J.P. Spatz, and A.D. Bershadsky, *Environmental sensing through focal adhesions.* Nat Rev Mol Cell Biol, 2009. 10. (1): p. 21-33.

57. Parsons, J.T., A.R. Horwitz, and M.A. Schwartz, *Cell adhesion: integrating cytoskeletal dynamics and cellular tension.* Nat Rev Mol Cell Biol, 2010. 11. (9): p. 633-643.

58. Totsukawa, G., Y. Yamakita, S. Yamashiro, D.J. Hartshorne, Y. Sasaki, and F. Matsumura, *Distinct roles of ROCK (Rho-kinase) and MLCK in spatial regulation of MLC phosphorylation for assembly of stress fibers and focal adhesions in 3T3 fibroblasts.* J Cell Biol, 2000. 150. (4): p. 797-806.

59. Tojkander, S., G. Gateva, and P. Lappalainen, *Actin stress fibers--assembly, dynamics and biological roles.* J Cell Sci, 2012. 125. (Pt 8): p. 1855-64.

60. Hezel, A.F. and N. Bardeesy, *LKB1; linking cell structure and tumor suppression.* Oncogene, 2008. 27. (55): p. 6908-19.

61. Houde, V.P., M.S. Ritorto, R. Gourlay, J. Varghese, P. Davies, N. Shpiro, K. Sakamoto, and D.R. Alessi, *Investigation of LKB1 Ser431 phosphorylation and Cys433 farnesylation using mouse knockin analysis reveals an unexpected role of prenylation in regulating AMPK activity.* Biochem J, 2014. 458. (1): p. 41-56.

62. Yoo, L.I., D.C. Chung, and J. Yuan, *LKB1--a master tumour suppressor of the small intestine and beyond.* Nat Rev Cancer, 2002. 2. (7): p. 529-35.

63. Dorfman, J. and I.G. Macara, *STRADalpha regulates LKB1 localization by blocking access to importin-alpha, and by association with Crm1 and exportin-7.* Mol Biol Cell, 2008. 19. (4): p. 1614-26.

64. Macara, I.G., *Transport into and out of the nucleus.* Microbiol Mol Biol Rev, 2001. 65. (4): p. 570-94, table of contents.

65. Esteve-Puig, R., F. Canals, N. Colomé, G. Merlino, and J.Á. Recio, *Uncoupling of the LKB1-AMPKα Energy Sensor Pathway by Growth Factors and Oncogenic BRAF^{V600E}.* PLoS ONE, 2009. 4. (3): p. e4771.

66. Eggers, C.M., E.R. Kline, D. Zhong, W. Zhou, and A.I. Marcus, *STE20-related kinase adaptor protein alpha (STRADalpha) regulates cell polarity and invasion through PAK1 signaling in LKB1-null cells.* J Biol Chem, 2012. 287. (22): p. 18758-68.

67. Baas, A.F., J. Boudeau, G.P. Sapkota, L. Smit, R. Medema, N.A. Morrice, D.R. Alessi, and H.C. Clevers, *Activation of the tumour suppressor kinase LKB1 by the STE20-like pseudokinase STRAD.* EMBO J, 2003. 22. (12): p. 3062-72.

68. Boudeau, J., A.F. Baas, M. Deak, N.A. Morrice, A. Kieloch, M. Schutkowski, A.R. Prescott, H.C. Clevers, and D.R. Alessi, *MO25alpha/beta interact with STRADalpha/beta enhancing their ability to bind, activate and localize LKB1 in the cytoplasm.* EMBO J, 2003. 22. (19): p. 5102-14.

69. Boudeau, J., J.W. Scott, N. Resta, M. Deak, A. Kieloch, D. Komander, D.G. Hardie, A.R. Prescott, D.M. van Aalten, and D.R. Alessi, *Analysis of the LKB1-STRAD-MO25 complex.* J Cell Sci, 2004. 117. (Pt 26): p. 6365-75.

70. Song, P., Y. Wu, J. Xu, Z. Xie, Y. Dong, M. Zhang, and M.H. Zou, *Reactive nitrogen species induced by hyperglycemia suppresses Akt signaling and triggers apoptosis by upregulating phosphatase PTEN (phosphatase and tensin homologue*

deleted on chromosome 10) in an LKB1-dependent manner. Circulation, 2007. 116. (14): p. 1585-95.

71. Collins, S.P., J.L. Reoma, D.M. Gamm, and M.D. Uhler, *LKB1, a novel serine/threonine protein kinase and potential tumour suppressor, is phosphorylated by cAMP-dependent protein kinase (PKA) and prenylated in vivo.* Biochem J, 2000. 345 Pt 3. p. 673-80.

72. Sanchez-Cespedes, M., P. Parrella, M. Esteller, S. Nomoto, B. Trink, J.M. Engles, W.H. Westra, J.G. Herman, and D. Sidransky, *Inactivation of LKB1/STK11 is a common event in adenocarcinomas of the lung.* Cancer Res, 2002. 62. (13): p. 3659-62.

73. Sapkota, G.P., J. Boudeau, M. Deak, A. Kieloch, N. Morrice, and D.R. Alessi, *Identification and characterization of four novel phosphorylation sites (Ser31, Ser325, Thr336 and Thr366) on LKB1/STK11, the protein kinase mutated in Peutz-Jeghers cancer syndrome.* Biochem J, 2002. 362. (Pt 2): p. 481-90.

74. Xie, Z., Y. Dong, R. Scholz, D. Neumann, and M.-H. Zou, *Phosphorylation of LKB1 at Serine 428 by Protein Kinase C-ζ Is Required for Metformin-Enhanced Activation of the AMP-Activated Protein Kinase in Endothelial Cells.* Circulation, 2008. 117. (7): p. 952-962.

75. Sapkota, G.P., A. Kieloch, J.M. Lizcano, S. Lain, J.S. Arthur, M.R. Williams, N. Morrice, M. Deak, and D.R. Alessi, *Phosphorylation of the protein kinase mutated in Peutz-Jeghers cancer syndrome, LKB1/STK11, at Ser431 by p90(RSK) and cAMP-dependent protein kinase, but not its farnesylation at Cys(433), is essential for LKB1 to suppress cell vrowth.* J Biol Chem, 2001. 276. (22): p. 19469-82.

76. Hemminki, A., D. Markie, I. Tomlinson, E. Avizienyte, S. Roth, A. Loukola, G. Bignell, W. Warren, M. Aminoff, P. Hoglund, H. Jarvinen, P. Kristo, K. Pelin, M. Ridanpaa, R. Salovaara, T. Toro, W. Bodmer, S. Olschwang, A.S. Olsen, M.R. Stratton, A. de la Chapelle, and L.A. Aaltonen, *A serine/threonine kinase gene defective in Peutz-Jeghers syndrome.* Nature, 1998. 391. (6663): p. 184-7.

77. Giardiello, F.M., S.B. Welsh, S.R. Hamilton, G.J. Offerhaus, A.M. Gittelsohn, S.V. Booker, A.J. Krush, J.H. Yardley, and G.D. Luk, *Increased risk of cancer in the Peutz-Jeghers syndrome.* N Engl J Med, 1987. 316. (24): p. 1511-4.

78. Spigelman, A.D., V. Murday, and R.K. Phillips, *Cancer and the Peutz-Jeghers syndrome.* Gut, 1989. 30. (11): p. 1588-90.

79. Dong, S.M., K.M. Kim, S.Y. Kim, M.S. Shin, E.Y. Na, S.H. Lee, W.S. Park, N.J. Yoo, J.J. Jang, C.Y. Yoon, J.W. Kim, S.Y. Kim, Y.M. Yang, S.H. Kim, C.S. Kim, and J.Y. Lee, *Frequent somatic mutations in serine/threonine kinase 11/Peutz-Jeghers syndrome gene in left-sided colon cancer.* Cancer Res, 1998. 58. (17): p. 3787-90.

80. Jenne, D.E., H. Reimann, J. Nezu, W. Friedel, S. Loff, R. Jeschke, O. Muller, W. Back, and M. Zimmer, *Peutz-Jeghers syndrome is caused by mutations in a novel serine threonine kinase.* Nat Genet, 1998. 18. (1): p. 38-43.

81. Mehenni, H., C. Gehrig, J. Nezu, A. Oku, M. Shimane, C. Rossier, N. Guex, J.L. Blouin, H.S. Scott, and S.E. Antonarakis, *Loss of LKB1 kinase activity in Peutz-Jeghers syndrome, and evidence for allelic and locus heterogeneity.* Am J Hum Genet, 1998. 63. (6): p. 1641-50.

82. Srivatsa, P.J., G.L. Keeney, and K.C. Podratz, *Disseminated cervical adenoma malignum and bilateral ovarian sex cord tumors with annular tubules associated with Peutz-Jeghers syndrome.* Gynecol Oncol, 1994. 53. (2): p. 256-64.

83. Alessi, D.R., K. Sakamoto, and J.R. Bayascas, *LKB1-dependent signaling pathways.* Annu Rev Biochem, 2006. 75. p. 137-63.

84. Jishage, K., J. Nezu, Y. Kawase, T. Iwata, M. Watanabe, A. Miyoshi, A. Ose, K. Habu, T. Kake, N. Kamada, O. Ueda, M. Kinoshita, D.E. Jenne, M. Shimane, and H. Suzuki, *Role of Lkb1, the causative gene of Peutz-Jegher's syndrome, in embryogenesis and polyposis.* Proc Natl Acad Sci U S A, 2002. 99. (13): p. 8903-8.

85. Bardeesy, N., M. Sinha, A.F. Hezel, S. Signoretti, N.A. Hathaway, N.E. Sharpless, M. Loda, D.R. Carrasco, and R.A. DePinho, *Loss of the Lkb1 tumour suppressor provokes intestinal polyposis but resistance to transformation.* Nature, 2002. 419. (6903): p. 162-7.

86. Miyoshi, H., M. Nakau, T.O. Ishikawa, M.F. Seldin, M. Oshima, and M.M. Taketo, *Gastrointestinal hamartomatous polyposis in Lkb1 heterozygous knockout mice.* Cancer Res, 2002. 62. (8): p. 2261-6.

87. Ji, H., M.R. Ramsey, D.N. Hayes, C. Fan, K. McNamara, P. Kozlowski, C. Torrice, M.C. Wu, T. Shimamura, S.A. Perera, M.C. Liang, D. Cai, G.N. Naumov, L. Bao, C.M. Contreras, D. Li, L. Chen, J. Krishnamurthy, J. Koivunen, L.R. Chirieac, R.F. Padera, R.T. Bronson, N.I. Lindeman, D.C. Christiani, X. Lin, G.I. Shapiro, P.A. Janne, B.E. Johnson, M. Meyerson, D.J. Kwiatkowski, D.H. Castrillon, N.

Bardeesy, N.E. Sharpless, and K.K. Wong, *LKB1 modulates lung cancer differentiation and metastasis.* Nature, 2007. 448. (7155): p. 807-10.

88. Hawley, S.A., J. Boudeau, J.L. Reid, K.J. Mustard, L. Udd, T.P. Makela, D.R. Alessi, and D.G. Hardie, *Complexes between the LKB1 tumor suppressor, STRAD alpha/beta and MO25 alpha/beta are upstream kinases in the AMP-activated protein kinase cascade.* J Biol, 2003. 2. (4): p. 28.

89. Shaw, R.J., M. Kosmatka, N. Bardeesy, R.L. Hurley, L.A. Witters, R.A. DePinho, and L.C. Cantley, *The tumor suppressor LKB1 kinase directly activates AMP-activated kinase and regulates apoptosis in response to energy stress.* Proc Natl Acad Sci U S A, 2004. 101. (10): p. 3329-35.

90. Barnes, A.P., B.N. Lilley, Y.A. Pan, L.J. Plummer, A.W. Powell, A.N. Raines, J.R. Sanes, and F. Polleux, *LKB1 and SAD kinases define a pathway required for the polarization of cortical neurons.* Cell, 2007. 129. (3): p. 549-63.

91. Brajenovic, M., G. Joberty, B. Kuster, T. Bouwmeester, and G. Drewes, *Comprehensive proteomic analysis of human Par protein complexes reveals an interconnected protein network.* J Biol Chem, 2004. 279. (13): p. 12804-11.

92. Cheng, H., P. Liu, Z.C. Wang, L. Zou, S. Santiago, V. Garbitt, O.V. Gjoerup, J.D. Iglehart, A. Miron, A.L. Richardson, W.C. Hahn, and J.J. Zhao, *SIK1 Couples LKB1 to p53-Dependent Anoikis and Suppresses Metastasis.* Science Signaling, 2009. 2. (80): p. ra35-ra35.

93. Kishi, M., Y.A. Pan, J.G. Crump, and J.R. Sanes, *Mammalian SAD Kinases Are Required for Neuronal Polarization.* Science, 2005. 307. (5711): p. 929-932.

94. Lizcano, J.M., O. Goransson, R. Toth, M. Deak, N.A. Morrice, J. Boudeau, S.A. Hawley, L. Udd, T.P. Makela, D.G. Hardie, and D.R. Alessi, *LKB1 is a master kinase that activates 13 kinases of the AMPK subfamily, including MARK/PAR-1.* EMBO J, 2004. 23. (4): p. 833-43.

95. Spicer, J., S. Rayter, N. Young, R. Elliott, A. Ashworth, and D. Smith, *Regulation of the Wnt signalling component PAR1A by the Peutz-Jeghers syndrome kinase LKB1.* Oncogene, 2003. 22. (30): p. 4752-6.

96. Vallenius, T., K. Vaahtomeri, B. Kovac, A.-M. Osiceanu, M. Viljanen, and T.P. Mäkelä, *An association between NUAK2 and MRIP reveals a novel mechanism for regulation of actin stress fibers.* Journal of Cell Science, 2011. 124. (3): p. 384-393.

97. Zagórska, A., M. Deak, D.G. Campbell, S. Banerjee, M. Hirano, S. Aizawa, A.R. Prescott, and D.R. Alessi, *New Roles for the LKB1-NUAK Pathway in Controlling Myosin Phosphatase Complexes and Cell Adhesion*. Vol. 3. 2010. ra25-ra25.

98. Guo, S. and K.J. Kemphues, *par-1, a gene required for establishing polarity in C. elegans embryos, encodes a putative Ser/Thr kinase that is asymmetrically distributed.* Cell, 1995. 81. (4): p. 611-20.

99. Watts, J.L., D.G. Morton, J. Bestman, and K.J. Kemphues, *The C. elegans par-4 gene encodes a putative serine-threonine kinase required for establishing embryonic asymmetry.* Development, 2000. 127. (7): p. 1467-75.

100. Martin, S.G. and D. St Johnston, *A role for Drosophila LKB1 in anterior-posterior axis formation and epithelial polarity.* Nature, 2003. 421. (6921): p. 379-384.

101. Amin, N., A. Khan, D. St Johnston, I. Tomlinson, S. Martin, J. Brenman, and H. McNeill, *LKB1 regulates polarity remodeling and adherens junction formation in the Drosophila eye.* Proc Natl Acad Sci U S A, 2009. 106. (22): p. 8941-6.

102. Baas, A.F., *LKB1: A Master Regulator of Cell Polarity*, in *Department of Immunology*. 2004, University Medical Center Utrecht: Grafische Communicatie, Rotterdam. p. 80.

103. Baas, A.F., J. Kuipers, N.N. van der Wel, E. Batlle, H.K. Koerten, P.J. Peters, and H.C. Clevers, *Complete polarization of single intestinal epithelial cells upon activation of LKB1 by STRAD.* Cell, 2004. 116. (3): p. 457-66.

104. Xu, X., D. Jin, J. Durgan, and A. Hall, *LKB1 controls human bronchial epithelial morphogenesis through p114RhoGEF dependent RhoA activation.* Mol Cell Biol, 2013.

105. Xu, X., T. Omelchenko, and A. Hall, *LKB1 tumor suppressor protein regulates actin filament assembly through Rho and its exchange factor Dbl independently of kinase activity.* BMC Cell Biol, 2010. 11. p. 77.

106. Totsukawa, G., Y. Wu, Y. Sasaki, D.J. Hartshorne, Y. Yamakita, S. Yamashiro, and F. Matsumura, *Distinct roles of MLCK and ROCK in the regulation of membrane protrusions and focal adhesion dynamics during cell migration of fibroblasts.* The Journal of Cell Biology, 2004. 164. (3): p. 427-439.

107. Gadea, G., M. de Toledo, C. Anguille, and P. Roux, *Loss of p53 promotes RhoA–ROCK-dependent cell migration and invasion in 3D matrices.* The Journal of Cell Biology, 2007. 178. (1): p. 23-30.

108. Kosla, J., D. Pankova, J. Plachy, O. Tolde, K. Bicanova, M. Dvorak, D. Rosel, and J. Brabek, *Metastasis of aggressive amoeboid sarcoma cells is dependent on Rho/ROCK/MLC signaling.* Cell Commun Signal, 2013. 11. p. 51.

109. Matsuoka, T. and M. Yashiro, *Rho/ROCK signaling in motility and metastasis of gastric cancer.* World J Gastroenterol, 2014. 20. (38): p. 13756-66.

110. Partanen, J.I., T.A. Tervonen, M. Myllynen, E. Lind, M. Imai, P. Katajisto, G.J. Dijkgraaf, P.E. Kovanen, T.P. Makela, Z. Werb, and J. Klefstrom, *Tumor suppressor function of Liver kinase B1 (Lkb1) is linked to regulation of epithelial integrity.* Proc Natl Acad Sci U S A, 2012. 109. (7): p. E388-97.

111. Roy, B.C., T. Kohno, R. Iwakawa, T. Moriguchi, T. Kiyono, K. Morishita, M. Sanchez-Cespedes, T. Akiyama, and J. Yokota, *Involvement of LKB1 in epithelial-mesenchymal transition (EMT) of human lung cancer cells.* Lung Cancer, 2010. 70. (2): p. 136-45.

112. Zhang, S., K. Schafer-Hales, F.R. Khuri, W. Zhou, P.M. Vertino, and A.I. Marcus, *The tumor suppressor LKB1 regulates lung cancer cell polarity by mediating cdc42 recruitment and activity.* Cancer Res, 2008. 68. (3): p. 740-8.

113. Liu, W., K.B. Monahan, A.D. Pfefferle, T. Shimamura, J. Sorrentino, K.T. Chan, D.W. Roadcap, D.W. Ollila, N.E. Thomas, D.H. Castrillon, C.R. Miller, C.M. Perou, K.K. Wong, J.E. Bear, and N.E. Sharpless, *LKB1/STK11 inactivation leads to expansion of a prometastatic tumor subpopulation in melanoma.* Cancer Cell, 2012. 21. (6): p. 751-64.

114. Hardie, D.G. and D.R. Alessi, *LKB1 and AMPK and the cancer-metabolism link - ten years after.* BMC Biol, 2013. 11. p. 36.

115. Kline, E.R., J. Shupe, M. Gilbert-Ross, W. Zhou, and A.I. Marcus, *LKB1 Represses Focal Adhesion Kinase (FAK) Signaling via a FAK-LKB1 Complex to Regulate FAK Site Maturation and Directional Persistence.* J Biol Chem, 2013. 288. (24): p. 17663-74.

116. Goodwin, J.M., R.U. Svensson, H.J. Lou, M.M. Winslow, B.E. Turk, and R.J. Shaw, *An AMPK-independent signaling pathway downstream of the LKB1 tumor suppressor controls Snail1 and metastatic potential.* Mol Cell, 2014. 55. (3): p. 436-50.

117. Carretero, J., T. Shimamura, K. Rikova, A.L. Jackson, M.D. Wilkerson, C.L. Borgman, M.S. Buttarazzi, B.A. Sanofsky, K.L. McNamara, K.A. Brandstetter, Z.E. Walton, T.-L. Gu, J.C. Silva, K. Crosby, G.I. Shapiro, S.-M. Maira, H. Ji, D.H. Castrillon, C.F. Kim, C. García-Echeverría, N. Bardeesy, N.E. Sharpless, N.D. Hayes, W.Y. Kim, J.A. Engelman, and K.-K. Wong, *Integrative Genomic and Proteomic Analyses Identify Targets for Lkb1-Deficient Metastatic Lung Tumors.* Cancer Cell, 2010. 17. (6): p. 547-559.

118. Hou, X., J.E. Liu, W. Liu, C.Y. Liu, Z.Y. Liu, and Z.Y. Sun, *A new role of NUAK1: directly phosphorylating p53 and regulating cell proliferation.* Oncogene, 2011. 30. (26): p. 2933-42.

119. Forcet, C., S. Etienne-Manneville, H. Gaude, L. Fournier, S. Debilly, M. Salmi, A. Baas, S. Olschwang, H. Clevers, and M. Billaud, *Functional analysis of Peutz-Jeghers mutations reveals that the LKB1 C-terminal region exerts a crucial role in regulating both the AMPK pathway and the cell polarity.* Hum Mol Genet, 2005. 14. (10): p. 1283-92.

120. Asada, N., K. Sanada, and Y. Fukada, *LKB1 regulates neuronal migration and neuronal differentiation in the developing neocortex through centrosomal positioning.* J Neurosci, 2007. 27. (43): p. 11769-75.

121. Konen, J., S. Wilkinson, B. Lee, H. Fu, W. Zhou, Y. Jiang, and A.I. Marcus, *LKB1 kinase-dependent and -independent defects disrupt polarity and adhesion signaling to drive collagen remodeling during invasion.* Mol Biol Cell, 2016. 27. (7): p. 1069-84.

122. Marcus, A.I. and W. Zhou, *LKB1 regulated pathways in lung cancer invasion and metastasis.* J Thorac Oncol, 2010. 5. (12): p. 1883-6.

123. Nakano, A. and S. Takashima, *LKB1 and AMP-activated protein kinase: regulators of cell polarity.* Genes Cells, 2012. 17. (9): p. 737-47.

124. Chan, K.T., S.B. Asokan, S.J. King, T. Bo, E.S. Dubose, W. Liu, M.E. Berginski, J.M. Simon, I.J. Davis, S.M. Gomez, N.E. Sharpless, and J.E. Bear, *LKB1 loss in melanoma disrupts directional migration toward extracellular matrix cues.* The Journal of Cell Biology, 2014. 207. (2): p. 299-315.

125. Matsumoto, S., R. Iwakawa, K. Takahashi, T. Kohno, Y. Nakanishi, Y. Matsuno, K. Suzuki, M. Nakamoto, E. Shimizu, J.D. Minna, and J. Yokota, *Prevalence and specificity of LKB1 genetic alterations in lung cancers.* Oncogene, 2007. 26. (40): p. 5911-8.

126. Wingo, S.N., T.D. Gallardo, E.A. Akbay, M.C. Liang, C.M. Contreras, T. Boren, T. Shimamura, D.S. Miller, N.E. Sharpless, N. Bardeesy, D.J. Kwiatkowski, J.O. Schorge, K.K. Wong, and D.H. Castrillon, *Somatic LKB1 mutations promote cervical cancer progression.* PLoS One, 2009. 4. (4): p. e5137.

127. Swaminathan, V., R.S. Fischer, and C.M. Waterman, *The FAK-Arp2/3 interaction promotes leading edge advance and haptosensing by coupling nascent adhesions to lamellipodia actin.* Mol Biol Cell, 2016.

128. Machacek, M. and G. Danuser, *Morphodynamic Profiling of Protrusion Phenotypes.* Biophysical Journal, 2006. 90. (4): p. 1439-1452.

129. Machacek, M., L. Hodgson, C. Welch, H. Elliott, O. Pertz, P. Nalbant, A. Abell, G.L. Johnson, K.M. Hahn, and G. Danuser, *Coordination of Rho GTPase activities during cell protrusion.* Nature, 2009. 461. (7260): p. 99-103.

130. Yuan, J., E. Bae, and X.-C. Tai. *A study on continuous max-flow and min-cut approaches*. in *2010 IEEE Conference on Computer Vision and Pattern Recognition (CVPR)*. 2010. San Francisco, CA: IEEE.

131. Ryan, G.L., H.M. Petroccia, N. Watanabe, and D. Vavylonis, *Excitable actin dynamics in lamellipodial protrusion and retraction.* Biophys J, 2012. 102. (7): p. 1493-502.

132. Zhuo, Y., T. Qian, Y. Wu, J. Seong, Y. Gong, H. Ma, Y. Wang, and S. Lu, *Subcellular and Dynamic Coordination between Src Activity and Cell Protrusion in Microenvironment.* Sci Rep, 2015. 5. p. 12963.

133. Katoh, K., Y. Kano, M. Amano, H. Onishi, K. Kaibuchi, and K. Fujiwara, *Rho-kinase--mediated contraction of isolated stress fibers.* J Cell Biol, 2001. 153. (3): p. 569-84.

134. Driscoll, M.K., W. Losert, K. Jacobson, and M. Kapustina, *Spatiotemporal relationships between the cell shape and the actomyosin cortex of periodically protruding cells.* Cytoskeleton (Hoboken), 2015. 72. (6): p. 268-81.

135. Gerisch, G., T. Bretschneider, A. Muller-Taubenberger, E. Simmeth, M. Ecke, S. Diez, and K. Anderson, *Mobile actin clusters and traveling waves in cells recovering from actin depolymerization.* Biophys J, 2004. 87. (5): p. 3493-503.

136. Buccione, R., J.D. Orth, and M.A. McNiven, *Foot and mouth: podosomes, invadopodia and circular dorsal ruffles.* Nat Rev Mol Cell Biol, 2004. 5. (8): p. 647-57.

137. Stokes, J.B., S.J. Adair, J.K. Slack-Davis, D.M. Walters, R.W. Tilghman, E.D. Hershey, B. Lowrey, K.S. Thomas, A.H. Bouton, R.F. Hwang, E.B. Stelow, J.T. Parsons, and T.W. Bauer, *Inhibition of focal adhesion kinase by PF-562,271 inhibits the growth and metastasis of pancreatic cancer concomitant with altering the tumor microenvironment.* Mol Cancer Ther, 2011. 10. (11): p. 2135-45.

138. Jay, D.G., *The clutch hypothesis revisited: ascribing the roles of actin-associated proteins in filopodial protrusion in the nerve growth cone.* J Neurobiol, 2000. 44. (2): p. 114-25.

139. Ishizaki, T., M. Uehata, I. Tamechika, J. Keel, K. Nonomura, M. Maekawa, and S. Narumiya, *Pharmacological properties of Y-27632, a specific inhibitor of rho-associated kinases.* Mol Pharmacol, 2000. 57. (5): p. 976-83.

140. Gao, Y., Q. Xiao, H. Ma, L. Li, J. Liu, Y. Feng, Z. Fang, J. Wu, X. Han, J. Zhang, Y. Sun, G. Wu, R. Padera, H. Chen, K.K. Wong, G. Ge, and H. Ji, *LKB1 inhibits lung cancer progression through lysyl oxidase and extracellular matrix remodeling.* Proc Natl Acad Sci U S A, 2010. 107. (44): p. 18892-7.

141. Carragher, N.O. and M.C. Frame, *Focal adhesion and actin dynamics: a place where kinases and proteases meet to promote invasion.* Trends Cell Biol, 2004. 14. (5): p. 241-9.

142. Kallergi, G., S. Agelaki, H. Markomanolaki, V. Georgoulias, and C. Stournaras, *Activation of FAK/PI3K/Rac1 signaling controls actin reorganization and inhibits cell motility in human cancer cells.* Cell Physiol Biochem, 2007. 20. (6): p. 977-86.

143. Serrels, B., A. Serrels, V.G. Brunton, M. Holt, G.W. McLean, C.H. Gray, G.E. Jones, and M.C. Frame, *Focal adhesion kinase controls actin assembly via a FERM-mediated interaction with the Arp2/3 complex.* Nat Cell Biol, 2007. 9. (9): p. 1046-56.

144. Yoon, K.A., J.L. Ku, H.S. Choi, S.C. Heo, S.Y. Jeong, Y.J. Park, N.K. Kim, J.C. Kim, P.M. Jung, and J.G. Park, *Germline mutations of the STK11 gene in Korean Peutz-Jeghers syndrome patients.* Br J Cancer, 2000. 82. (8): p. 1403-6.

145. Guldberg, P., P. thor Straten, V. Ahrenkiel, T. Seremet, A.F. Kirkin, and J. Zeuthen, *Somatic mutation of the Peutz-Jeghers syndrome gene, LKB1/STK11, in malignant melanoma.* Oncogene, 1999. 18. (9): p. 1777-80.

146. Jaleel, M., A. McBride, J.M. Lizcano, M. Deak, R. Toth, N.A. Morrice, and D.R. Alessi, *Identification of the sucrose non-fermenting related kinase SNRK, as a novel LKB1 substrate.* FEBS Lett, 2005. 579. (6): p. 1417-23.

147. Havel, L.S., E.R. Kline, A.M. Salgueiro, and A.I. Marcus, *Vimentin regulates lung cancer cell adhesion through a VAV2-Rac1 pathway to control focal adhesion kinase activity.* Oncogene, 2014.

148. Ladhani, O., C. Sanchez-Martinez, J.L. Orgaz, B. Jimenez, and O.V. Volpert, *Pigment epithelium-derived factor blocks tumor extravasation by suppressing amoeboid morphology and mesenchymal proteolysis.* Neoplasia, 2011. 13. (7): p. 633-42.

149. Nogawa, H. and T. Mizuno, *Mesenchymal control over elongating and branching morphogenesis in salivary gland development.* J Embryol Exp Morphol, 1981. 66. p. 209-21.

150. Bredfeldt, J.S., Y. Liu, M.W. Conklin, P.J. Keely, T.R. Mackie, and K.W. Eliceiri, *Automated quantification of aligned collagen for human breast carcinoma prognosis.* J Pathol Inform, 2014. 5. p. 28.

151. Morley, S., M.H. Hager, S.G. Pollan, B. Knudsen, D. Di Vizio, and M.R. Freeman, *Trading in your spindles for blebs: the amoeboid tumor cell phenotype in prostate cancer.* Asian Journal of Andrology, 2014. 16. (4): p. 530-535.

152. Wolf, K., I. Mazo, H. Leung, K. Engelke, U.H. von Andrian, E.I. Deryugina, A.Y. Strongin, E.-B. Bröcker, and P. Friedl, *Compensation mechanism in tumor cell migration: mesenchymal–amoeboid transition after blocking of pericellular proteolysis.* The Journal of Cell Biology, 2003. 160. (2): p. 267-277.

153. Wolf, K., R. Müller, S. Borgmann, E.-B. Bröcker, and P. Friedl, *Amoeboid shape change and contact guidance: T-lymphocyte crawling through fibrillar collagen is independent of matrix remodeling by MMPs and other proteases*. Vol. 102. 2003. 3262-3269.

154. Lo, B., G. Strasser, M. Sagolla, C.D. Austin, M. Junttila, and I. Mellman, *Lkb1 regulates organogenesis and early oncogenesis along AMPK-dependent and -independent pathways.* The Journal of Cell Biology, 2012. 199. (7): p. 1117-1130.

155. Friedl, P. and K. Wolf, *Tumour-cell invasion and migration: diversity and escape mechanisms.* Nat Rev Cancer, 2003. 3. (5): p. 362-74.

156. Mandeville, J.T., M.A. Lawson, and F.R. Maxfield, *Dynamic imaging of neutrophil migration in three dimensions: mechanical interactions between cells and matrix.* J Leukoc Biol, 1997. 61. (2): p. 188-200.

157. Li, J., J. Liu, P. Li, X. Mao, W. Li, J. Yang, and P. Liu, *Loss of LKB1 disrupts breast epithelial cell polarity and promotes breast cancer metastasis and invasion.* J Exp Clin Cancer Res, 2014. 33. p. 70.

158. Kakiuchi, M., T. Nishizawa, H. Ueda, K. Gotoh, A. Tanaka, A. Hayashi, S. Yamamoto, K. Tatsuno, H. Katoh, Y. Watanabe, T. Ichimura, T. Ushiku, S. Funahashi, K. Tateishi, I. Wada, N. Shimizu, S. Nomura, K. Koike, Y. Seto, M. Fukayama, H. Aburatani, and S. Ishikawa, *Recurrent gain-of-function mutations of RHOA in diffuse-type gastric carcinoma.* Nat Genet, 2014. 46. (6): p. 583-587.

159. Wang, K., S.T. Yuen, J. Xu, S.P. Lee, H.H.N. Yan, S.T. Shi, H.C. Siu, S. Deng, K.M. Chu, S. Law, K.H. Chan, A.S.Y. Chan, W.Y. Tsui, S.L. Ho, A.K.W. Chan, J.L.K. Man, V. Foglizzo, M.K. Ng, A.S. Chan, Y.P. Ching, G.H.W. Cheng, T. Xie, J. Fernandez, V.S.W. Li, H. Clevers, P.A. Rejto, M. Mao, and S.Y. Leung, *Whole-genome sequencing and comprehensive molecular profiling identify new driver mutations in gastric cancer.* Nat Genet, 2014. 46. (6): p. 573-582.

160. Han, X., F. Li, Z. Fang, Y. Gao, F. Li, R. Fang, S. Yao, Y. Sun, L. Li, W. Zhang, H. Ma, Q. Xiao, G. Ge, J. Fang, H. Wang, L. Zhang, K.K. Wong, H. Chen, Y. Hou, and H. Ji, *Transdifferentiation of lung adenocarcinoma in mice with Lkb1 deficiency to squamous cell carcinoma.* Nat Commun, 2014. 5. p. 3261.

161. Erler, J.T., K.L. Bennewith, M. Nicolau, N. Dornhofer, C. Kong, Q.-T. Le, J.-T.A. Chi, S.S. Jeffrey, and A.J. Giaccia, *Lysyl oxidase is essential for hypoxia-induced metastasis.* Nature, 2006. 440. (7088): p. 1222-1226.

162. Haston, W.S., J.M. Shields, and P.C. Wilkinson, *Lymphocyte locomotion and attachment on two-dimensional surfaces and in three-dimensional matrices.* J Cell Biol, 1982. 92. (3): p. 747-52.

163. Rosel, D., J. Brabek, O. Tolde, C.T. Mierke, D.P. Zitterbart, C. Raupach, K. Bicanova, P. Kollmannsberger, D. Pankova, P. Vesely, P. Folk, and B. Fabry, *Up-regulation of Rho/ROCK signaling in sarcoma cells drives invasion and increased generation of protrusive forces.* Mol Cancer Res, 2008. 6. (9): p. 1410-20.

164. Sahai, E. and C.J. Marshall, *Differing modes of tumour cell invasion have distinct requirements for Rho/ROCK signalling and extracellular proteolysis.* Nat Cell Biol, 2003. 5. (8): p. 711-719.

165. Wyckoff, J.B., S.E. Pinner, S. Gschmeissner, J.S. Condeelis, and E. Sahai, *ROCK- and myosin-dependent matrix deformation enables protease-independent tumor-cell invasion in vivo.* Curr Biol, 2006. 16. (15): p. 1515-23.

166. Ryerson, A.B., C.R. Eheman, S.F. Altekruse, J.W. Ward, A. Jemal, R.L. Sherman, S.J. Henley, D. Holtzman, A. Lake, A.M. Noone, R.N. Anderson, J. Ma, K.N. Ly, K.A. Cronin, L. Penberthy, and B.A. Kohler, *Annual Report to the Nation on the*

Status of Cancer, 1975-2012, featuring the increasing incidence of liver cancer. Cancer, 2016. 122. (9): p. 1312-37.

167. Resta, N., C. Simone, C. Mareni, M. Montera, M. Gentile, F. Susca, R. Gristina, S. Pozzi, L. Bertario, P. Bufo, N. Carlomagno, M. Ingrosso, F.P. Rossini, R. Tenconi, and G. Guanti, *STK11 mutations in Peutz-Jeghers syndrome and sporadic colon cancer.* Cancer Res, 1998. 58. (21): p. 4799-801.

168. Shackelford, D.B. and R.J. Shaw, *The LKB1-AMPK pathway: metabolism and growth control in tumour suppression.* Nat Rev Cancer, 2009. 9. (8): p. 563-75.

169. Jackson, E.L., N. Willis, K. Mercer, R.T. Bronson, D. Crowley, R. Montoya, T. Jacks, and D.A. Tuveson, *Analysis of lung tumor initiation and progression using conditional expression of oncogenic K-ras.* Genes Dev, 2001. 15. (24): p. 3243-8.

170. Jonkers, J., R. Meuwissen, H. van der Gulden, H. Peterse, M. van der Valk, and A. Berns, *Synergistic tumor suppressor activity of BRCA2 and p53 in a conditional mouse model for breast cancer.* Nat Genet, 2001. 29. (4): p. 418-25.

171. Serrano, M., H. Lee, L. Chin, C. Cordon-Cardo, D. Beach, and R.A. DePinho, *Role of the INK4a locus in tumor suppression and cell mortality.* Cell, 1996. 85. (1): p. 27-37.

172. de Leng, W.W., J.J. Keller, S. Luiten, A.R. Musler, M. Jansen, A.F. Baas, F.W. de Rooij, J.J. Gille, F.H. Menko, G.J. Offerhaus, and M.A. Weterman, *STRAD in Peutz-Jeghers syndrome and sporadic cancers.* J Clin Pathol, 2005. 58. (10): p. 1091-5.

173. Jiang, W.G., *Membrane ruffling of cancer cells: a parameter of tumour cell motility and invasion.* Eur J Surg Oncol, 1995. 21. (3): p. 307-9.

174. Johnston, C.L., H.C. Cox, J.J. Gomm, and R.C. Coombes, *bFGF and aFGF induce membrane ruffling in breast cancer cells but not in normal breast epithelial cells: FGFR-4 involvement.* Biochemical Journal, 1995. 306. (Pt 2): p. 609-616.

175. Allard, J. and A. Mogilner, *Traveling waves in actin dynamics and cell motility.* Current opinion in cell biology, 2013. 25. (1): p. 107-115.

176. Bretschneider, T., K. Anderson, M. Ecke, A. Muller-Taubenberger, B. Schroth-Diez, H.C. Ishikawa-Ankerhold, and G. Gerisch, *The three-dimensional dynamics of actin waves, a model of cytoskeletal self-organization.* Biophys J, 2009. 96. (7): p. 2888-900.

177. Driscoll, M.K., C. McCann, R. Kopace, T. Homan, J.T. Fourkas, C. Parent, and W. Losert, *Cell Shape Dynamics: From Waves to Migration.* PLoS Comput Biol, 2012. 8. (3): p. e1002392.

178. Zhou, J., Y. Hayakawa, Timothy C. Wang, and Adam J. Bass, *RhoA Mutations Identified in Diffuse Gastric Cancer.* Cancer Cell, 2014. 26. (1): p. 9-11.

179. Chang, C.F., M.W. Lee, P.Y. Kuo, Y.J. Wang, Y.H. Tu, and S.C. Hung, *Three-dimensional collagen fiber remodeling by mesenchymal stem cells requires the integrin-matrix interaction.* J Biomed Mater Res A, 2007. 80. (2): p. 466-74.

180. Kagami, S., S. Kondo, K. Loster, W. Reutter, T. Kuhara, K. Yasutomo, and Y. Kuroda, *Alpha1beta1 integrin-mediated collagen matrix remodeling by rat mesangial cells is differentially regulated by transforming growth factor-beta and platelet-derived growth factor-BB.* J Am Soc Nephrol, 1999. 10. (4): p. 779-89.

181. Oliveira, C.R., C. Marqueti Rde, M.R. Cominetti, E.S. Douat, J.U. Ribeiro, C.L. Pontes, A. Borghi-Silva, and H.S. Selistre-de-Araujo, *Effects of blocking*

alphavbeta3 integrin by a recombinant RGD disintegrin on remodeling of wound healing after induction of incisional hernia in rats. Acta Cir Bras, 2015. 30. (2): p. 134-42.